Curl and Warp Analysis of the LTPP SPS-2 Site in Arizona

PUBLICATION NO. FHWA-HRT-12-068

DECEMBER 2012

U.S. Department of Transportation
Federal Highway Administration

Research, Development, and Technology
Turner-Fairbank Highway Research Center
6300 Georgetown Pike
McLean, VA 22101-2296

FOREWORD

This study examined the roughness and roughness progression of 21 test sections on the Long-Term Pavement Performance (LTPP) Specific Pavement Studies (SPS)-2 site in Arizona over the first 16 years of the experiment. The site included 12 test sections from the standard experiment and 9 supplemental test sections selected by the Arizona Department of Transportation.

Traditional profile analyses revealed roughness caused by transverse and longitudinal cracking on some test sections and some localized roughness caused by built-in defects. However, the analyses showed that curl and warp contributed to, and in some cases dominated, the roughness on many of the test sections. In addition, roughness did not increase steadily with time because of diurnal and seasonal changes in slab curl and warp.

Jorge E. Pagán-Ortiz
Director, Office of Infrastructure
Research and Development

TECHNICAL REPORT DOCUMENTATION PAGE

1. Report No. FHWA-HRT-12-068	2. Government Accession No.	3. Recipient's Catalog No.
4. Title and Subtitle Curl and Warp Analysis of the LTPP SPS-2 Site in Arizona		5. Report Date December 2012
		6. Performing Organization Code
7. Author(s) Steven M. Karamihas and Kevin Senn		8. Performing Organization Report No. UMTRI-2012-28
9. Performing Organization Name and Address Nichols Consulting Engineers 1885 S. Arlington Ave., Suite 111 Reno, NV 89509		10. Work Unit No. (TRAIS)
		11. Contract or Grant No. DTFH61-06-C-00027
12. Sponsoring Agency Name and Address Turner-Fairbank Highway Research Center Federal Highway Administration 6300 Georgetown Pike McLean, VA 22101-2296		13. Type of Report and Period Covered Final Report
		14. Sponsoring Agency Code

15. Supplementary Notes
The FHWA Contracting Officer's Technical Representative (COTR) was Larry Wiser, HRDI-30.

16. Abstract

This study examined the roughness and roughness progression of 21 test sections on the LTPP SPS-2 site in Arizona over the first 16 years of the experiment. The site included 12 test sections from the standard experiment and 9 supplemental test sections selected by the Arizona Department of Transportation.

Traditional profile analyses revealed roughness caused by transverse and longitudinal cracking on some test sections and some localized roughness caused by built-in defects. However, the analyses showed that curl and warp contributed to, and in some cases dominated, the roughness on many of the test sections. In addition, roughness did not increase steadily with time because of diurnal and seasonal changes in slab curl and warp.

This study applied objective profile analyses to quantify the level of curl and warp on each section. These automated algorithms estimated the gross strain gradient needed to deform each slab into the shape present in the measured profile and produced a pseudo strain gradient (PSG) value. The levels of curl and warp within each profile are summarized by the average PSG value.

For the jointed concrete test sections, variations in average PSG over time explained many of the changes in roughness over time. This included diurnal variations in slab curl, which often caused the overall progression in roughness to appear disorderly throughout the experiment. PSG analysis also revealed that the overall level of curl and warp increased throughout the life of the experiment, with commensurate increases in the roughness.

This limited study demonstrated the potential value of applying the methods herein to other jointed portland cement concrete pavements, including other SPS-2 sites.

17. Key Word Road roughness, Longitudinal profile, International Roughness Index, LTPP, Pavement testing, Pavement rehabilitation, Jointed concrete pavement, Slab curl and warp	18. Distribution Statement No restrictions. This document is available to the public through the National Technical Information Service, Springfield, VA 22161

19. Security Classif. (of this report) Unclassified	20. Security Classif. (of this page) Unclassified	21. No. of Pages 110	22. Price

Form DOT F 1700.7 (8-72) **Reproduction of completed page authorized**

SI* (MODERN METRIC) CONVERSION FACTORS

APPROXIMATE CONVERSIONS TO SI UNITS

Symbol	When You Know	Multiply By	To Find	Symbol
		LENGTH		
in	inches	25.4	millimeters	mm
ft	feet	0.305	meters	m
yd	yards	0.914	meters	m
mi	miles	1.61	kilometers	km
		AREA		
in^2	square inches	645.2	square millimeters	mm^2
ft^2	square feet	0.093	square meters	m^2
yd^2	square yard	0.836	square meters	m^2
ac	acres	0.405	hectares	ha
mi^2	square miles	2.59	square kilometers	km^2
		VOLUME		
fl oz	fluid ounces	29.57	milliliters	mL
gal	gallons	3.785	liters	L
ft^3	cubic feet	0.028	cubic meters	m^3
yd^3	cubic yards	0.765	cubic meters	m^3
	NOTE: volumes greater than 1000 L shall be shown in m^3			
		MASS		
oz	ounces	28.35	grams	g
lb	pounds	0.454	kilograms	kg
T	short tons (2000 lb)	0.907	megagrams (or "metric ton")	Mg (or "t")
		TEMPERATURE (exact degrees)		
^oF	Fahrenheit	5 (F-32)/9 or (F-32)/1.8	Celsius	^oC
		ILLUMINATION		
fc	foot-candles	10.76	lux	lx
fl	foot-Lamberts	3.426	candela/m^2	cd/m^2
		FORCE and PRESSURE or STRESS		
lbf	poundforce	4.45	newtons	N
lbf/in^2	poundforce per square inch	6.89	kilopascals	kPa

APPROXIMATE CONVERSIONS FROM SI UNITS

Symbol	When You Know	Multiply By	To Find	Symbol
		LENGTH		
mm	millimeters	0.039	inches	in
m	meters	3.28	feet	ft
m	meters	1.09	yards	yd
km	kilometers	0.621	miles	mi
		AREA		
mm^2	square millimeters	0.0016	square inches	in^2
m^2	square meters	10.764	square feet	ft^2
m^2	square meters	1.195	square yards	yd^2
ha	hectares	2.47	acres	ac
km^2	square kilometers	0.386	square miles	mi^2
		VOLUME		
mL	milliliters	0.034	fluid ounces	fl oz
L	liters	0.264	gallons	gal
m^3	cubic meters	35.314	cubic feet	ft^3
m^3	cubic meters	1.307	cubic yards	yd^3
		MASS		
g	grams	0.035	ounces	oz
kg	kilograms	2.202	pounds	lb
Mg (or "t")	megagrams (or "metric ton")	1.103	short tons (2000 lb)	T
		TEMPERATURE (exact degrees)		
^oC	Celsius	1.8C+32	Fahrenheit	^oF
		ILLUMINATION		
lx	lux	0.0929	foot-candles	fc
cd/m^2	candela/m^2	0.2919	foot-Lamberts	fl
		FORCE and PRESSURE or STRESS		
N	newtons	0.225	poundforce	lbf
kPa	kilopascals	0.145	poundforce per square inch	lbf/in^2

*SI is the symbol for the International System of Units. Appropriate rounding should be made to comply with Section 4 of ASTM E380.
(Revised March 2003)

TABLE OF CONTENTS

LIST OF FIGURES

LIST OF TABLES

LIST OF ACRONYMS

AC	Asphalt concrete
ADOT	Arizona Department of Transportation
BTB	Bituminous-treated base
DGAB	Dense-graded aggregate base
FHWA	Federal Highway Administration
GPS	General Pavement Studies
HRI	Half-car Roughness Index
IRI	International Roughness Index
LCB	Lean concrete base
LTPP	Long-Term Pavement Performance
MRI	Mean Roughness Index
PATB	Permeable asphalt-treated base
PBTB	Permeable bituminous-treated base
PCC	Portland cement concrete
PSD	Power spectral density
PSG	Pseudo strain gradient
RN	Ride Number
SEE	Standard estimate of error
SMP	Seasonal Monitoring Program
SPS	Specific Pavement Studies

INTRODUCTION

This report provides the results of profile and roughness analyses for the Long-Term Pavement Performance (LTPP) Specific Pavement Studies (SPS)-2 site in Arizona. The analyses emphasized the roles of curl and warp in the development of roughness. SPS-2 sites were established for the study of rigid pavement structural factors, including concrete slab thickness, concrete strength, base material, permeability, and lane width.[(1)] These test pavements were constructed on eastbound Interstate 10 from April 1993 through January 1994. The site includes 21 test sections and extends from milepost 106 to 109. Some properties of the sections are listed in table 1.

Table 1. Arizona SPS-2 Site Structural Factors.

Section	Lane Width (ft)	PCC Flexural Strength (psi)	Layer Thickness (inches)			Layer Type		
			Layer 1	Layer 2	Layer 3	Layer 1	Layer 2	Layer 3
0213	14	550	8	6		PCC	DGAB	
0214	12	900	8	6		PCC	DGAB	
0215	12	550	11	6		PCC	DGAB	
0216	14	900	11	6		PCC	DGAB	
0217	14	550	8	6		PCC	LCB	
0218	12	900	8	6		PCC	LCB	
0219	12	550	11	6		PCC	LCB	
0220	14	900	11	6		PCC	LCB	
0221	14	550	8	4	4	PCC	PATB	DGAB
0222	12	900	8	4	4	PCC	PATB	DGAB
0223	12	550	11	4	4	PCC	PATB	DGAB
0224	14	900	11	4	4	PCC	PATB	DGAB
0260	—	—	8.5	4		AC	DGAB	
0261	—	—	8.5	4		AC	DGAB	
0262	14	550	8	6		PCC	DGAB	
0263	14	550	8	4	4	PCC	PBTB	DGAB
0264	12	550	8.5	4	4	PCC	PBTB	DGAB
0265	12	550	8.5	6		PCC	DGAB	
0266	14	550	12.5	4		PCC	DGAB	
0267	14	550	11	4		PCC	BTB	
0268	14	550	8	4		PCC	BTB	

— Value unknown
Blank cell indicates that layer is not present in section
AC = Asphalt concrete
BTB = Bituminous-treated base
DGAB = Dense-graded aggregate base
LCB = Lean concrete base
PATB = Permeable asphalt-treated base
PCC = Portland cement concrete
PBTB = Permeable bituminous-treated base

Twelve sections, 0213–0224, were constructed as part of the standard SPS-2 experiment. These sections have the same design characteristics as the standard 12 sections that appear on several other SPS-2 sites within the LTPP study. They are all doweled jointed plain concrete pavements. This site also includes four undoweled sections with skewed joints, SPS-2A-type sections 0262–0265. Their doweled counterparts are 0213, 0221, 0223, and 0215, respectively. Three additional sections of doweled jointed plain concrete, 0266–0268, were included with specialized designs of interest to the Arizona Department of Transportation (ADOT). Asphalt concrete (AC) sections 0260 and 0261 were also included by ADOT.

This report seeks to characterize the surface roughness of these sections over time and link the observations to records of pavement distress and its development. Road profile measurements were collected on this site about once per year since the winter after it was opened to traffic. Profile data were also collected on section 0215 on 16 additional dates.

This study applied algorithms for estimating the level of curl and warp present in the pavement and its effect on surface roughness. The algorithms included slab-by-slab quantification of curl and warp throughout the monitoring history of the site. The analysis framework for this was established in a recent Federal Highway Administration (FHWA) study of seasonal and diurnal changes in jointed concrete pavement roughness.[(2)] This method applies Westergaard's theory to establish the likely shape of a curled slab and a curve fitting algorithm to quantify the level of curling in each slab.

The study related aggregated measurements of curl and warp within each profile measurement to the International Roughness Index (IRI). The observed statistical relationship between changes in curl and warp and changes in IRI for a given section provided a way distinguish the long-term roughness caused by distress from short- and long-term changes in roughness associated with curl and warp. Estimates of curl and warp from the profiles also provide the opportunity to study underlying environmental causes, but that aspect was not explored in this study.

This study also analyzed the profiles in detail using profile analysis methods employed in the study of other SPS sites in Arizona. (See references 3–7.) These methods include calculating roughness index values, examining the spatial distribution of roughness within a section, viewing profiles with post-processing filters, and examining spectral properties. The study applied the traditional analysis methods to the AC sections (0260 and 0261) in an attempt to treat them as control sections for comparison to the portland cement concrete (PCC) sections.

DATA COLLECTION AND ANALYSES

PROFILE DATA SYNCHRONIZATION

Profile data were collected over the entire Arizona SPS-2 site during 15 visits, as shown in table 2. Raw profile data were available for all 15 visits. In each visit, a minimum of seven repeat profile measurements were made. The measurements for all visits included sections 0213–0224 and sections 0260–0268.

Table 2. Profile Measurement Visits of the SPS-2 Site.

Visit	Date	Time	Repeats
01	25-Jan-1994	06:10	9
02	05-Mar-1995	11:21	9
03	27-Jan-1997	11:23–12:49	9
04	04-Dec-1997	11:06–13:07	7
05	08-Dec-1998	10:29–11:27	7
06	15-Nov-1999	11:39–12:39	7
07	30-Nov-2000	13:38–15:01	9
08	08-Nov-2001	11:09–12:40	9
09	30-Oct-2002	12:41–14:07	9
10	04-Feb-2004	13:47–15:12	9
11	12-Dec-2004	16:16–18:37	9
12	11-Aug-2006	04:18–06:26	9
	13-Aug-2006	00:17–04:28	9
13	30-Dec-2007	10:06–13:21	9
14	20-Sep-2008	00:37–03:36	9
15	25-Jan-2010	16:09–19:00	9

Note: In visit 12, one portion of the site was measured on the first date and the remaining portion was measured two days later.

Profile data were also collected over section 0215 on 16 additional dates as part of the Seasonal Monitoring Program (SMP). On most of the measurement dates for this section, profiles were collected in the morning and the afternoon. In others, the profiles were collected in the early and late morning. In this report, each group of runs is treated as a distinct visit. Table 3 lists the dates and times of each visit. These visits covered 4 seasons in 1998 and 12 consecutive seasons starting in the winter of 2001.

Profiles of individual test sections were extracted directly from the raw measurements and aligned using an automated trace comparison algorithm. This was done for two reasons. First, profiles were collected at a sample interval of 0.98 inches in visits 03–08 and S01–S14 and at a sample interval of about 0.77 inches in visits 09–11 and S15–S28. These data appeared in the database after the application of an 11.8-inch moving average and decimation to a sample interval of 5.91 inches. The raw data contained the more detailed profiles. Second, this study depended on consistency of the profile starting and ending points with the construction layout and consistency of the section limits with time. Appendix A describes the extraction of individual test section profiles from the raw measurements and the process of ensuring the profiles had consistent alignment.

Table 3. Seasonal Visits of Section 0215.

Visit	Date	Repeats	Time
S01	15-Jan-1998	7	11:33–11:53
S02	15-Jan-1998	5	16:43–16:52
S03	13-Apr-1998	5	10:13–10:30
S04	13-Apr-1998	5	15:20–15:31
S05	09-Jul-1998	5	08:23–08:45
S06	09-Jul-1998	5	12:11–12:26
S07	30-Sep-1998	5	11:59–12:15
S08	30-Sep-1998	7	14:34–15:05
S09	09-Dec-2001	7	09:21–09:46
S10	09-Dec-2001	9	14:58–15:30
S11	24-Jan-2002	7	10:12–10:38
S12	24-Jan-2002	9	14:56–15:33
S13	15-Mar-2002	7	09:40–10:11
S14	15-Mar-2002	7	14:30–15:01
S15	09-Oct-2002	9	08:43–09:34
S16	09-Oct-2002	9	13:47–14:35
S17	20-Dec-2002	9	09:05–09:43
S18	20-Dec-2002	9	13:24–14:08
S19	07-Mar-2003	9	09:24–09:54
S20	07-Mar-2003	9	13:57–14:37
S21	25-Jul-2003	9	04:24–05:06
S22	25-Jul-2003	9	08:34–09:12
S23	24-Nov-2003	9	09:32–10:17
S24	24-Nov-2003	9	14:23–15:04
S25	14-Dec-2003	9	10:33–11:10
S26	14-Dec-2003	9	15:16–15:56
S27	22-Apr-2004	9	04:59–05:38
S28	22-Apr-2004	9	09:49–10:25
S29	15-Jul-2004	9	04:17–04:50
S30	15-Jul-2004	9	09:02–09:40
S31	09-Sep-2004	9	08:35–09:05
S32	09-Sep-2004	9	15:53–16:25

DATA QUALITY SCREENING

Each visit of each test section included five, seven, or nine repeat profile measurements. Data quality screening was performed to select five repeat profile measurements per section from each visit. Among the group of available runs, the five measurements that exhibited the best agreement with each other were selected. Agreement between two profiles was judged by cross correlating the profiles after applying the IRI filter rather than the overall IRI values. This method compares the profile traces rather than the overall index. Achieving high correlation requires that the details of the profile shape affecting roughness agree as well as the overall roughness level.[8]

The average correlation level produced by these calculations provided a numerical assessment of the repeatability within each set of repeat measurements. Overall, most sets of selected repeat measurements exhibited good repeatability. In some cases, localized surface distress reduced

repeatability. The inconsistency in profiles in these areas occurred because of slight variations in the lateral tracking position of the profiles as the profiler passed over transversely inconsistent surface features. The most prominent example of this inconsistency occurred in the later visits of section 0213 on the left side of the lane.

Appendix B describes the process of selecting five repeat measurements for each visit of each section and provides a list of the selected profiles with a repeatability score. Appendix C provides the standard deviation of left and right IRI values for each set of repeat measurements.

SUMMARY ROUGHNESS VALUES

Appendix C provides roughness progression plots for all 21 test sections. These plots show the left and right IRI values from each visit over the 16-year monitoring period. Appendix C also lists the IRI, Half-car Roughness Index (HRI), and Ride Number (RN) of each section for each visit. These roughness values are the average of the five repeat measurements selected by data quality screening. The measurements are not necessarily the same five repeat measurements selected for the LTPP public database. Appendix C also provides the standard deviation of IRI over the five repeat measurements. This helps identify erratic roughness values that are the result of transverse variations in the profile caused by surface distresses.

Figure 1 and figure 2 show left and right IRI values for sections 0213 and 0215 over their monitoring period. The graph for section 0213 includes 30 summary IRI values, 2 per visit over 15 visits. The graph for section 0215 includes extra IRI values from the seasonal visits listed in table 3. The figures show the IRI values versus time in years. In this case, *years* is defined as the number of years between the measurement date and the date the site was opened to traffic (1-Oct-1993).

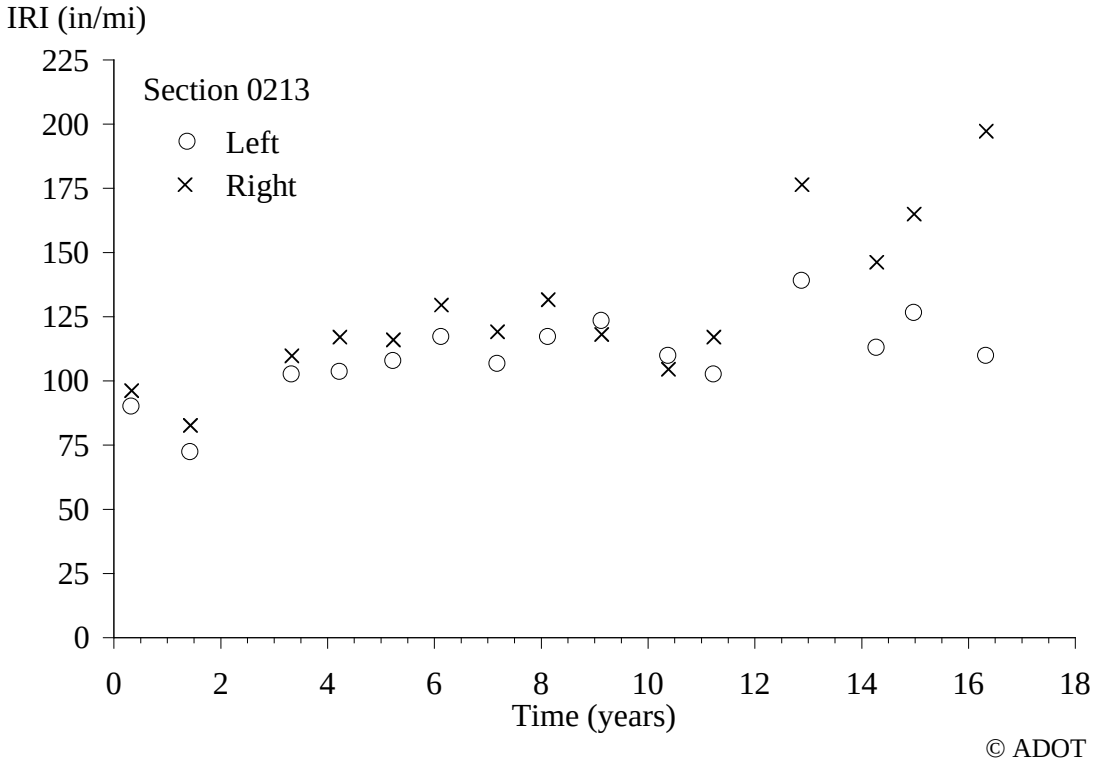

Figure 1. Graph. IRI Progression for Section 0213.

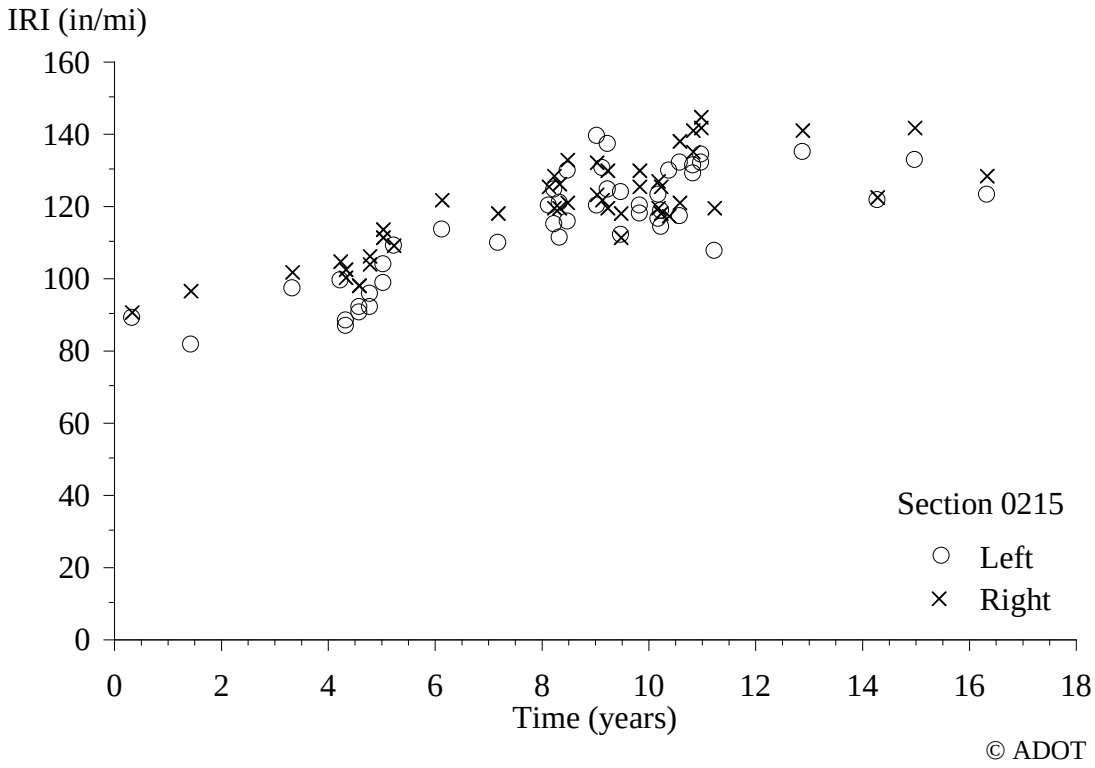

Figure 2. Graph. IRI Progression for Section 0215.

On section 0213, the IRI increases overall, but the roughness does not increase consistently as time progresses. For example, the IRI values in visit 01 (0.32 years) are greater than the values in visit 02 (1.42 years), and the IRI values in visit 12 (12.86 years) are much greater than in visit 11 (11.20 years) or visit 13 (14.25 years). In addition, the right IRI increases over the last three visits, whereas the left IRI does not. The analyses in this report show that the first two observations are due to diurnal changes in curl and warp and the third is not.

On section 0215, the IRI progression reverses direction many times. The eras from 4 to 6 years and 8 to 11 years include several pairs of IRI values from two different times on the same day and a series of seasonal measurements. Of the 16 diurnal pairs collected on section 0215 (listed in table 3), the later set of repeat measurements produced IRI values that were between 2.2 inches/mi above and 19.0 inches/mi below the earlier set of repeat measurements from the same day. In addition, the four seasonal visits that took place in year 9 produced a range of IRI values of 27.2 inches/mi on the left side and 20.5 inches/mi on the right side.

The analyses in the next sections aim to explain the inconsistent progression in IRI on all the test sections and show that some short-term changes in IRI are due to curl and warp and others are not.

TRADITIONAL PROFILE ANALYSES

This study applied typical diagnostic profile analyses such as inspection of filtered elevation profile plots, roughness profile plots, and power spectral density plots to explain the roughness, roughness distribution, and roughness progression of each section. Appendix D provides detailed findings from these analyses that support the discussion of each section in the summary.

These analyses showed that slab curl and warp contributed to, and in some cases dominated, the roughness of many of the test sections. In addition, changes in curl and warp offered a possible explanation for the disorderly progression in roughness with time that occurred on some of the test sections. For example, section 0215 exhibited a very unsteady progression in roughness with time, including large diurnal and seasonal changes in years 4–6 and 8–12.

The analyses in the following sections helped account for changes in slab curl and warp to determine what share of the roughness of each profile was due to slab effects.

CURL AND WARP ANALYSIS

Statistical analysis segregated the portion of roughness caused by curl and warp within a profile from the rest of the irregularities. The levels of curl and warp present within each profile were estimated using slab-by-slab analysis of local profile segments. The procedure quantified the level of curl and warp on each slab using a pseudo strain gradient (PSG). PSG is the gross strain gradient required to deform a slab into the shape that appears within the measured slab profile from a flat baseline.

The PSG value for each slab was derived using a curve fit between the measured profile and an expected curled slab shape using the Westergaard equation. The Westergaard equation requires estimates of pavement mechanical properties (summarized by the radius of relative stiffness). As such, the idealized slab shape was different for each test section. Estimates of these properties were developed using the LTPP database.

Appendix E describes the process of identifying the slab boundaries, and appendix F describes the methodology for estimating PSG given the measured profile and pavement mechanical properties for each slab. Figure 3 shows results for a left-side profile of section 0213 collected in visit 09 (20-Oct-2002). The figure shows the PSG value for each slab along the profile, where slabs 0 and 33 straddle the boundaries of the section and slabs -1 and 34 are outside the section boundaries. The figure shows PSG in units of microstrain per inch (με/inch). Negative values indicate upward curl, which means that the slab edges have a higher elevation than the center.

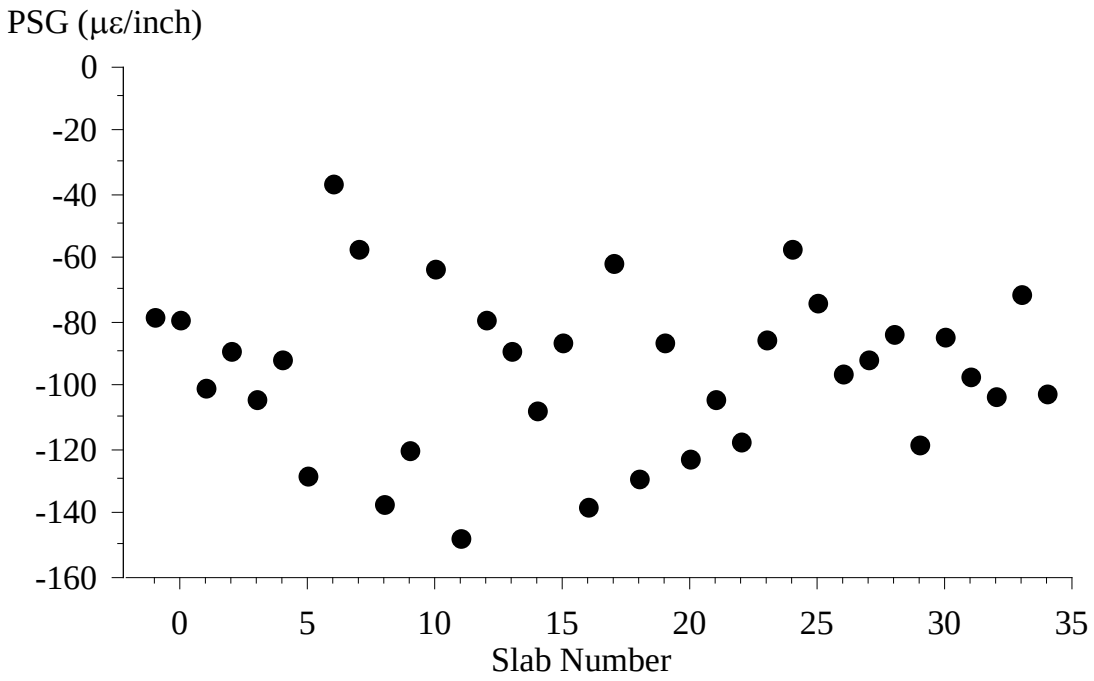

Figure 3. Graph. Left Profile PSG Values from Visit 09 of Section 0213.

Figure 3 provides an example of the variation in upward curl along the left profile of section 0213. For the purposes of examining trends over time, the average PSG value summarizes the overall curl and warp observed for the entire section. The average PSG value is -95.5 με/inch for the profile in figure 3. This is a weighted average, where the PSG of each slab contributes to the section average in proportion to the length that appears within the section. Thus, the PSG of slabs -1 and 34 do not affect the average, and the PSG of slabs 0 and 33 influence the average less than slabs 1–32.

Because this study includes five repeat measurements from each visit of each section, the average PSG values are further averaged over the five repeat measurements. For example, the five left-side profiles of section 0213 from visit 09 (30-Oct-2002) yielded sectionwide average PSG values of -95.5 to -93.0 με/inch, with an average value of -94.5 με/inch. Unless otherwise specified, the PSG values provided in this report are averaged over five repeat profile measurements.

PSG Progression

Figure 4 shows the variation in average PSG for the left side of section 0213 throughout the experiment. The value of -94.5 με/inch, previously discussed for visit 09, appears on the plot 9.08 years into the experiment.

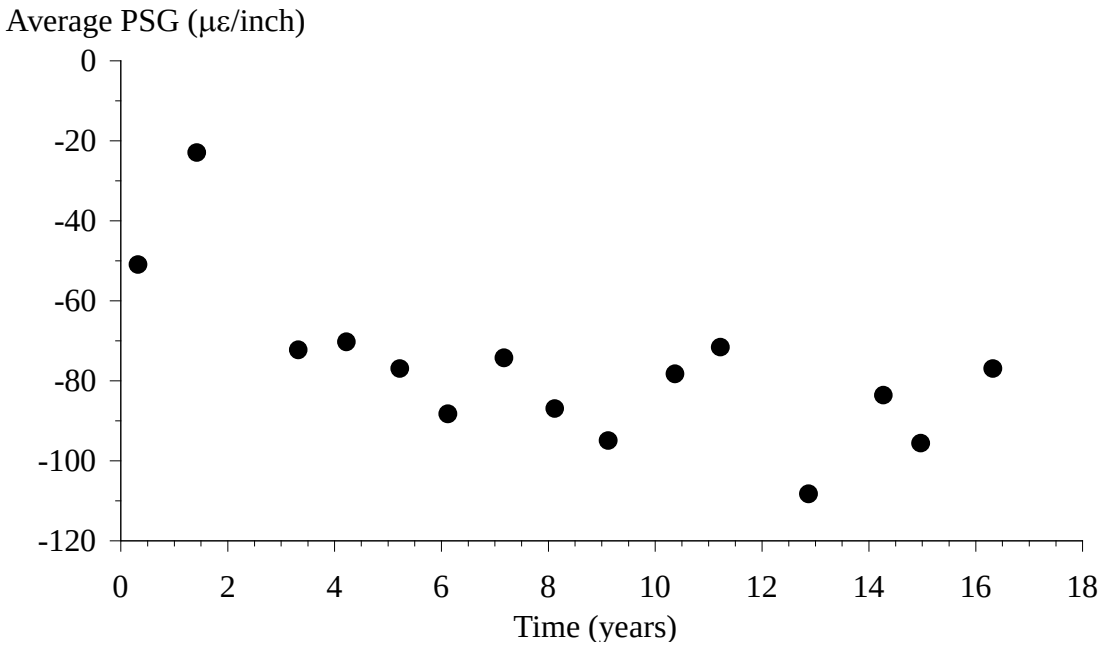

Figure 4. Graph. Average PSG versus Time for Left Side of Section 0213.

The data in figure 4 provide a way to examine the gross changes in curl and warp over time for the left profile of section 0213. The levels of downward curl shown in figure 4 and the left IRI shown in figure 1 follow similar trends, including the following:

- Curling is more severe in visit 01 (0.32 years) than in visit 02 (1.42 years), and the IRI is higher in visit 01 than in visit 02.

- Curling is more severe in visit 09 (9.08 years) than in the two visits before and the two visits afterward, and the IRI is higher in visit 09 than in the two visits before and the two visits afterward.

- Curling is greater in visits 12 (12.86 years) and 14 (14.97 years) than in visits 11 (11.20 years), 13 (14.25 years), and 15 (16.32 years), and the IRI is higher in visits 12 and 14 than in visits 11, 13, and 15.

Indeed, the variations in absolute average IRI over time imitate many of the details of the variations in PSG over time for the left side of section 0213.

Inspection of PSG values versus time showed a similar relationship between PSG and IRI over most of the test sections in the experiment. In some cases, variation in PSG was proportional to variation in IRI but only over the early part of the experiment and during eras of the pavement life where distress remained constant. The following section examines the relationship between PSG and IRI in detail.

Several trends in the variation of PSG over time on multiple sections help explain the disorderly progression in IRI shown in the figures in appendix C. First, on many of the test sections, like section 0213, the upward curl was much more severe in visit 01 (25-Jan-1994) than in visit 02

(5-Mar-1995) or the PSG reversed from negative (upward curl) in visit 01 to positive (downward curl) in visit 02. Visit 01 was conducted at about 6 a.m., and visit 02 was conducted at 11 a.m.

Second, PSG values were more negative in visits 12 (11-Aug-2006) and 14 (20-Sep-2008) than in visits 11 (12-Dec-2004), 13 (30-Dec-2007), and 15 (25-Jan-2010) on sections 0213, 0215–0219, 0220, 0222, and 0262–0268. This indicates a decrease in upward curling in visits 11, 13, and 15 compared to visits 12 and 14. Visits 12 and 14 occurred shortly after midnight, and visits 11, 13, and 15 occurred after sunrise. Section 0214 also exhibited a decrease in downward curl in visits 12 and 14.

Third, sections 0215, 0219, 0223, 0224, and 0264–0266 exhibited a net increase in the magnitude of upward curl over the life of the experiment. The trend was not orderly on any of the test sections, and it typically included the short-term variations discussed for visits 01 and 02 and visits 11–15. Figure 5 provides an example, showing the average PSG for the left- and right-side profiles of each visit for section 0223. Diurnal cycles in temperature and sunlight explain the short-term variations in PSG but not the trend toward increasing upward curl over the life of the experiment.

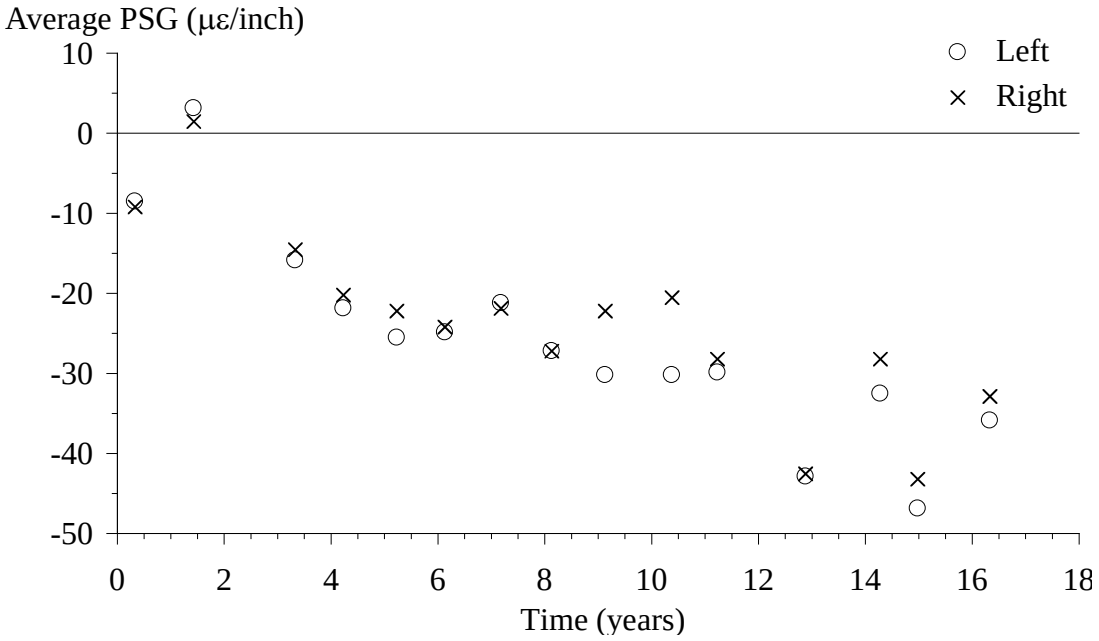

Figure 5. Graph. Average PSG versus Time for Section 0223.

In contrast to the rest of the test sections, section 0214 exhibited a trend from upward curl at the start of the experiment to increasingly downward curl at the end. As shown in figure 6, the PSG values increased most aggressively from negative to positive in years 4–10. Figure 7 shows that the slabs curled upward throughout the section in visit 01 (0.32 years). However, the trend toward downward curl is strongest near the start of the section in visit 10 (10.34 years) and becomes increasingly weak toward the end of the section. A decrease in severity of map cracking from the beginning to the end of the section may explain this trend.

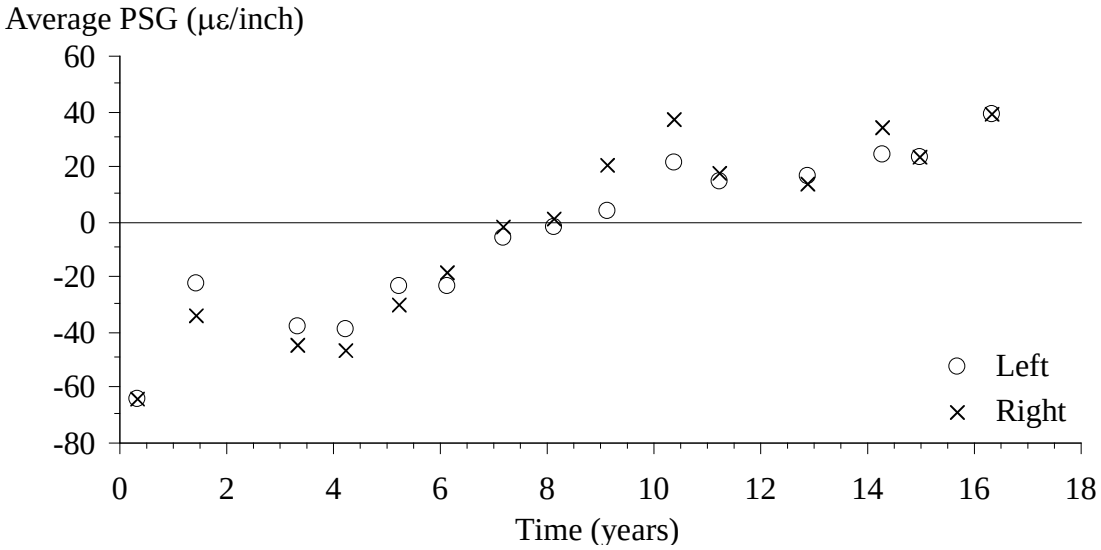

Figure 6. Graph. Average PSG versus Time for Section 0214.

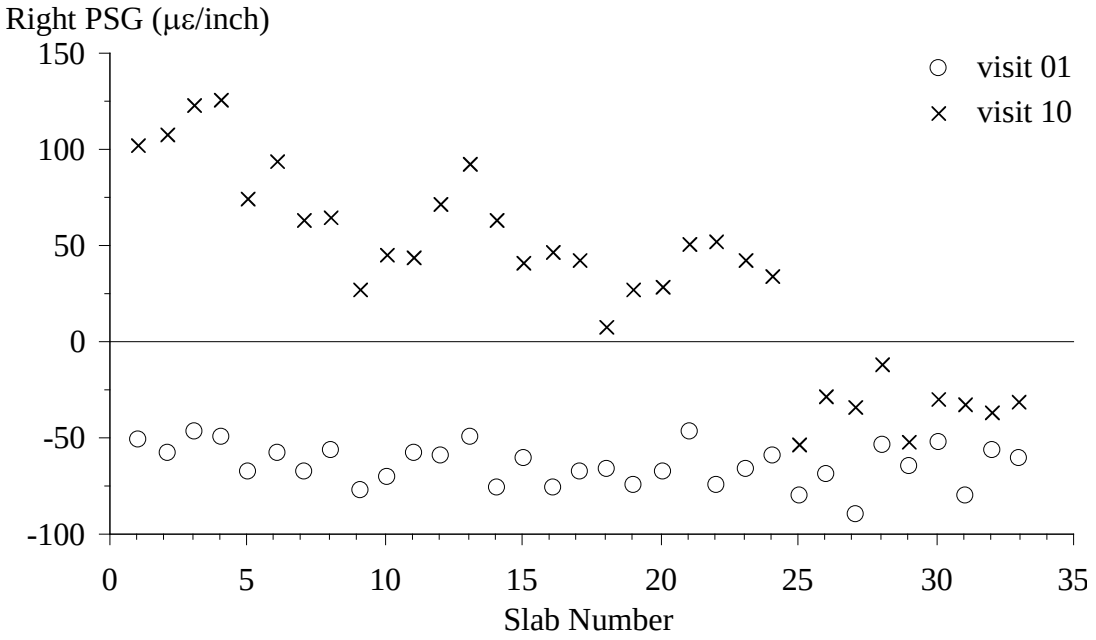

Figure 7. Graph. Right PSG Values from Visits 01 and 10 of Section 0214.

Relationship Between PSG and IRI

This section addresses the penalty to IRI caused by curling. On the low-strength sections, a very strong statistical relationship was found between variations in PSG and variations in IRI. Using this relationship, the roughness caused by slab curl was separated from the roughness caused by other sources. This provided a way to look for increases in IRI caused by surface deterioration without the erratic changes caused by variations in curl and warp over time. This also provided a way to directly estimate the improvement in IRI that is possible with a reduction in slab curl.

Originally, the study sought to relate PSG to IRI theoretically. For example, an artificial profile constructed using a pattern of 15-ft-long slabs with profiles equivalent to the Westergaard equations

showed increases in IRI of 1.74 inches/mi per 1 με/inch increase in PSG when the radius of relative stiffness was 39.37 inches. However, statistical observations using measured profiles showed that the variation in IRI with PSG was roughly three-quarters as large. This is because more roughness appeared at transitions between slabs in the theoretical profile, where the slope break between slabs was sharper. In the measured profiles, the slope at slab ends was not as large, most likely due to the influence of dowel bars and slab weight, which were not included in the model that produced the theoretical slab profile.

Instead, the statistical relationship between IRI and PSG was derived using detailed profile measurements collected for the FHWA project "Inertial Profile Data for Pavement Performance Analysis."[(2)] Measurements from the FHWA study include 124 profiles of sections 0213–0224 collected over a 1-year cycle. The measurements include four seasonal visits (17-Aug-2003, 13-Dec-2003, 9-Mar-2004, and 3-Jul-2004) and four rounds of measurement per visit (before sunrise, after sunrise, mid-afternoon, and after sunset). Seven or more repeat profiles were collected in each of the 16 rounds of measurement. One of the data collection rounds commenced less than 11 h after LTPP visit 11 (12-Dec-2003).

The FHWA profile measurements occurred throughout a diverse mix of ground temperature, air temperature, weather, and intensity of solar radiation. Thus, large changes were observed in curl and warp without large changes in other surface conditions that affect IRI, such as distress. Unfortunately, the profiles from the FHWA study did not cover sections 0260–0268.

Figure 8 shows the relationship between IRI and PSG on the right side of section 0215 using the FHWA data set. The figure shows a distinct IRI-PSG pair for each of 122 passes by the profiler. A least-squares linear fit indicates that the IRI changes 1.3754 inches/mi per 1 με/inch of change in PSG, with a standard estimate of error (SEE) of 2.23 inches/mi. The close relationship observed depends on using measurements collected over a relatively short portion of the pavement life so that changes do not occur because of other contributors to the IRI, such as surface distress. The high correlation is also due to the large range of observed PSG values.

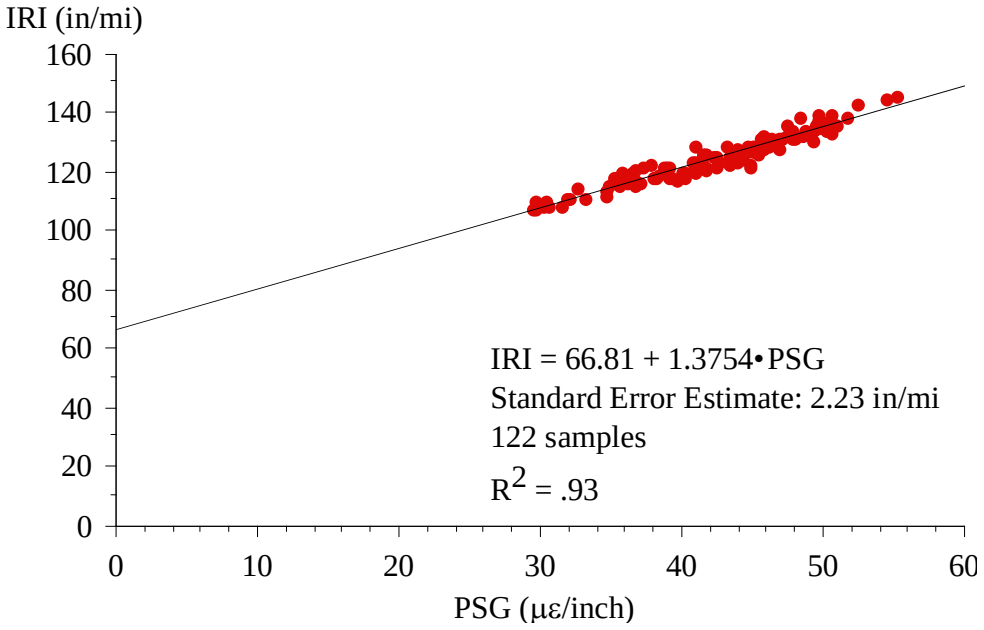

Figure 8. Graph. IRI versus PSG for Right Side of Section 0215 (FHWA Data).

Figure 8 provides noteworthy insight into the contribution of curl and warp to the roughness of section 0215. The PSG values for the right side covered a range of 30–55 με/inch in just 1 year, and the IRI exhibited a commensurate variation of 38 inches/mi. Further, the plot suggests that if the apparent curl were eliminated, the IRI of the right side would be about 67 inches/mi, which is less than half the peak value.

Linear regression of IRI against PSG demonstrated a similar level of correlation for the low-strength test sections in the standard experiment. Table 4 lists the slope, intercept, SEE, and correlation coefficient for the left- and right-side profiles of these sections.

Table 4. Regression Results for IRI and PSG on Low-Strength Test Sections.

Section	Side	Slope ((inches/mi)/(με/inch))	Intercept (inches/mi)	SEE (inches/mi)	R^2
0213	Left	0.8969	39.97	1.19	0.99
	Right	0.8859	48.95	4.64	0.86
0217	Left	1.0511	50.90	2.51	0.96
	Right	1.1348	42.11	2.15	0.96
0221	Left	0.8307	42.03	3.60	0.90
	Right	0.9346	36.00	2.52	0.96
0215	Left	1.3182	60.40	1.84	0.95
	Right	1.3754	66.81	2.23	0.93
0219	Left	1.4938	52.02	4.02	0.92
	Right	1.5094	69.97	2.17	0.98
0223	Left	1.3995	52.27	2.83	0.94
	Right	1.3686	60.36	2.14	0.96

In table 4, the test sections are listed in order of surface layer thickness. This illustrates the similarity in the IRI-PSG slope among structurally similar pavements. A similar dependence of the slope on radius of relative stiffness appeared in the theoretical calculations. At a higher radius of relative stiffness, IRI is higher for the same strain gradient in an artificial profile constructed using the Westergaard equation. The consistency between this trend and the influence of radius of relative stiffness on the IRI-PSG slope derived empirically is a sign that the Westergaard equation may have been an appropriate choice of an idealized profile on the low-strength test sections.

The dependence of IRI on PSG was also characterized using LTPP data from section 0215. This was possible because section 0215 is in SMP, and data collected from November 2001 through December 2004 included 3 regular profiling visits and 24 seasonal visits. Figure 9 shows the linear regression for IRI against PSG for the 135 associated profiler passes. The slope, intercept, and SEE are all exceptionally similar to the observations from the FHWA data. For the left side, the LTPP data produced a slope of 1.442 inches/mi per 1 με/inch.

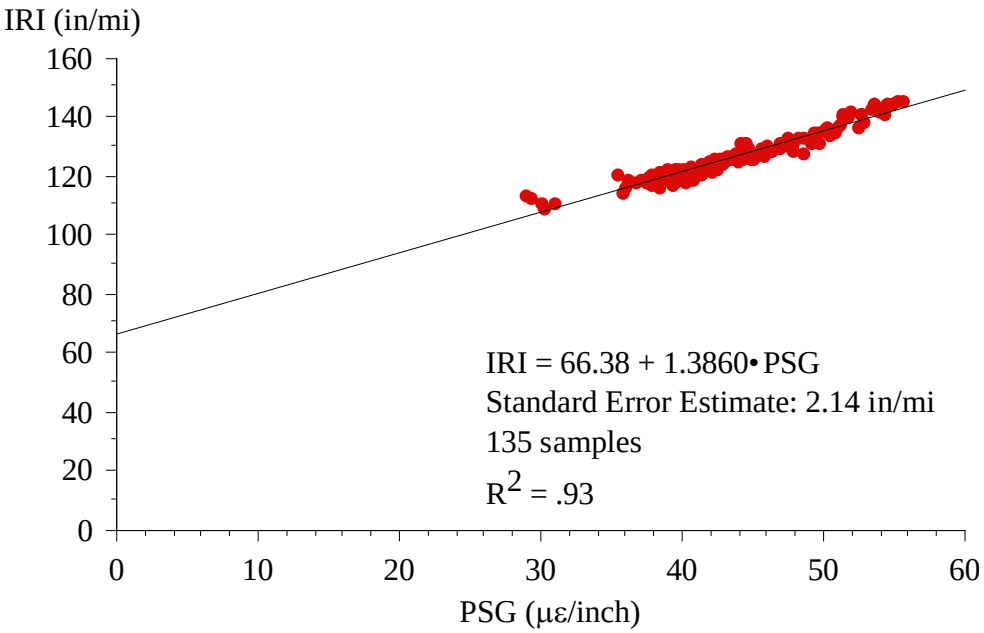

Figure 9. Graph. IRI versus PSG for Right Side of Section 0215 (LTPP SMP Data).

The agreement between figure 8 and figure 9 demonstrates that the IRI-PSG relationship derived from one data set may be applied to data from another, so long as appropriate measurement practices are followed. (An analytical procedure with this quality is called “transportable” in the classic road roughness literature.[9]) The consistency between data sets also indicates that the SMP produced sufficient data to investigate the IRI-PSG relationship and other rigid SMP test sections may also produce sufficient data for this analysis.

Unfortunately, the regression for the high-strength sections often produced low correlation. Table 5 lists the statistics produced by the FHWA data set for the high-strength sections. In some cases, the low overall range in PSG values over the 16 rounds of testing caused low correlation to IRI. Curl and warp also caused only a small share of the overall roughness on many of the high-strength sections, which often led to poor curve fits in the slab-by-slab analysis. High correlation (and low SEE) existed for the right-side profiles on sections 0218, 0220, and 0222. However, the variations in IRI over the monitoring period were low relative to the SEE for these sections as compared to the low-strength sections.

Table 5. Regression Results for IRI and PSG on High-Strength Test Sections.

Section	Side	Slope ((inches/mi)/(με/inch))	Intercept (inches/mi)	SEE (inches/mi)	R^2
0214	Left	0.3726	74.32	5.85	0.02
	Right	0.8089	44.30	1.87	0.72
0218	Left	0.2879	71.08	3.39	0.19
	Right	1.0129	41.36	2.07	0.90
0222	Left	0.5281	60.37	4.85	0.72
	Right	0.7001	41.51	2.29	0.96
0216	Left	3.3459	49.39	3.80	0.54
	Right	0.8603	82.18	2.12	0.21
0220	Left	0.8482	65.20	5.86	0.18
	Right	1.1765	53.60	2.04	0.88
0224	Left	0.6488	69.75	7.43	0.26
	Right	0.5674	65.18	2.15	0.80

Effect of Curling on IRI

For the low-strength sections, the relationship between IRI and PSG was sufficient to support empirical estimates of the contributions curl and warp make to each IRI value. This was done by obtaining the absolute average PSG value for a given visit of a given section, applying the slope from table 4 to it, and subtracting the result from the raw IRI value. Graphically, this is equivalent to placing a point in the appropriate location on an IRI versus PSG plot such as figure 8 and using the IRI-PSG slope to project the point to the IRI axis.

The product of the PSG and the slope from table 4 is the portion of the IRI associated with curl, warp, and other profile features that consistently appear with the same shape as the Westergaard equation. The balance is the roughness linked to other sources, such as built-in defects and surface distress. Figure 10 through figure 21 provide the results of this method for the low-strength test sections.

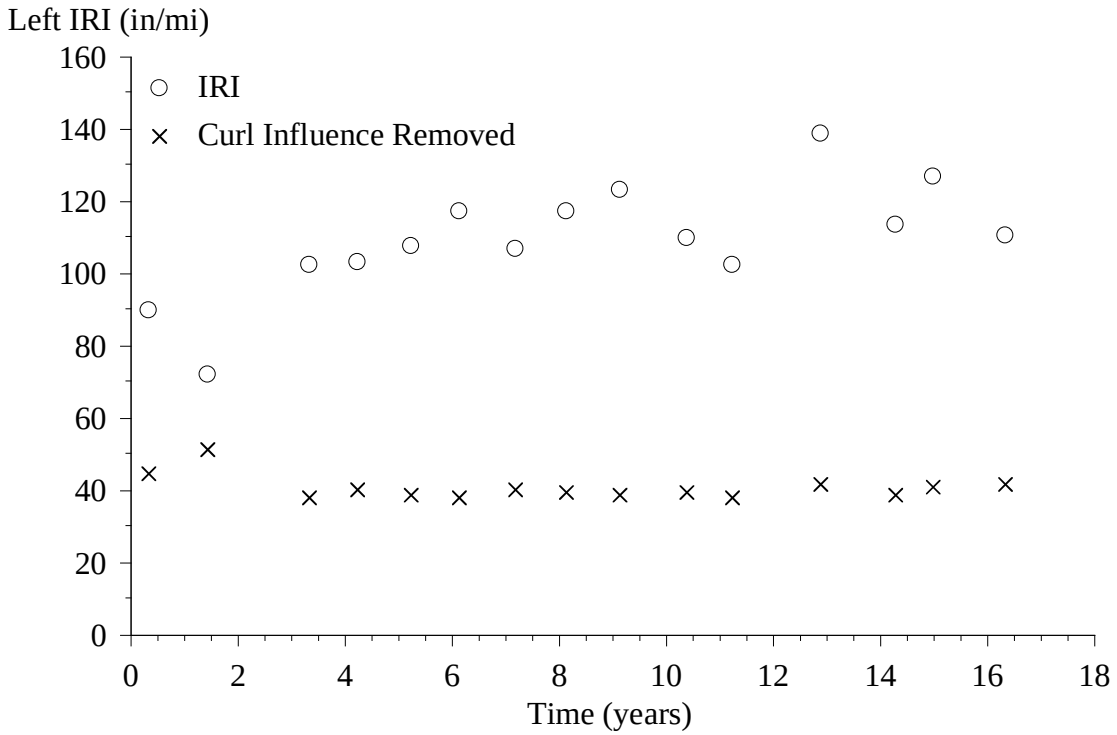

Figure 10. Graph. Left IRI Progression for Section 0213.

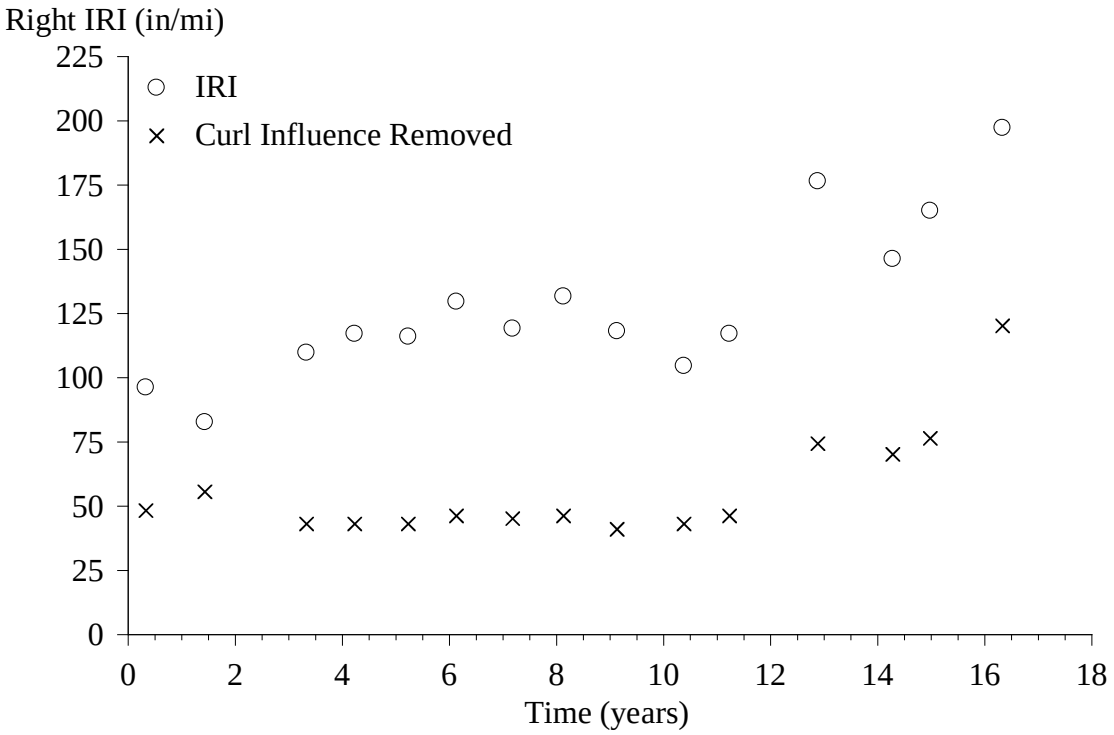

Figure 11. Graph. Right IRI Progression for Section 0213.

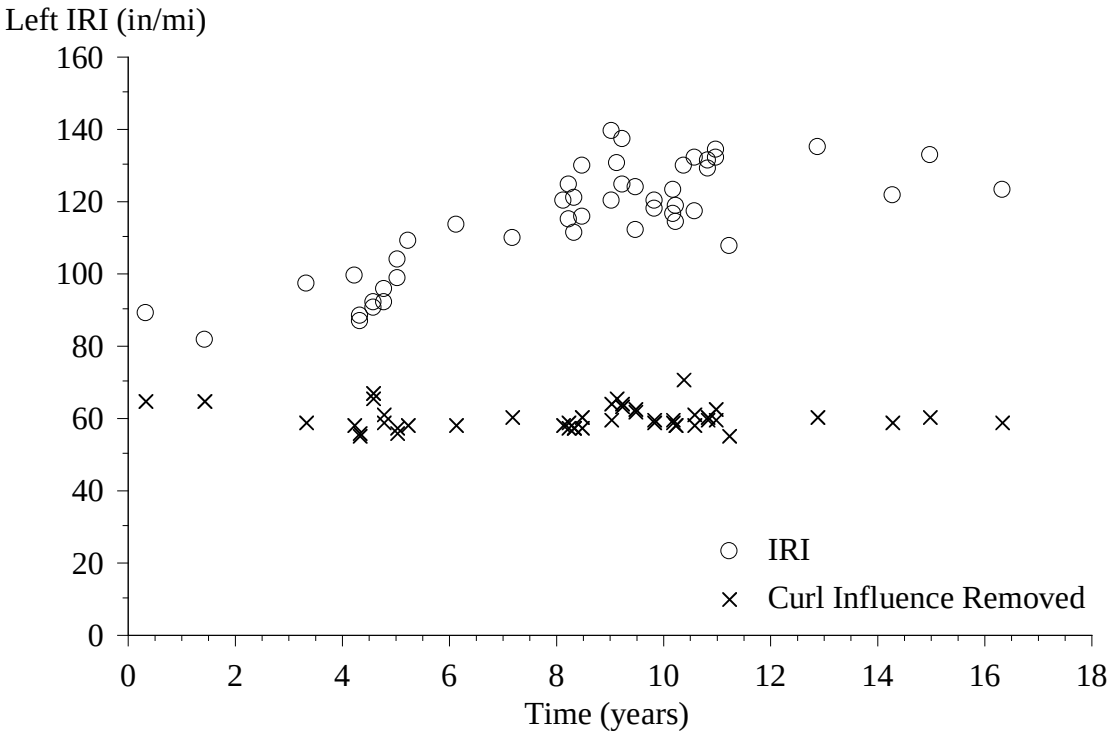

Figure 12. Graph. Left IRI Progression for Section 0215.

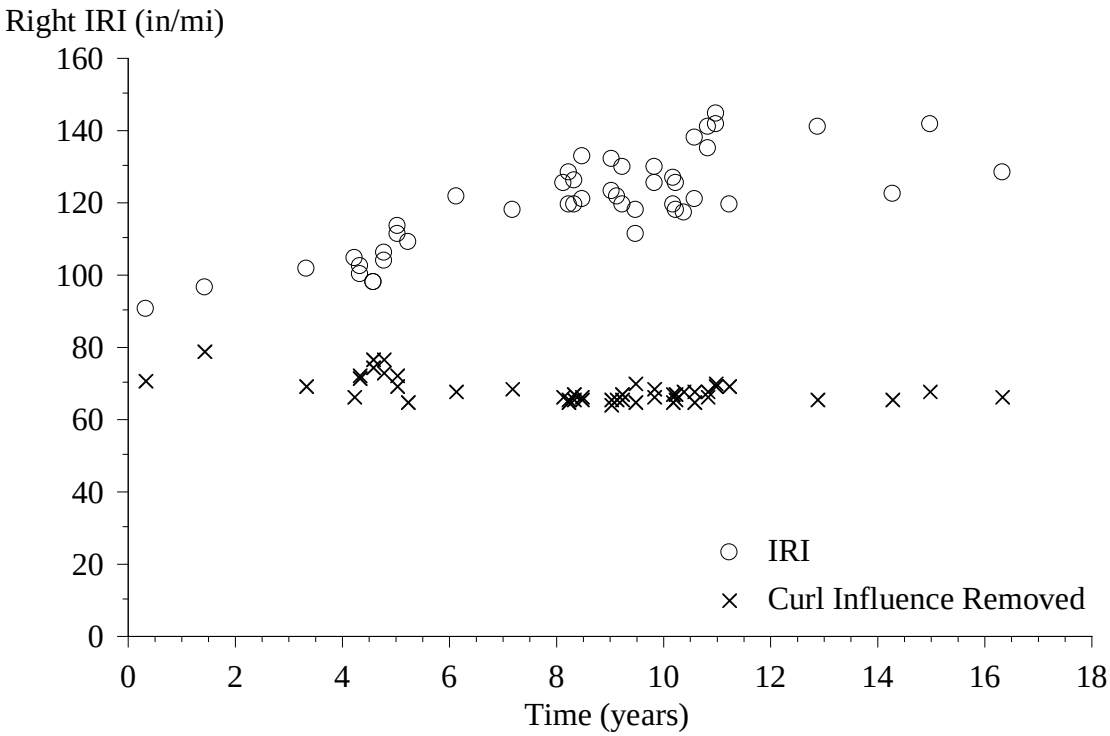

Figure 13. Graph. Right IRI Progression for Section 0215.

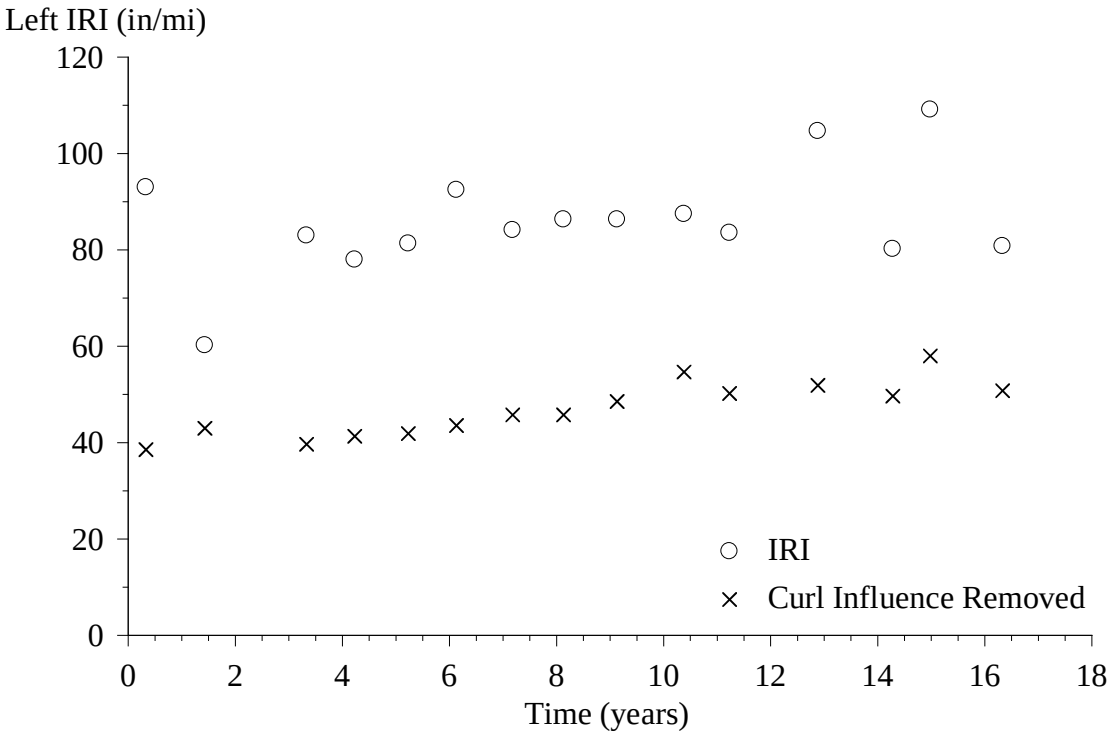

Figure 14. Graph. Left IRI Progression for Section 0217.

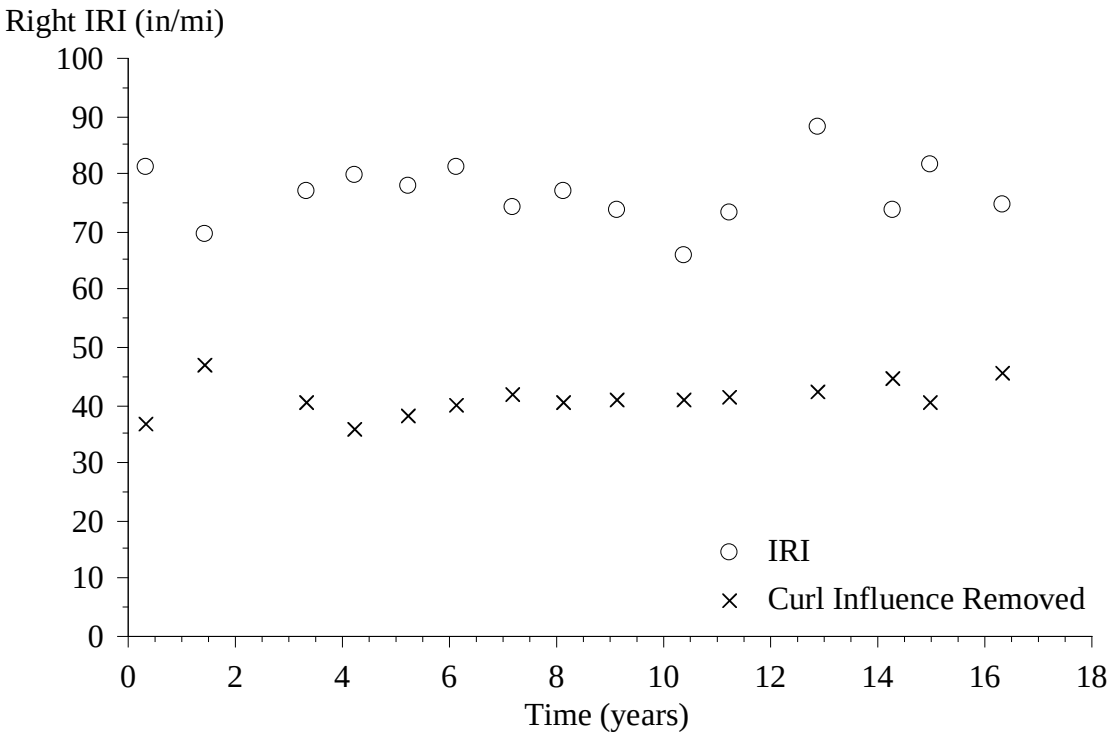

Figure 15. Graph. Right IRI Progression for Section 0217.

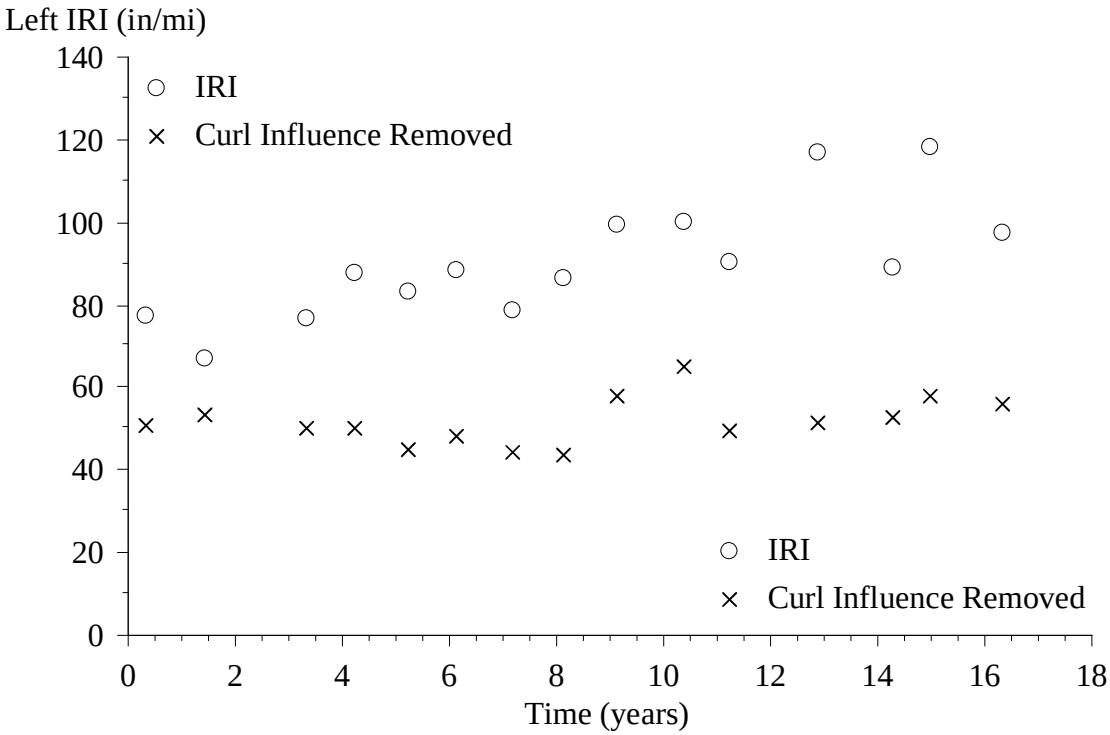

Figure 16. Graph. Left IRI Progression for Section 0219.

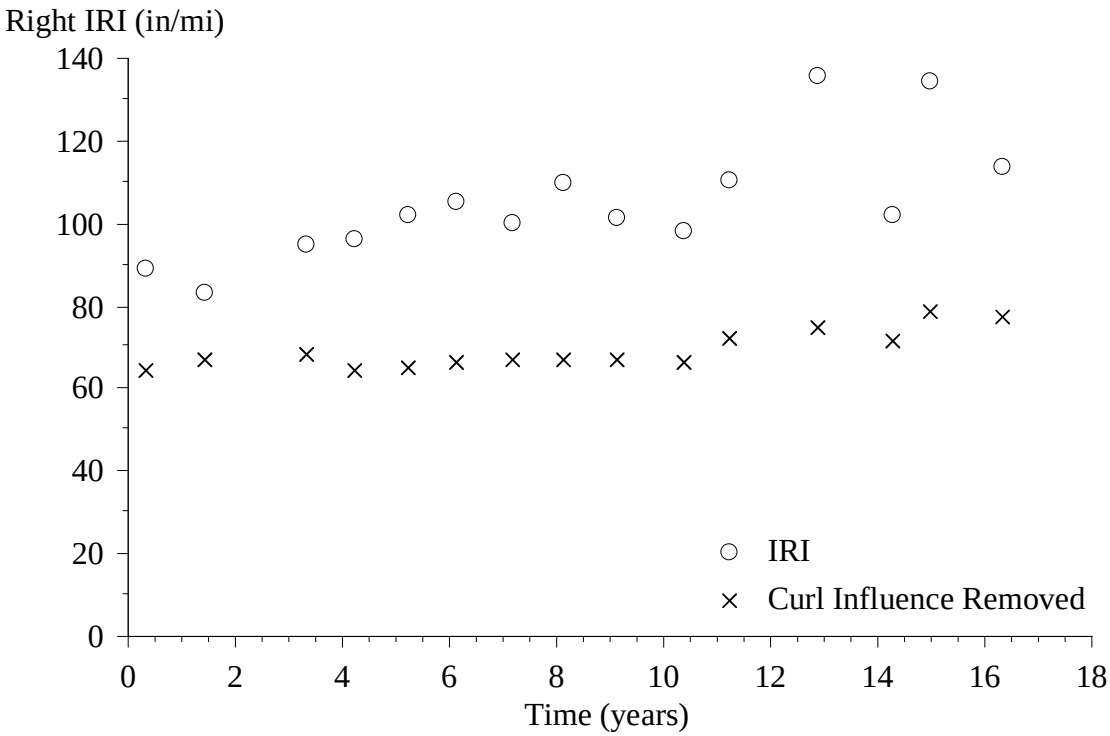

Figure 17. Graph. Right IRI Progression for Section 0219.

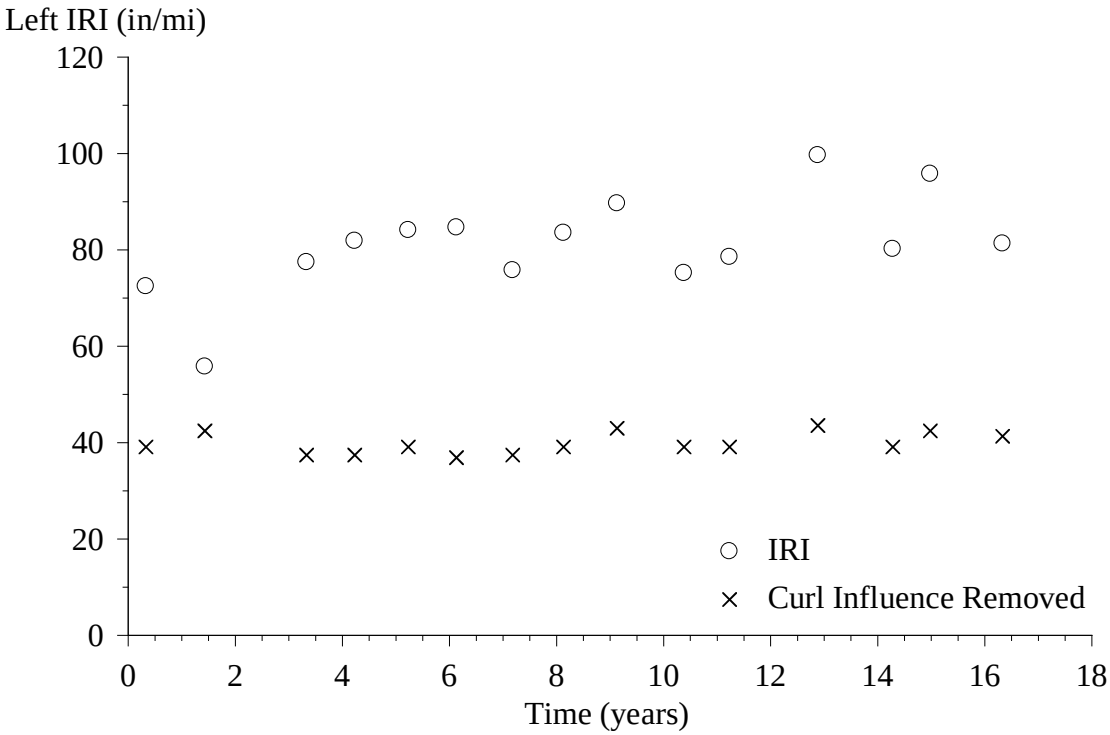

Figure 18. Graph. Left IRI Progression for Section 0221.

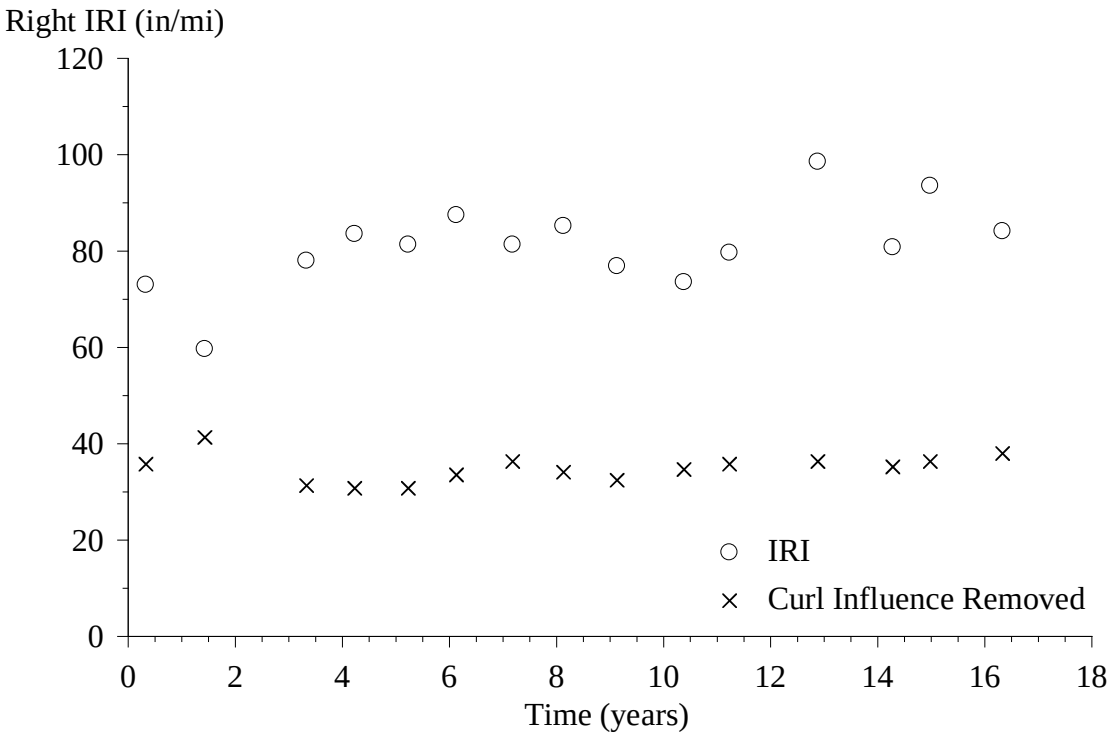

Figure 19. Graph. Right IRI Progression for Section 0221.

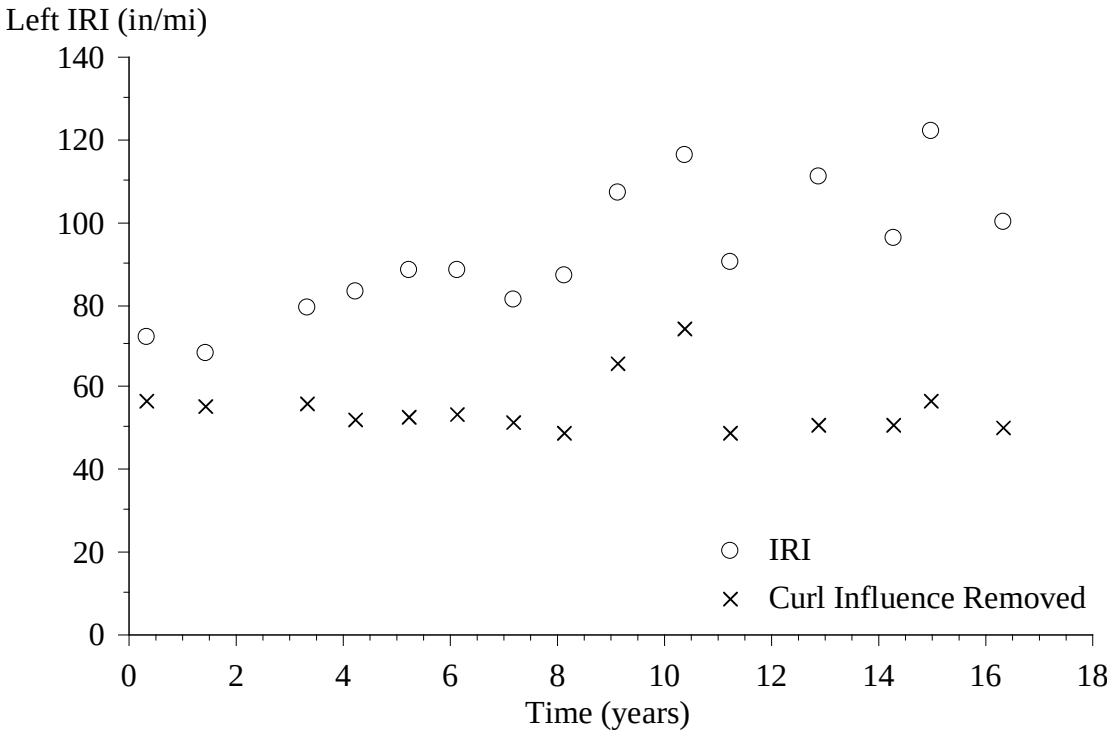

Figure 20. Graph. Left IRI Progression for Section 0223.

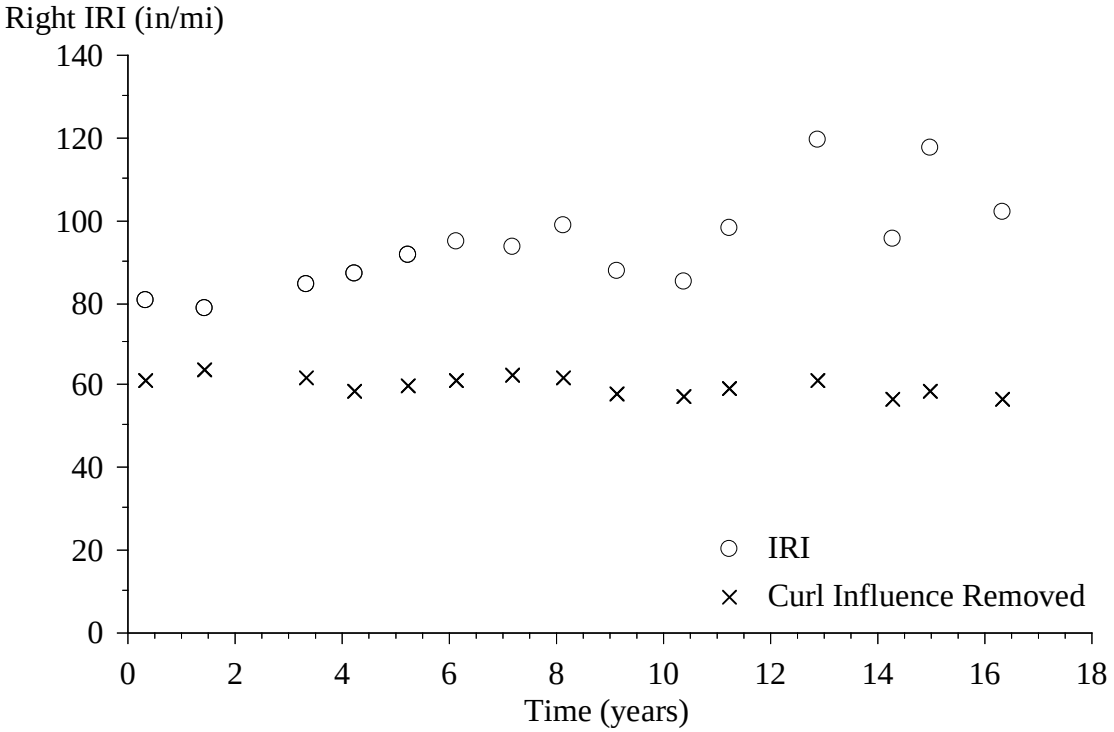

Figure 21. Graph. Right IRI Progression for Section 0223.

This analysis depends on some key assumptions. First, the idealized slab shape must be appropriate. If so, the individual curve fits for slab profiles will have high quality, like the example in appendix F. Second, empirical derivation of IRI-PSG slope requires measurements over a large range of PSG

values. Third, these analyses used the average absolute PSG value as a basis for comparison to IRI. As such, the quality of the relationship breaks down for test sections where some slabs curl upward and others curl downward. This was often the case in visit 02 (1.42 years). Lastly, the method may overestimate the influence of curl and warp on IRI if other roughness is present that appears consistently as a pattern with the same characteristic length as the joint spacing. It is important to monitor the quality of the curve fits and qualitatively look for potential features of this type.

Figure 10 and figure 11 provide sample results for section 0213. The figures show the progression in left and right IRI and the portion of the IRI that remained after removing the influence of curl and warp. On section 0213, the overall IRI values increased over time, but they were erratic. This analysis shows that, without curl and warp, the roughness on the left side was steady throughout the experiment, and the roughness on the right side was steady over the first 11 years of the experiment.

Since longitudinal cracking caused the increase in IRI on the right side after 11 years, it also contributed to the roughness in the plot after removing the influence of curl and warp (see appendix D). The right side of section 0213 provides an example of using the IRI-PSG relationship to distinguish the roughness progression caused by curl and warp from the roughness progression caused by surface distress.

Figure 12 and figure 13 provide sample results for section 0215, including the seasonal visits. As on section 0213, the raw IRI values increased erratically on section 0215, with additional scatter caused by IRI values that differed between morning and afternoon passes. For example, seasonal visits S11 and S12 (8.31 years) produced an IRI on the left side of 121.8 inches/mi at 10 a.m. and 111.6 inches/mi at 3 p.m. With the influence of curl and warp removed, these values changed to 58.0 and 57.7 inches/mi, respectively.

With the influence of curl and warp removed, the IRI values for section 0215 progressed much less erratically. Further, the overall IRI level held steady over the experiment. This suggests that a long-term increase in upward curl and warp caused net increases in raw IRI of 35 inches/mi on the left side and 39 inches/mi on the right side.

Figure 14 through figure 21 show the results for sections 0217, 0219, 0221, and 0223. These sections also exhibited erratic changes in IRI caused by curl and warp. With the influence of curl and warp removed, the IRI values were much lower and either increased slowly or held steady throughout the experiment, with two exceptions. On the left side of sections 0219 and 0223, the IRI values were much higher in visits 09 (9.08 years) and 10 (10.34 years) than in the previous and following visits, even after removing the influence of curl and warp (see figure 16 and figure 20). This is because other factors caused the increased roughness.

On both sections, spectral analysis for the left side profiles revealed additional content in the 8–11-ft wavelength range in visits 09 (9.08 years) and 10 (10.34 years) that did not appear in other visits. This phenomenon appeared prominently on sections 0214, 0216, 0218, 0219, 0223, and 0224 and to a lesser extent on sections 0215, 0217, 0220, and 0222. In many cases, this effect increased the IRI of some but not all repeat measurements. Appendix D provides an example for section 0224, where the effect was strongest. On many of these sections, the IRI progression plots (appendix C) or the standard deviation of IRI for the left side (appendix B) showed some evidence of this effect,

but the influence of curl and warp obscured it. The source of additional roughness in the 8–11-ft wavelength range is not clear, but the affected test sections all appear as a group along the site.

FAULTING ANALYSIS

Traditional profile analysis also revealed that faulting contributed heavily to the roughness of some test sections. A simple algorithm provided faulting estimates at each joint. This included an algorithm for finding the joints, as described in appendix E, and a simple calculation of the difference in elevation downstream of the joint and elevation upstream of the joint.

To exclude the narrow dips at the joint from the calculation, the faulting algorithm excluded 6 inches of profile on either side of the joint and used the average elevation over 6 inches of profile on either side of the excluded area. In visits 01 (0.32 years) and 02 (1.42 years), only one profile point appeared within this range for the approach and leave slabs. In later visits, the calculation included at least six points on either side of the joint.

All test sections except 0262 and 0265 produced average faulting values of less than 0.05 inches throughout the experiment. As described in appendix D, sections 0262 and 0265 faulted, the severity of faulting grew throughout the experiment, and the increase in IRI with time was primarily due to faulting. Figure 22 and figure 23 show the faulting estimates for the left and right profiles on these sections.

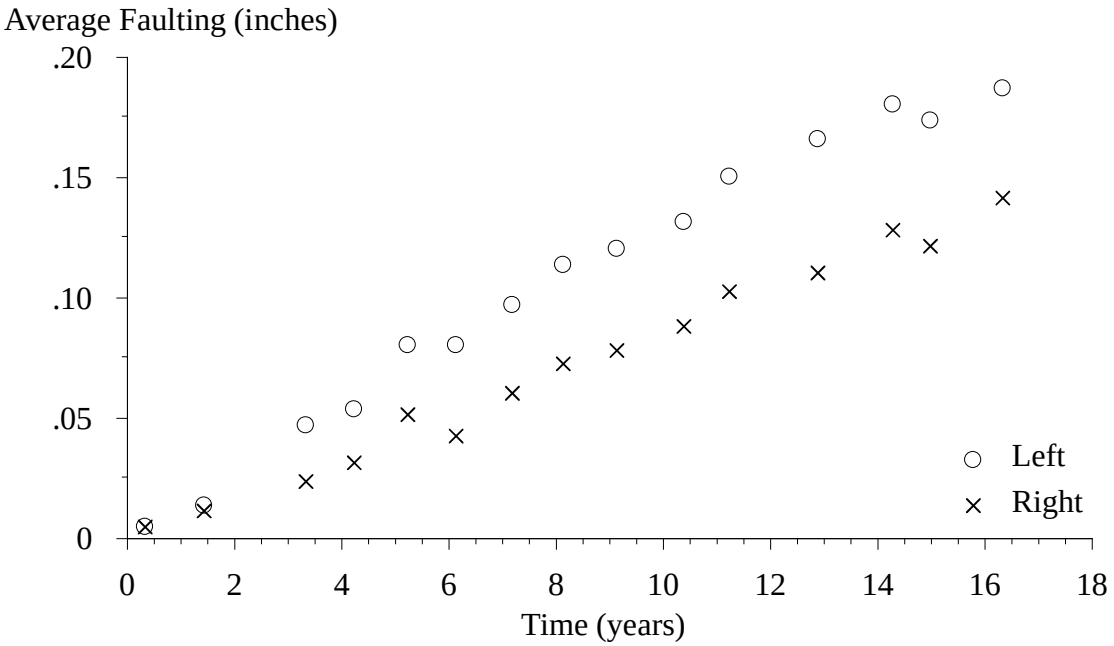

Figure 22. Graph. Faulting for Section 0262.

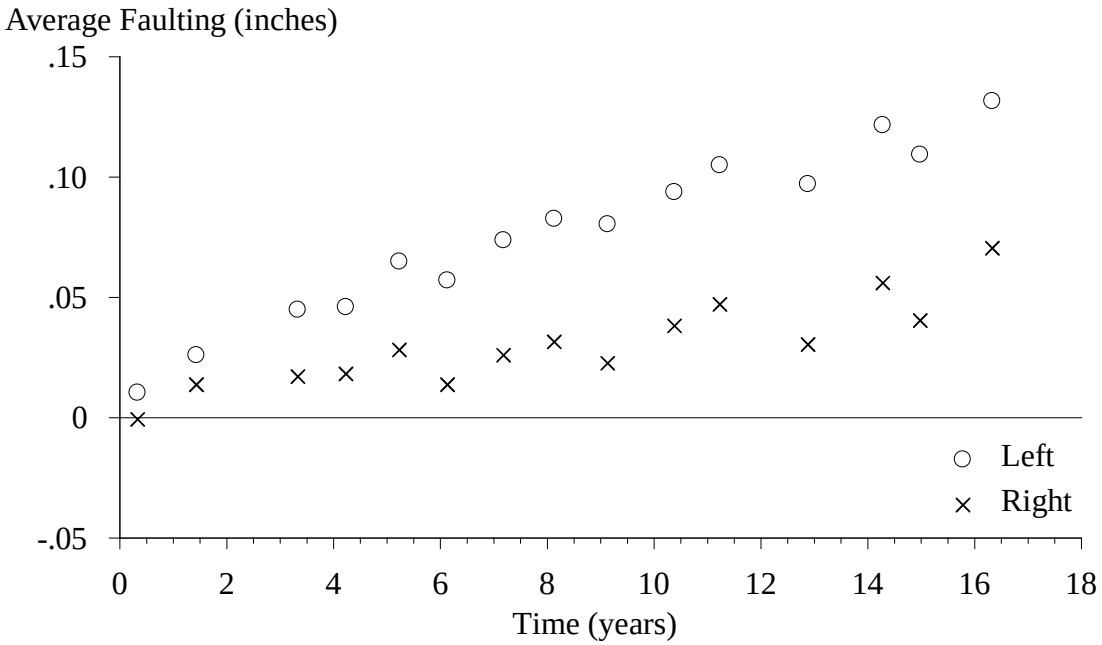

Figure 23. Graph. Faulting for Section 0265.

SUMMARY

This study examined the roughness and roughness progression of 21 test sections on the LTPP SPS-2 site in Arizona. The site included 12 test sections from the standard experiment and 9 supplemental test sections selected by ADOT. The standard test sections included a matrix of variations in surface layer thickness, surface layer strength, and base type. The supplemental sections included four test sections that were similar to their counterparts from the standard experiment but without dowel bars. The supplemental test sections also included three other jointed plain concrete pavement designs of interest to ADOT and two AC test sections.

Traditional profile analyses revealed roughness caused by transverse and longitudinal cracking on some test sections and some localized roughness caused by built-in defects. However, spectral analysis and filtered profile plots showed that curl and warp contributed to, and in some cases dominated, the roughness on many of the test sections. In addition, the progression of roughness throughout the experiment often followed a disorderly trend because of diurnal and seasonal changes in slab curl and warp. This study applied objective profile analyses to quantify the level of curl and warp on each section. These automated algorithms estimated the gross strain gradient needed to deform each slab into the shape present in the measured profile and produced a PSG value. The levels of curl and warp within each profile are summarized by the average PSG value.

For the 19 jointed concrete test sections, variations in average PSG over time and slab-by-slab PSG along the pavement explained many of the changes in IRI over time. This included diurnal variations in slab curl, which often caused the overall progression in IRI to appear disorderly throughout the experiment. PSG analysis also revealed that the level of curl and warp increased overall throughout the life of the experiment, with commensurate increases in the IRI.

LOW-STRENGTH SECTIONS, STANDARD EXPERIMENT

Table 6 summarizes the observations for the low-strength sections in the base experiment. The table lists key structural factors of each section and provides the net change in IRI values from the initial visit (0.32 years) to the final visit (16.32 years) for the left and right side. The table also lists the net change in PSG values from the initial to the final visit and the prevailing direction of curl in the final visit. For these test sections, a negative value indicates an increase in upward curl and a positive value indicates a decrease in upward curl.

Table 6. Summary Results, Low-Strength Sections.

Section	0213	0217	0221	0215	0219	0223
PCC Flexural Strength (psi)	550	550	550	550	550	550
Surface Layer Thickness (inches)	8	8	8	11	11	11
Base Type	DGAB	LCB	PATB	DGAB	LCB	PATB
Direction of Curl	Up	Up	Up	Up	Up	Up
IRI Change (inches/mi)						
Left	20	-12	9	34	20	28
Right	101	-7	11	38	24	22
PSG Change (με/inch)						
Left	-26	24	-8	-33	-10	-28
Right	-12	16	-10	-35	-6	-24
IRI Change, Curl Removed (inches/mi)						
Left	-3	12	2	-6	6	-6
Right	72	9	2	-5	12	-5

DGAB = Dense-graded aggregate base
LCB = Lean concrete base
PATB = Permeable asphalt-treated base
PCC = Portland cement concrete

Table 6 shows that a strong relationship exists between the change in PSG and the change in IRI, even though the specific relationship depends on the pavement structural properties (see table 4). For example, the highest change in PSG of the 11-inch-thick sections occurred on section 0215, which showed the highest change in IRI. Further, section 0217, where the level of curl decreased, showed a net decrease in IRI.

On the six low-strength test sections in the standard experiment, the correlation between IRI and PSG was very high. This permitted statistical analysis that isolated the portion of the overall roughness caused by curl and warp from the remainder of the roughness. With the influence of curl and warp removed, the balance of roughness often followed a more orderly trend. This allowed investigation of sources of roughness, such as distress, that were otherwise obscured by the influence of curl and warp. It also identified instances in which the roughness progressed due solely to changes in curl and warp, where the test section had not deteriorated despite the increase in overall IRI.

Table 6 also lists the change in IRI with the influence of curl removed. In this case, the balance of the roughness held steady throughout the monitoring period on sections 0215, 0217, and 0221. This was also the case on sections 0219 and 0223, with the exception of two left IRI values from years 9 and 10 that stood out as higher than the rest. Profile analysis showed that the additional roughness was isolated to the 8–11-ft wavelength range. Otherwise, the curl-removed IRI on these sections held steady at a relatively low value or increased slightly from an initially low value.

With the influence of curl and warp removed, the balance of the roughness on section 0213 held steady throughout the experiment on the left side but increased after 11 years on the right side. Patches of narrow dips caused by longitudinal cracking appeared in the left-side profiles in the second half of the monitoring period, and they caused localized roughness starting in year 12 of the experiment.

Other observations from the low-strength sections include the following:

- **Section 0213:** Section 0213 included a long bump followed by a long dip in all profiles. This feature of the profile included a 0.9-inch transition from the peak of the bump to the lowest part of the dip over 40 ft of pavement.

- **Section 0217:** Section 0217 included transverse and longitudinal cracking starting in year 3 of the experiment. The transverse cracks caused narrow dips in the profiles at some mid-slab positions that increased in severity throughout the rest of the monitoring period.

- **Section 0221:** One of the slabs within section 0221 experienced severe aggregate loss early in the experiment. The distress surveys listed scaling along the right side of the slab. This area and a few others were sealed with fiberglass by year 14. Nevertheless, the slab with the most severe aggregate loss caused localized roughness in the right-side profiles by the end of the monitoring period.

HIGH-STRENGTH SECTIONS, STANDARD EXPERIMENT

Table 7 lists summary results for the high-strength sections. As a group, the high strength sections exhibited smaller increases in roughness. As in the low-strength group, the sections with lean concrete base (LCB) either increased in roughness less than counterparts with other base types or decreased in roughness.

Table 7. Summary Results, High-Strength Sections.

Section	0214	0218	0222	0216	0220	0224
PCC Flexural Strength (psi)	900	900	900	900	900	900
Surface Layer Thickness (inches)	8	8	8	11	11	11
Base Type	DGAB	LCB	PATB	DGAB	LCB	PATB
Direction of Curl						
Initial (0.32 years)	Up	Up	Up	Up	Up	Up
Final (16.32 years)	Down	Up	Up	Down	Up	Up
IRI Change (inches/mi)						
Left	15	-14	4	3	3	20
Right	19	-15	-1	18	3	16
PSG Change (με/inch)						
Left	103	48	1	32	14	-13
Right	103	56	8	27	6	-15

DGAB = Dense-graded aggregate base
LCB = Lean concrete base
PATB = Permeable asphalt-treated base

Table 7 lists the net change in PSG for each section. On sections 0218, 0220, and 0222, a positive number indicates a reduction in upward curl. The IRI either reduced or held steady on these sections. On sections 0214 and 0216, a positive value indicates a change from upward curl at the start of the experiment to downward curl at the end. On section 0214, the transition toward downward curl was more aggressive on the first half of the section, and a group of slabs in the second half of the section maintained a reduced level of upward curl. In this case, the effect on IRI depended on the initial level of downward curl. On section 0224, upward curl increased overall.

SUPPLEMENTAL SECTIONS

Table 8 lists summary results for the supplemental sections. Sections 0262–0265 match the designs of sections 0213, 0221, 0223, and 0215, respectively, except that they are undoweled. All of the supplemental sections were curled upward (on average) in the initial visit (0.32 years) and the final visit (16.32 years), but some exhibited downward curl in the second visit (1.42 years). Sections 0262 and 0265 faulted, and the faulting progressed from virtually none to an average value of about 0.15 inches on section 0262 and 0.10 inches on section 0265.

Table 8. Summary Results, Supplemental Sections.

Section	0262	0263	0264	0265	0266	0267	0268
PCC Flexural Strength (psi)	550	550	550	550	550	550	550
Surface Layer Thickness (inches)	8	8	8.5	8.5	12.5	11	8
Base Type	DGAB	PBTB	PBTB	DGAB	DGAB	BTB	BTB
Direction of Curl	Up	Up	Up	Up	Up	Up	Up
IRI Change (inches/mi)							
Left	123	19	23	49	24	-2	9
Right	162	9	31	91	19	-14	7
PSG Change (με/inch)							
Left	-52	-13	-21	-32	-20	-8	-17
Right	-49	-18	-19	-33	-19	-6	-12

BTB = Bituminous-treated base
DGAB = Dense-graded aggregate base
PATB = Permeable asphalt-treated base
PCC = Portland cement concrete

AC SECTIONS

The IRI increased on section 0260 by 64 inches/mi on the left side and 9 inches/mi on the right side. Two areas of localized roughness on the left side of the section account for the increase in IRI. These areas included small potholes, patching, longitudinal cracks, and pools of sealant.

The IRI increased on section 0261 by 17 inches/mi on the left side and 58 inches/mi on the right side. Dips appeared at several transverse cracks starting 10 years into the experiment that exacerbated the roughness of the section in both wheel paths. In addition, a distressed area on the right side developed into a pothole. This caused localized roughness in the final profiling visit.

RECOMMENDATIONS

This report demonstrated the potential for isolating the effect of curl and warp from other sources of roughness in the study of long-term pavement performance due to the strong statistical relationship between changes in IRI and changes in PSG. This report also demonstrated that long-term increases in IRI may be caused solely by changes in curl and warp and do not necessarily indicate structural failure or increased surface distress. However, the statistical methods used in this study required a high volume of profile measurements. Refinement of the methods for more general applications with broader validity and less ambitious data requirements requires further study. The following investigations are recommended:

- Study structural models other than the original Westergaard equations that may improve the prediction of slab profiles near the joints on pavements with dowels. This may also permit the theoretical determination of the IRI-PSG slope and reduce measurement effort.

- Apply the method to other SPS-2 and General Pavement Studies (GPS)-3 sites to generalize the IRI-PSG relationship for each pavement design. This would reduce the measurement effort needed to apply the methods investigated in this study and provide the same detailed assessment of the long-term behavior of pavements at other SPS-2 and GPS-3 sites.

- Seek a refinement to the method that permits full analysis on high-strength sections and on pavement for which curl and warp is a small contributor to IRI. This may require an alternative method of estimating the dependence of IRI on PSG or the development of an alternative to PSG.

- Refine the process of obtaining the radius of relative stiffness and quantify the sensitivity of the results to the quality of the estimate.

- Investigate a version of the method that relates raw PSG, rather than average absolute PSG, to IRI.

- Relate PSG to environmental factors.

APPENDIX A. DATA EXTRACTION

This appendix describes the process of extracting profile measurements for each test section from longer measurements that cover multiple test sections. The process described ensured that repeat measurements within a given visit and sets of repeat measurements from multiple visits have consistent boundaries.

CROSS CORRELATION

Searching for the longitudinal offset between repeat profile measurements that provides the best agreement between them is a helpful way to refine the synchronization. This can be done by inspecting filtered profile plots, but it is very time consuming. Visual assessment is also somewhat subjective when two profiles do not agree well, which is often the case when measurements are made several years apart. Rather than visual inspection, an automated procedure was used for finding the longitudinal offset between measurements.

The procedure is based on a customized version of cross correlation.[10] In this procedure, a basis measurement that is considered to have the correct longitudinal positioning is designated. A candidate profile is then searched for the longitudinal offset that provides the highest cross correlation to the basis measurement. A high level of cross correlation requires a good match of profile shape, the location of isolated rough spots, and overall roughness level. Therefore, the correlation level is often only high when the two measurements are synchronized. Great care was required for the profiles in this study, because local peaks in correlation were observed every 15 ft, where joints from the two profiles aligned. However, the highest correlation level was only observed when the profiles were truly synchronized. When the optimal offset is found, a profile is extracted from the candidate measurement with the proper overall length and endpoint positions. For the rest of this discussion, this process will be referred to as *automated synchronization*.

For this application, cross correlation was performed after the IRI filter was applied to the profiles rather than using unfiltered profiles. This helped assign the proper weighting to relevant profile features. In particular, it increased the weighting of short-wavelength roughness that may appear at joints. This enhanced the effectiveness of the automated synchronization procedure. The long-wavelength content within the IRI output helped ensure the longitudinal positioning was nearly correct, and the short-wavelength content was able to leverage roughness near joints to fine-tune the positioning.

SYNCHRONIZATION

In visits 01–11, the profiler covered all test sections in each pass with a single, long run. In visits 12–15, the profiler covered portions of the site in each pass, and the site was split into either four or five groups of test sections.

Profiles of individual test sections were extracted from the raw measurements using the following steps:

1. Establish a basis measurement for each section from visit 08. This was done using the event markers from a raw measurement. The first repeat measurement was used for this purpose.

Event markers appeared at the start of every section and at the end of every section except section 0214. The locations of the event markers were compared to the layout provided in the construction report.[1] They exhibited a linear relationship with a bias of less than 0.014 percent, and no individual section starting point differed by more than 5 ft. All of the sections were assumed to begin at the appropriate event marker and continue for 500 ft.

2. Automatically synchronize the other eight repeats from visit 08 to the basis set.

3. Automatically synchronize the measurements from the previous visit to the current basis set.

4. Replace the basis set with a new set of synchronized measurements from the first repeat of the current visit.

5. Repeat steps 3 and 4 until visit 01 is complete.

Data for visits 09–15 were provided after visits 01–08 were synchronized. Visits 09–15 were synchronized using steps 3–5 but going forward in time.

LONGITUDINAL DISTANCE MEASUREMENT

When the longitudinal placement of the individual sections within each measurement were compared to the layout within the basis set, the slope of the linear fit ranged from 0.9995 to 1.0000. Thus, the longitudinal distance measurement for the nine profile measurements of visit 08 was consistent within 0.05 percent. This is a very high level of agreement in longitudinal distance measurement. Figure 24 shows the disagreement in longitudinal distance measurement for visits 01–11 using the original basis set as a reference. In visits 12–15, the site was not covered in a single, long run in each pass, so the visits were excluded from this analysis. In the figure, a range of disagreement for each visit exists because up to nine repeat profile measurements were made. The variation between repeat measurements within a visit appears as the width of each bar in the figure. Because the longitudinal distance measurement was based on the rotation of a drive wheel, the variations were most likely caused by variations in speed, lateral wander, and tire inflation pressure.[11] If tire inflation pressure were the dominant cause, the disagreement would grow more positive with each successive repeat measurement as the tire heated up. This is because the tire rolling radius would increase, and the profiler would register less wheel rotation for the same travel distance. This appeared to be the case for visits 04–10, but the effect was never greater than 0.10 percent of the overall distance.

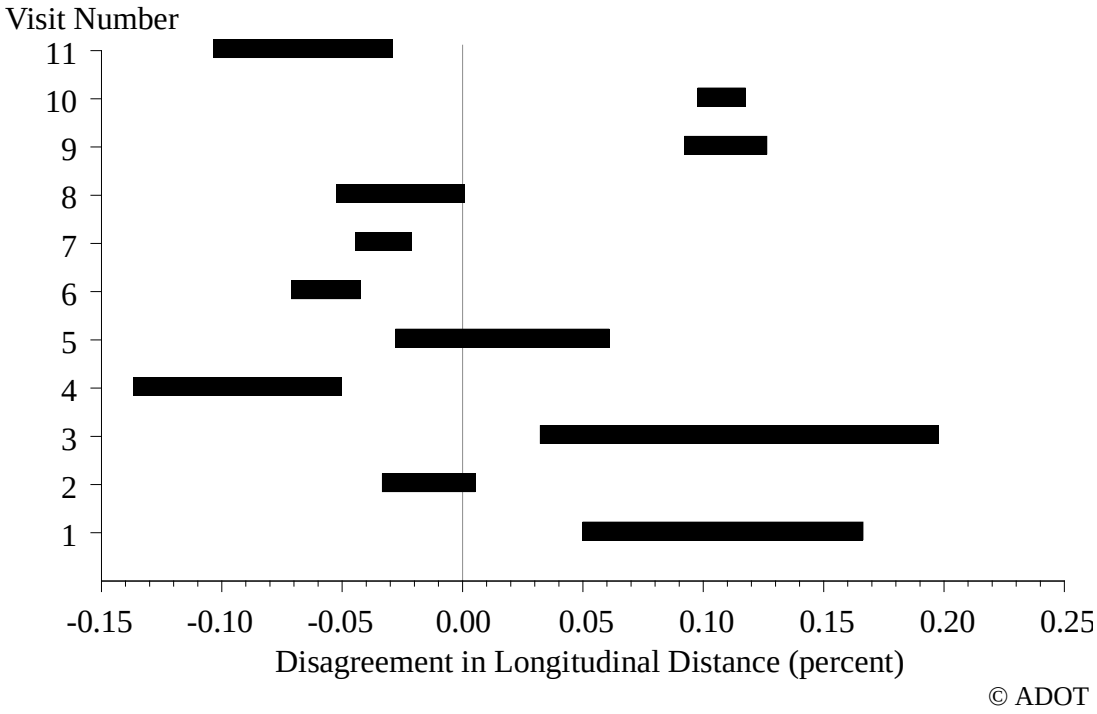

Figure 24. Graph. Consistency in Longitudinal Distance Measurement.

The variation between visits in figure 24 was caused by differences in distance measurement instrument calibration. The longitudinal distance measured by a profiler is not a true horizontal distance. It includes additional components because the profiler must travel up and down undulations in the road. This component can be minimized by calibrating the profiler to true horizontal distance. However, if a profiler operates on a road with grade changes and roughness that are not similar to the site used for longitudinal distance measurement calibration, some error will exist. For consistent results, tire inflation pressure must also be close to the level used during calibration.

Modest inconsistency in longitudinal distance measurement between visits is not critical as long as the profiles of individual sections are extracted using event markers rather than longitudinal distance from the start of each profile measurement. A high level of inconsistency, however, could interfere with comparisons between profile features and distress surveys. Errors in profile index values, such as IRI, are also roughly of the same order as errors in longitudinal distance measurement.[(11)] Figure 24 shows that longitudinal distance was measured with a very high level of agreement throughout all 11 visits.

APPENDIX B. DATA QUALITY SCREENING

A screening process was performed to select five repeat profile measurements from each visit of each section. The five measurements selected from the group of either five, seven, or nine available runs were those that exhibited the best agreement with each other. In this case, agreement between any two profile measurements was judged by cross correlating them after applying the IRI filter.[10] In this method, the IRI filter is applied to the profiles, then the output signals, rather than the overall index, are compared. High correlation by this method requires that the overall roughness is in agreement, as well as the details of the profile shape that affect IRI. The IRI filter was applied before correlation in this case for the following reasons:

- Direct correlation of unfiltered profiles places a premium on long-wavelength content but ignores much of the contribution of short-wavelength content.
- Correlation of IRI filter output emphasizes profile features in (approximate) proportion to their effect on the overall roughness.
- Correlation of IRI filter output provides a good tradeoff between emphasizing localized rough features at distressed areas in the pavement and placing too much weight on short-duration, narrow features (spikes) that are not likely to agree between measurements. This is because the IRI filter amplifies short-wavelength content but attenuates macrotexture, megatexture, and spikes.
- A relationship has been demonstrated between the cross correlation level of IRI filter output and the expected agreement in overall IRI.[10]

The method was performed with a special provision for correcting modest longitudinal distance measurement errors.

Each comparison between profiles produced a single value that summarized their level of agreement. When 9 repeat profile measurements were available, they produced a total of 36 correlation values. Any subgroup of 5 measurements could be summarized by averaging the appropriate 10 correlation values. The subgroup that produced the highest average was selected, and the other repeats were excluded from the analyses discussed in this report. Table 9 through table 29 list the selected repeats for each visit of each section and the composite correlation level produced by them.

The process used for selecting five repeat measurements from a larger group is similar to the practice within LTPP except that it uses composite agreement in profiles rather than the overall index value. The correlation levels listed in table 9 through table 29 provide a repeatability score and appraise the agreement between profile measurements for each visit of each section. When two profiles produce a correlation level above 0.82, their IRI values are expected to agree within 10 percent most (95 percent) of the time. Above this threshold, the agreement between profiles is usually acceptable for studying the influence of distresses on the profile. When two profiles produce a correlation level above 0.92, they are expected to agree within 5 percent most of the time. Above this threshold, the agreement between profiles is good. Correlation above 0.92 often depends on consistent lateral tracking of the profiler and may be very difficult to achieve on highly distressed surfaces. The IRI values in this report are the average of five observations, which tightens the tolerance even further.

Table 9. Selected Repeats for Section 0213.

Visit	Repeat Number					Composite Correlation
01	2	3	6	7	8	0.935
02	2	5	6	7	9	0.902
03	1	3	5	6	8	0.971
04	1	3	4	5	7	0.953
05	1	2	5	6	7	0.965
06	1	3	4	5	6	0.963
07	4	5	6	7	9	0.948
08	1	2	4	7	9	0.936
09	1	3	4	5	7	0.948
10	1	2	6	7	8	0.947
11	2	3	4	7	9	0.900
12	1	4	5	7	8	0.853
13	1	2	3	4	5	0.812
14	1	3	4	5	6	0.771
15	1	4	5	7	9	0.769

Table 10. Selected Repeats for Section 0214.

Visit	Repeat Numbers					Composite Correlation
01	2	3	5	6	8	0.909
02	2	4	6	7	8	0.822
03	2	3	4	5	8	0.912
04	1	3	4	5	7	0.900
05	1	3	4	5	6	0.903
06	2	3	4	6	7	0.926
07	1	2	5	6	8	0.953
08	1	2	5	6	7	0.950
09	1	3	5	6	8	0.937
10	2	3	5	6	8	0.935
11	3	5	6	7	8	0.924
12	2	3	4	7	8	0.945
13	4	5	6	8	9	0.959
14	1	3	4	7	8	0.927
15	2	4	5	6	9	0.955

Table 11. Selected Repeats for Section 0215.

Visit	Repeat Numbers					Composite Correlation
01	1	3	4	5	8	0.930
02	1	3	5	7	8	0.920
03	5	6	7	8	9	0.962
04	1	3	4	5	7	0.922
05	1	2	4	6	7	0.967
06	1	2	4	6	7	0.955
07	1	3	4	8	9	0.976
08	4	5	6	7	9	0.987
09	3	5	6	7	8	0.943
10	1	3	5	8	9	0.933
11	1	2	3	5	7	0.948
12	2	4	5	6	7	0.981
13	2	3	4	7	9	0.976
14	1	2	7	8	9	0.969
15	2	3	4	5	8	0.965
S01	2	3	4	5	7	0.936
S02	1	2	3	4	5	0.966
S03	1	2	3	4	5	0.955
S04	1	2	3	4	5	0.921
S05	1	2	3	4	5	0.937
S06	1	2	3	4	5	0.959
S07	1	2	3	4	5	0.936
S08	2	3	4	5	6	0.959
S09	1	2	3	4	7	0.977
S10	1	3	4	5	9	0.972
S11	2	3	5	6	7	0.979
S12	1	2	3	6	8	0.983
S13	1	3	4	5	7	0.979
S14	2	3	5	6	7	0.965
S15	4	5	6	7	9	0.960
S16	1	2	3	4	5	0.965
S17	1	2	3	4	6	0.976
S18	1	4	7	8	9	0.947
S19	2	3	5	6	9	0.963
S20	2	4	6	7	9	0.960
S21	1	3	4	5	6	0.972
S22	3	4	6	7	9	0.975
S23	3	4	5	8	9	0.964
S24	1	4	5	6	9	0.957
S25	1	2	4	7	9	0.975
S26	1	2	4	5	6	0.973
S27	1	2	3	8	9	0.972
S28	4	6	7	8	9	0.961
S29	1	2	3	4	8	0.973
S30	2	4	6	7	8	0.978
S31	3	4	6	7	8	0.978
S32	1	2	3	4	6	0.976

Table 12. Selected Repeats for Section 0216.

Visit	Repeat Numbers					Composite Correlation
01	3	5	6	8	9	0.922
02	3	5	7	8	9	0.892
03	1	2	3	5	7	0.927
04	1	2	4	5	6	0.930
05	1	2	3	5	6	0.951
06	2	3	4	5	6	0.948
07	2	3	4	6	9	0.968
08	2	3	4	6	8	0.957
09	1	2	4	5	8	0.930
10	1	3	4	6	7	0.937
11	2	4	5	6	9	0.910
12	1	4	6	7	8	0.949
13	2	4	7	8	9	0.954
14	2	3	6	8	9	0.938
15	1	2	3	4	8	0.948

Table 13. Selected Repeats for Section 0217.

Visit	Repeat Numbers					Composite Correlation
01	4	6	7	8	9	0.925
02	1	4	5	6	8	0.876
03	3	4	6	8	9	0.951
04	2	3	4	6	7	0.916
05	1	2	3	6	7	0.915
06	1	2	4	5	7	0.939
07	4	5	6	8	9	0.963
08	1	2	3	6	9	0.957
09	1	2	3	4	5	0.921
10	1	2	3	7	9	0.907
11	1	2	6	7	9	0.875
12	1	3	5	6	7	0.957
13	2	3	4	6	9	0.911
14	1	2	5	7	9	0.933
15	1	5	6	7	9	0.838

Table 14. Selected Repeats for Section 0218.

Visit	Repeat Numbers					Composite Correlation
01	1	2	5	7	9	0.898
02	2	4	5	8	9	0.818
03	1	3	6	7	9	0.909
04	1	3	4	5	7	0.891
05	1	2	3	4	5	0.888
06	2	3	4	6	7	0.923
07	1	2	3	6	9	0.944
08	1	3	4	7	8	0.951
09	2	3	5	6	7	0.892
10	1	2	4	7	9	0.906
11	1	2	3	6	7	0.889
12	4	5	6	7	9	0.928
13	2	3	6	8	9	0.931
14	1	3	7	8	9	0.947
15	1	3	6	7	8	0.921

Table 15. Selected Repeats for Section 0219.

Visit	Repeat Numbers					Composite Correlation
01	3	5	6	7	9	0.902
02	1	2	5	6	8	0.870
03	2	4	7	8	9	0.931
04	1	3	4	6	7	0.920
05	1	2	3	5	7	0.928
06	2	3	4	6	7	0.942
07	2	4	6	8	9	0.955
08	1	2	5	6	8	0.954
09	1	2	3	7	9	0.923
10	1	2	5	6	8	0.932
11	4	5	6	7	8	0.936
12	1	4	6	7	8	0.970
13	2	3	4	8	9	0.954
14	1	3	4	5	6	0.951
15	4	5	6	7	9	0.931

Table 16. Selected Repeats for Section 0220.

Visit	Repeat Numbers					Composite Correlation
01	5	6	7	8	9	0.910
02	3	4	5	6	9	0.871
03	1	2	6	7	8	0.917
04	1	3	4	6	7	0.898
05	2	3	4	6	7	0.950
06	1	2	5	6	7	0.950
07	1	2	5	7	9	0.935
08	2	3	4	5	6	0.958
09	1	2	3	6	8	0.915
10	2	3	4	6	7	0.929
11	1	2	5	6	9	0.938
12	3	4	6	7	8	0.936
13	2	3	6	7	9	0.932
14	2	4	5	6	7	0.944
15	1	3	6	8	9	0.936

Table 17. Selected Repeats for Section 0221.

Visit	Repeat Numbers					Composite Correlation
01	1	4	6	8	9	0.890
02	4	6	7	8	9	0.838
03	1	2	4	6	9	0.901
04	1	2	4	5	6	0.882
05	1	2	3	5	6	0.936
06	1	2	4	5	7	0.946
07	1	2	5	6	9	0.932
08	1	5	6	8	9	0.946
09	1	5	6	7	8	0.825
10	1	3	4	6	8	0.861
11	2	4	5	6	7	0.857
12	3	4	5	6	7	0.943
13	1	2	3	5	6	0.907
14	1	2	3	4	6	0.949
15	2	5	7	8	9	0.934

Table 18. Selected Repeats for Section 0222.

Visit	Repeat Numbers					Composite Correlation
01	4	5	6	8	9	0.898
02	1	4	5	6	7	0.816
03	1	3	5	6	9	0.942
04	1	3	5	6	7	0.857
05	2	3	4	6	7	0.929
06	2	3	4	5	7	0.920
07	2	4	5	6	8	0.943
08	2	4	5	7	8	0.948
09	1	2	4	6	7	0.900
10	1	2	3	5	6	0.880
11	2	3	4	6	8	0.853
12	2	3	6	7	8	0.935
13	2	3	5	6	9	0.931
14	2	3	4	6	7	0.914
15	2	6	7	8	9	0.910

Table 19. Selected Repeat for Section 0223.

Visit	Repeat Numbers					Composite Correlation
01	1	2	6	7	9	0.892
02	1	3	4	8	9	0.893
03	4	5	6	7	9	0.934
04	3	4	5	6	7	0.948
05	1	2	3	6	7	0.943
06	1	2	3	4	6	0.953
07	1	2	3	6	8	0.956
08	3	4	5	6	9	0.960
09	3	6	7	8	9	0.949
10	1	2	3	5	8	0.914
11	5	6	7	8	9	0.946
12	2	4	5	6	9	0.972
13	2	3	4	8	9	0.956
14	3	5	6	8	9	0.965
15	3	4	6	8	9	0.951

Table 20. Selected Repeats for Section 0224.

Visit	Repeat Numbers					Composite Correlation
01	3	4	6	8	9	0.894
02	4	5	6	8	9	0.837
03	2	3	4	6	7	0.907
04	1	2	3	4	5	0.863
05	1	2	3	6	7	0.873
06	2	3	5	6	7	0.921
07	2	3	5	6	7	0.940
08	2	4	6	7	8	0.932
09	1	2	4	5	8	0.917
10	2	4	6	8	9	0.960
11	1	2	4	7	9	0.873
12	1	2	6	7	8	0.939
13	5	6	7	8	9	0.950
14	3	6	7	8	9	0.905
15	1	2	3	5	9	0.918

Table 21. Selected Repeats for Section 0260.

Visit	Repeat Numbers					Composite Correlation
01	1	2	3	4	7	0.939
02	3	5	6	8	9	0.899
03	1	2	5	6	8	0.932
04	3	4	5	6	7	0.885
05	1	2	4	5	7	0.921
06	2	4	5	6	7	0.920
07	1	3	4	6	9	0.952
08	2	3	6	7	9	0.962
09	1	3	4	6	8	0.921
10	1	2	5	7	8	0.897
11	1	2	5	6	7	0.837
12	1	3	4	6	8	0.889
13	1	3	5	6	8	0.799
14	1	2	3	4	6	0.882
15	1	3	4	5	6	0.866

Table 22. Selected Repeats for Section 0261.

Visit	Repeat Numbers					Composite Correlation
01	3	5	6	8	9	0.916
02	2	4	6	7	9	0.872
03	5	6	7	8	9	0.910
04	1	3	5	6	7	0.857
05	3	4	5	6	7	0.926
06	1	2	4	5	7	0.896
07	3	4	5	6	7	0.937
08	1	3	4	5	7	0.940
09	1	2	3	4	9	0.866
10	1	2	5	6	7	0.860
11	1	4	5	6	7	0.766
12	4	5	6	8	9	0.882
13	2	3	4	7	8	0.893
14	1	2	3	6	7	0.877
15	1	2	3	5	9	0.922

Table 23. Selected Repeats for Section 0262.

Visit	Repeat Numbers					Composite Correlation
01	4	5	6	8	9	0.867
02	1	4	5	7	9	0.859
03	2	3	5	6	7	0.965
04	2	3	4	5	7	0.969
05	1	2	3	4	5	0.981
06	2	3	4	5	6	0.980
07	2	5	6	8	9	0.981
08	2	3	5	6	7	0.986
09	1	2	3	4	6	0.976
10	2	3	4	6	7	0.975
11	2	3	4	6	7	0.978
12	1	4	5	8	9	0.982
13	2	3	5	7	9	0.949
14	1	4	7	8	9	0.959
15	1	2	5	8	9	0.974

Table 24. Selected Repeats for Section 0263.

Visit	Repeat Numbers					Composite Correlation
01	3	6	7	8	9	0.839
02	1	6	7	8	9	0.813
03	1	2	3	5	9	0.940
04	1	2	3	4	5	0.936
05	2	3	4	5	7	0.939
06	1	2	3	4	6	0.942
07	1	3	5	7	9	0.947
08	2	3	5	7	9	0.944
09	2	5	6	7	8	0.884
10	1	2	4	5	9	0.932
11	1	2	4	5	7	0.855
12	2	3	4	6	7	0.949
13	2	4	5	6	8	0.941
14	2	3	5	7	8	0.939
15	2	3	4	5	6	0.899

Table 25. Selected Repeats for Section 0264.

Visit	Repeat Numbers					Composite Correlation
01	2	3	4	5	8	0.906
02	1	5	6	7	8	0.931
03	1	2	4	6	8	0.938
04	2	3	4	5	6	0.940
05	2	3	5	6	7	0.964
06	1	2	3	6	7	0.951
07	1	2	5	6	8	0.962
08	1	4	5	6	7	0.969
09	1	3	4	7	8	0.904
10	3	4	5	7	8	0.894
11	1	2	4	5	6	0.911
12	1	3	6	8	9	0.968
13	2	4	6	8	9	0.946
14	1	2	4	6	7	0.962
15	1	2	3	4	5	0.937

Table 26. Selected Repeats for Section 0265.

Visit	Repeat Numbers					Composite Correlation
01	1	2	4	5	8	0.915
02	4	5	6	7	9	0.879
03	1	3	4	6	7	0.958
04	3	4	5	6	7	0.927
05	1	4	5	6	7	0.950
06	1	2	4	6	7	0.937
07	2	4	6	7	8	0.976
08	2	3	4	5	6	0.965
09	2	3	4	5	7	0.923
10	3	6	7	8	9	0.935
11	2	4	5	6	7	0.916
12	2	3	7	8	9	0.974
13	3	4	6	8	9	0.966
14	1	2	4	6	7	0.962
15	1	2	3	6	7	0.977

Table 27. Selected Repeats for Section 0266.

Visit	Repeat Numbers					Composite Correlation
01	1	4	6	7	9	0.886
02	1	2	3	5	6	0.885
03	1	2	7	8	9	0.941
04	1	2	3	4	6	0.901
05	1	2	3	4	6	0.972
06	1	2	3	5	6	0.943
07	1	4	6	7	8	0.958
08	2	3	4	5	6	0.963
09	3	4	7	8	9	0.902
10	1	3	5	7	8	0.949
11	1	4	5	7	9	0.934
12	1	2	5	6	9	0.947
13	1	2	4	5	8	0.960
14	1	3	4	5	8	0.950
15	1	3	4	5	6	0.937

Table 28. Selected Repeats for Section 0267.

Visit	Repeat Numbers					Composite Correlation
01	1	3	6	7	9	0.888
02	4	5	6	7	8	0.878
03	4	5	6	8	9	0.919
04	1	2	3	4	6	0.872
05	1	2	4	5	6	0.921
06	2	3	4	5	7	0.949
07	1	2	3	7	9	0.955
08	1	4	6	7	9	0.960
09	2	3	5	6	8	0.874
10	2	3	5	7	9	0.930
11	1	2	5	6	7	0.926
12	1	2	4	6	9	0.869
13	1	4	6	7	8	0.878
14	1	2	4	5	6	0.907
15	1	2	3	4	6	0.909

Table 29. Selected Repeats for Section 0268.

Visit	Repeat Numbers					Composite Correlation
01	1	2	5	6	9	0.851
02	1	3	5	6	8	0.813
03	4	5	7	8	9	0.919
04	1	2	4	6	7	0.863
05	1	2	4	5	6	0.904
06	2	3	5	6	7	0.956
07	1	3	4	8	9	0.932
08	2	3	6	7	9	0.947
09	1	2	3	5	6	0.831
10	1	5	6	8	9	0.924
11	3	4	6	7	9	0.875
12	2	3	6	7	8	0.939
13	3	4	5	7	9	0.931
14	1	2	5	6	9	0.883
15	2	3	4	6	9	0.873

Only 9 of the 347 sets of selected repeat measurements listed in table 9 through table 29 exhibited a composite correlation below 0.82. Measurements of sections 0215 and 0262 produced the highest repeatability scores, whereas some profiles from visit 02 and from later visits of section 0213 produced the lowest scores. Fortunately, correlation was never low enough to impede the automated synchronization process. However, low repeatability scores prompted inspection of profile plots to help identify the cause. In visit 02, most of the profiles included short-wavelength content that was not correlated between repeat measurements. The effect was greatest in sections 0214, 0218, 0222, 0263, and 0268. It is suspected that the effect was caused by coarse surface texture, but that cannot be verified.

Other observations were as follows:

- **Section 0213, visits 13–15:** The right profiles of these visits included deep, narrow dips or patches of narrow dips that appeared in some areas in each profile with inconsistent size and placement.

- **Section 0260, later visits:** Agreement between profiles was diminished by patches of uncorrelated deep, narrow dips in the left profiles from 50 to 65 ft from the start of the section and from 330 to 360 ft from the start of the section. This is an AC section.

- **Section 0261, visit 11:** Localized roughness appeared on the right side from 474 to 479 ft from the start of the section in four of the five profiles and with inconsistent shape and placement on the left side from 355 to 375 ft from the start of the section. Visits 09 and 10 also included inconsistent measurement of these features. This is an AC section.

- **Sections 0267 and 0268, visit 09:** The short-wavelength content from the visit did not agree well, and the profiles included some extraneous narrow dips.

APPENDIX C. ROUGHNESS VALUES

This appendix lists left IRI, right IRI, Mean Roughness Index (MRI), HRI, and RN values for each visit of each section. The roughness values are the average for five repeat runs. The five runs were selected from a group of as many as nine by automated comparison of profiles, as described in appendix B. Values of standard deviation are also provided for left and right IRI to reveal cases of high variability among the five measurements. However, the screening procedure used to select the five repeats usually helped reduce the level of scatter.

The discussion of roughness in the main report emphasizes the left and right IRI. Nevertheless, the other indexes provide useful additional information. MRI is the average of the left and right IRI values. HRI is calculated by converting the IRI filter into a half-car model.[(12)] This is done by collapsing the left and right profile into a single profile in which each point is the average of the corresponding left and right elevation. The IRI filter is then applied to the resulting signal. HRI is similar to IRI except that side-to-side deviations in the profile are eliminated. The result is that the HRI value for a pair of profiles will always be lower than the corresponding MRI value. Comparing HRI and MRI values provides a crude indication of the significance of roll (i.e., side-by-side variation in profile) to the overall roughness. When HRI is low compared to MRI, roll is significant. This is common among asphalt pavements.[(13)] Certain types of pavement distress, such as longitudinal cracking, may also cause significant differences between HRI and MRI.

Figure 25 compares HRI to MRI for the profile measurements on PCC sections. This includes 1,585 pairs of roughness values and excludes AC sections 0260 and 0261. The figure shows a best-fit line with a zero intercept and a line of equality. The slope of the line is 0.914. A typical range for concrete pavement is 0.90–0.95. A better linear fit was found without forcing a zero intercept. A simple linear fit produced a slope of about 0.979 and an intercept of about -6.9 inches/mi.

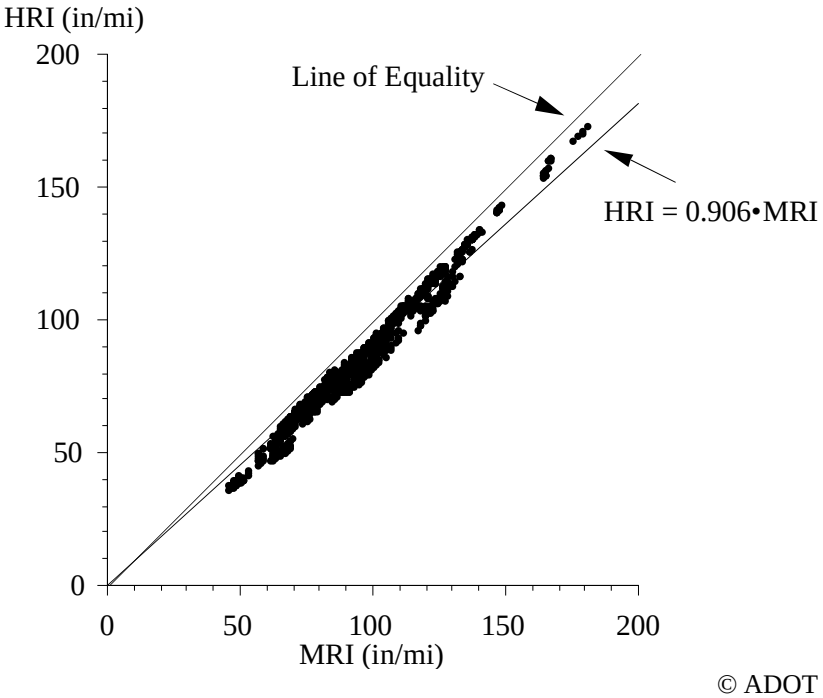

Figure 25. Graph. Comparison of HRI to MRI.

RN has shown a closer relationship to road-user opinions than other indexes.[14] As such, it may help distinguish the segments from each other by ride quality. Further, the effect on RN may help quantify the impact of distress on ride when the roughness of a section is dominated by a particular type of distress. In particular, a very low RN value coupled with moderate IRI values indicates a high level of short-wavelength roughness and potential sensitivity to narrow dips and measurement errors caused by coarse surface texture.

Table 30 provides the roughness values. The table also lists the date of each measurement and the time in years since the site was opened to traffic. Figure 26 through figure 46 show left and right IRI versus time in years for all 21 test sections. As before, *years* is defined as the number of years between the measurement date and the date the site was opened to traffic (1-Oct-1993).

Table 30. Roughness Values.

Section	Date	Years	Left IRI (inches/mi)		Right IRI (inches/mi)		MRI (inches/mi)	HRI (inches/mi)	RN
			Average	SD	Average	SD			
0213	25-Jan-94	0.32	91	1.7	97	1.5	94	86	3.63
	5-Mar-95	1.42	72	1.0	83	1.7	78	69	3.75
	27-Jan-97	3.32	103	0.9	110	1.1	107	101	3.53
	4-Dec-97	4.18	104	2.6	117	2.0	111	105	3.50
	8-Dec-98	5.19	108	1.1	117	1.5	112	107	3.46
	15-Nov-99	6.12	118	0.7	131	1.0	124	118	3.33
	30-Nov-00	7.16	107	1.1	119	1.4	113	106	3.42
	8-Nov-01	8.10	118	1.2	133	1.5	125	119	3.29
	30-Oct-02	9.08	124	0.6	119	2.4	122	116	3.36
	4-Feb-04	10.34	110	1.4	105	3.3	108	101	3.48
	12-Dec-04	11.20	103	1.2	117	3.2	110	103	3.32
	11-Aug-06	12.86	139	1.0	177	5.5	158	149	2.39
	30-Dec-07	14.25	114	0.8	147	6.9	131	121	2.56
	20-Sep-08	14.97	127	1.0	166	6.8	147	136	2.56
	25-Jan-10	16.32	111	1.3	198	3.5	155	140	2.00
0214	25-Jan-94	0.32	85	1.9	80	1.9	83	80	3.65
	5-Mar-95	1.42	55	0.5	59	1.7	57	50	3.78
	27-Jan-97	3.32	76	3.2	64	2.6	70	65	3.80
	4-Dec-97	4.18	70	2.6	69	1.9	70	65	3.79
	8-Dec-98	5.19	67	3.3	68	0.9	68	62	3.80
	15-Nov-99	6.12	85	2.0	71	1.8	78	71	3.70
	30-Nov-00	7.16	81	0.8	71	1.2	76	70	3.68
	8-Nov-01	8.10	79	2.5	79	0.5	79	73	3.62
	30-Oct-02	9.08	94	3.4	78	1.0	86	78	3.47
	4-Feb-04	10.34	101	3.1	87	1.4	94	85	3.38
	12-Dec-04	11.20	80	2.9	83	1.0	81	75	3.46
	13-Aug-06	12.87	81	1.9	83	0.8	82	75	3.44
	30-Dec-07	14.25	102	1.3	93	1.8	97	90	3.31
	20-Sep-08	14.97	96	3.0	85	1.7	91	84	3.39
	25-Jan-10	16.32	100	2.0	99	0.9	100	94	3.27

Table 30. Roughness Values—Continued.

Section	Date	Years	Left IRI (inches/mi)		Right IRI (inches/mi)		MRI (inches/ mi)	HRI (inches/ mi)	RN
			Average	SD	Average	SD			
0215	25-Jan-94	0.32	89	0.8	91	1.4	90	80	3.66
	5-Mar-95	1.42	82	0.9	97	3.2	89	80	3.61
	27-Jan-97	3.32	98	0.7	102	1.4	100	91	3.60
	4-Dec-97	4.18	100	3.6	105	2.2	103	94	3.52
	15-Jan-98	4.29	89	0.8	101	2.3	95	86	3.61
	15-Jan-98	4.29	87	0.7	103	0.9	95	87	3.61
	13-Apr-98	4.53	92	0.9	99	1.7	96	86	3.60
	13-Apr-98	4.53	91	1.2	98	1.6	95	85	3.60
	9-Jul-98	4.77	96	1.7	107	2.3	101	91	3.54
	9-Jul-98	4.77	93	0.7	105	1.9	99	88	3.54
	30-Sep-98	5.00	105	1.1	114	2.3	109	100	3.47
	30-Sep-98	5.00	99	2.3	112	1.6	105	96	3.48
	8-Dec-98	5.19	109	1.2	110	2.1	109	101	3.46
	15-Nov-99	6.12	114	1.9	123	1.5	118	110	3.41
	30-Nov-00	7.16	111	0.5	119	1.4	115	106	3.44
	8-Nov-01	8.10	121	0.5	126	0.7	124	116	3.34
	9-Dec-01	8.19	125	0.3	129	0.6	127	120	3.32
	9-Dec-01	8.19	116	0.9	120	0.6	118	111	3.42
	24-Jan-02	8.31	122	1.2	127	0.9	124	117	3.34
	24-Jan-02	8.31	112	0.3	120	1.1	116	108	3.43
	15-Mar-02	8.45	130	1.2	133	1.3	132	125	3.27
	15-Mar-02	8.45	117	0.7	122	2.8	119	112	3.40
	9-Oct-02	9.02	140	1.3	132	3.0	136	130	3.24
	9-Oct-02	9.02	121	1.4	123	1.4	122	116	3.35
	30-Oct-02	9.08	131	6.1	122	1.1	127	119	3.33
	20-Dec-02	9.22	137	0.8	131	1.3	134	128	3.25
	20-Dec-02	9.22	125	4.4	120	1.6	123	115	3.37
	7-Mar-03	9.43	124	1.5	119	2.1	122	115	3.35
	7-Mar-03	9.43	112	0.7	112	2.0	112	105	3.45
	25-Jul-03	9.81	121	0.3	130	1.2	126	119	3.32
	25-Jul-03	9.81	119	1.0	126	1.0	122	115	3.33
	24-Nov-03	10.15	124	1.7	127	0.9	125	119	3.29
	24-Nov-03	10.15	117	1.2	120	2.2	118	112	3.39
	14-Dec-03	10.20	119	0.8	126	1.0	122	115	3.32
	14-Dec-03	10.20	115	1.4	119	0.6	117	110	3.39
	4-Feb-04	10.34	130	3.3	118	2.4	124	116	3.35
	22-Apr-04	10.56	133	0.4	139	2.1	136	129	3.22
	22-Apr-04	10.56	118	1.1	121	1.6	120	113	3.36
	15-Jul-04	10.79	132	1.3	142	1.7	137	131	3.21
	15-Jul-04	10.79	129	0.3	135	0.9	132	126	3.24
	9-Sep-04	10.94	135	0.1	145	0.7	140	134	3.18
	9-Sep-04	10.94	132	0.7	142	1.6	137	131	3.19

Table 30. Roughness Values—Continued.

Section	Date	Years	Left IRI (inches/mi)		Right IRI (inches/mi)		MRI (inches/ mi)	HRI (inches/ mi)	RN
			Average	SD	Average	SD			
0215	12-Dec-04	11.20	108	1.9	120	1.3	114	107	3.39
	13-Aug-06	12.87	135	0.6	141	0.9	138	133	3.18
	30-Dec-07	14.25	122	0.5	123	1.0	123	116	3.32
	20-Sep-08	14.97	134	0.9	142	1.6	138	132	3.18
	25-Jan-10	16.32	124	1.5	129	1.0	126	119	3.28
0216	25-Jan-94	0.32	90	2.4	87	2.3	89	81	3.57
	5-Mar-95	1.42	83	1.5	89	1.8	86	75	3.54
	27-Jan-97	3.32	87	3.7	84	0.8	86	76	3.65
	4-Dec-97	4.18	86	0.7	85	2.5	85	76	3.61
	8-Dec-98	5.19	88	0.9	87	1.8	88	78	3.59
	15-Nov-99	6.12	93	2.7	86	0.6	89	79	3.63
	30-Nov-00	7.16	85	1.3	88	0.7	87	78	3.65
	8-Nov-01	8.10	85	1.2	91	1.3	88	78	3.62
	30-Oct-02	9.08	98	3.9	92	1.3	95	80	3.52
	4-Feb-04	10.34	99	3.2	99	1.6	99	84	3.47
	12-Dec-04	11.20	88	1.6	99	2.7	94	85	3.50
	13-Aug-06	12.87	88	1.4	99	1.5	94	85	3.49
	30-Dec-07	14.25	98	1.6	101	1.5	99	88	3.44
	20-Sep-08	14.97	100	2.8	97	0.4	99	85	3.47
	25-Jan-10	16.32	93	1.0	105	1.8	99	90	3.42
0217	25-Jan-94	0.32	93	0.5	82	1.1	87	79	3.59
	5-Mar-95	1.42	61	1.5	70	2.1	65	56	3.81
	27-Jan-97	3.32	83	0.7	78	1.3	80	71	3.76
	4-Dec-97	4.18	79	3.7	80	2.6	79	72	3.78
	8-Dec-98	5.19	82	3.2	78	2.8	80	72	3.76
	15-Nov-99	6.12	93	2.2	81	0.9	87	77	3.73
	30-Nov-00	7.16	85	1.6	75	0.6	80	70	3.81
	8-Nov-01	8.10	87	2.2	77	1.7	82	74	3.78
	30-Oct-02	9.08	87	1.5	74	0.8	80	70	3.73
	4-Feb-04	10.34	88	3.3	66	1.4	77	65	3.79
	12-Dec-04	11.20	84	4.3	74	2.0	79	69	3.75
	11-Aug-06	12.86	105	1.7	89	2.1	97	89	3.62
	30-Dec-07	14.25	80	2.5	74	1.6	77	66	3.60
	20-Sep-08	14.97	110	3.5	82	1.9	96	86	3.61
	25-Jan-10	16.32	81	1.6	75	3.0	78	68	3.26

Table 30. Roughness Values—Continued.

Section	Date	Years	Left IRI (inches/mi)		Right IRI (inches/mi)		MRI (inches/ mi)	HRI (inches/ mi)	RN
			Average	SD	Average	SD			
0218	25-Jan-94	0.32	92	3.7	85	1.9	88	83	3.54
	5-Mar-95	1.42	65	1.3	59	1.6	62	53	3.74
	27-Jan-97	3.32	74	1.5	56	0.4	65	58	3.81
	4-Dec-97	4.18	73	1.4	61	2.0	67	60	3.77
	8-Dec-98	5.19	74	0.9	60	1.2	67	60	3.77
	15-Nov-99	6.12	79	1.9	65	0.7	72	65	3.77
	30-Nov-00	7.16	72	1.1	60	0.7	66	58	3.82
	8-Nov-01	8.10	71	1.0	62	0.6	67	59	3.82
	30-Oct-02	9.08	85	4.7	56	0.9	70	63	3.75
	4-Feb-04	10.34	82	3.2	56	1.3	69	61	3.76
	12-Dec-04	11.20	72	1.4	64	2.1	68	59	3.76
	13-Aug-06	12.87	77	1.1	71	0.8	74	66	3.70
	30-Dec-07	14.25	83	2.5	68	1.7	76	67	3.70
	20-Sep-08	14.97	80	1.2	76	0.8	78	69	3.66
	25-Jan-10	16.32	78	1.4	70	1.3	74	65	3.68
0219	25-Jan-94	0.32	78	1.5	90	2.1	84	75	3.60
	5-Mar-95	1.42	67	1.1	84	1.4	76	66	3.63
	27-Jan-97	3.32	77	1.6	95	1.3	86	78	3.68
	4-Dec-97	4.18	88	3.9	97	1.6	92	84	3.63
	8-Dec-98	5.19	84	3.8	102	1.6	93	86	3.63
	15-Nov-99	6.12	89	2.5	105	2.3	97	90	3.59
	30-Nov-00	7.16	79	0.4	101	1.2	90	82	3.67
	8-Nov-01	8.10	87	1.8	110	3.2	99	92	3.59
	30-Oct-02	9.08	100	1.6	102	1.6	101	92	3.53
	4-Feb-04	10.34	101	4.4	98	1.6	100	91	3.52
	12-Dec-04	11.20	91	2.8	111	2.0	101	94	3.54
	13-Aug-06	12.87	117	1.5	136	1.4	127	121	3.24
	30-Dec-07	14.25	90	1.2	102	1.0	96	89	3.54
	20-Sep-08	14.97	118	2.4	135	3.3	126	121	3.29
	25-Jan-10	16.32	98	2.7	114	1.5	106	99	3.42
0220	25-Jan-94	0.32	77	2.1	80	1.8	78	74	3.70
	5-Mar-95	1.42	66	1.4	72	1.2	69	62	3.74
	27-Jan-97	3.32	66	3.6	72	1.7	69	64	3.87
	4-Dec-97	4.18	70	1.8	73	1.6	71	67	3.84
	8-Dec-98	5.19	69	0.6	73	1.4	71	67	3.86
	15-Nov-99	6.12	69	1.0	77	1.4	73	68	3.85
	30-Nov-00	7.16	77	4.7	69	1.3	73	68	3.86
	8-Nov-01	8.10	68	1.0	78	0.5	73	67	3.86
	30-Oct-02	9.08	82	2.1	69	1.2	76	71	3.77
	4-Feb-04	10.34	89	4.5	69	0.5	79	73	3.75
	12-Dec-04	11.20	73	1.6	80	1.9	77	71	3.75
	13-Aug-06	12.87	75	1.8	82	1.0	79	73	3.71
	30-Dec-07	14.25	86	1.9	85	1.6	85	80	3.63
	20-Sep-08	14.97	91	2.2	79	0.8	85	80	3.63
	25-Jan-10	16.32	80	2.4	83	1.7	82	76	3.65

Table 30. Roughness Values—Continued.

Section	Date	Years	Left IRI (inches/mi)		Right IRI (inches/mi)		MRI (inches/ mi)	HRI (inches/ mi)	RN
			Average	SD	Average	SD			
0221	25-Jan-94	0.32	73	1.9	73	1.7	73	65	3.72
	5-Mar-95	1.42	56	0.7	60	1.4	58	48	3.82
	27-Jan-97	3.32	78	1.6	78	0.4	78	71	3.76
	4-Dec-97	4.18	82	3.3	84	2.3	83	77	3.59
	8-Dec-98	5.19	85	2.8	82	1.7	83	77	3.66
	15-Nov-99	6.12	85	1.8	88	1.0	86	79	3.61
	30-Nov-00	7.16	76	1.2	82	1.6	79	71	3.62
	8-Nov-01	8.10	84	2.0	85	0.9	85	79	3.63
	30-Oct-02	9.08	90	6.3	77	2.4	84	77	3.46
	4-Feb-04	10.34	76	1.3	74	3.8	75	67	3.63
	12-Dec-04	11.20	79	2.9	80	1.3	79	72	3.61
	11-Aug-06	12.86	100	0.9	99	0.9	100	94	3.43
	30-Dec-07	14.25	81	1.3	81	1.6	81	74	3.52
	20-Sep-08	14.97	96	1.3	94	1.8	95	88	3.43
	25-Jan-10	16.32	82	1.3	84	1.5	83	76	3.40
0222	25-Jan-94	0.32	72	1.1	71	1.7	72	65	3.74
	5-Mar-95	1.42	58	1.4	56	1.1	57	47	3.82
	27-Jan-97	3.32	72	0.9	55	0.7	64	55	3.85
	4-Dec-97	4.18	64	2.8	63	1.8	63	55	3.82
	8-Dec-98	5.19	66	0.4	63	1.3	64	56	3.80
	15-Nov-99	6.12	79	2.5	64	0.8	72	64	3.78
	30-Nov-00	7.16	77	1.9	60	0.4	69	61	3.83
	8-Nov-01	8.10	68	1.6	64	0.8	66	57	3.84
	30-Oct-02	9.08	88	4.3	57	0.7	73	64	3.73
	4-Feb-04	10.34	87	6.3	58	1.1	72	64	3.72
	12-Dec-04	11.20	69	3.1	66	0.9	67	58	3.77
	13-Aug-06	12.87	72	0.8	73	1.7	73	63	3.75
	30-Dec-07	14.25	91	2.3	69	0.9	80	73	3.67
	20-Sep-08	14.97	78	2.1	75	1.5	76	69	3.69
	25-Jan-10	16.32	76	1.7	70	1.7	73	64	3.72
0223	25-Jan-94	0.32	73	1.5	81	3.1	77	66	3.70
	5-Mar-95	1.42	69	0.9	79	1.3	74	63	3.68
	27-Jan-97	3.32	80	1.5	85	1.2	82	71	3.69
	4-Dec-97	4.18	83	0.7	88	1.4	85	76	3.69
	8-Dec-98	5.19	89	2.2	92	1.5	90	82	3.64
	15-Nov-99	6.12	89	1.7	95	1.4	92	84	3.62
	30-Nov-00	7.16	82	1.3	94	0.8	88	79	3.66
	8-Nov-01	8.10	87	1.8	99	1.1	93	85	3.61
	30-Oct-02	9.08	108	1.3	88	0.9	98	90	3.56
	4-Feb-04	10.34	117	5.8	86	1.1	101	93	3.52
	12-Dec-04	11.20	91	2.5	98	1.3	95	87	3.54
	13-Aug-06	12.87	111	1.5	120	1.3	116	109	3.37
	30-Dec-07	14.25	97	1.6	96	2.2	96	90	3.51
	20-Sep-08	14.97	122	2.5	118	0.8	120	115	3.35
	25-Jan-10	16.32	101	2.9	102	1.2	102	95	3.47

Table 30. Roughness Values—Continued.

Section	Date	Years	Left IRI (inches/mi)		Right IRI (inches/mi)		MRI (inches/ mi)	HRI (inches/ mi)	RN
			Average	SD	Average	SD			
0224	25-Jan-94	0.32	65	0.5	67	1.7	66	61	3.80
	5-Mar-95	1.42	60	1.8	71	3.6	66	60	3.74
	27-Jan-97	3.32	73	3.2	69	0.8	71	66	3.84
	4-Dec-97	4.18	64	5.5	71	2.3	67	61	3.84
	8-Dec-98	5.19	64	5.5	75	3.3	69	64	3.83
	15-Nov-99	6.12	80	5.2	71	1.5	76	71	3.83
	30-Nov-00	7.16	83	4.3	69	0.4	76	72	3.84
	8-Nov-01	8.10	66	3.3	77	0.8	72	66	3.82
	30-Oct-02	9.08	84	2.7	72	0.9	78	72	3.77
	4-Feb-04	10.34	114	2.1	71	1.0	93	86	3.65
	12-Dec-04	11.20	70	5.0	79	1.7	75	69	3.78
	13-Aug-06	12.87	78	3.6	74	1.1	76	72	3.78
	30-Dec-07	14.25	79	1.7	77	0.9	78	74	3.75
	20-Sep-08	14.97	89	6.6	78	1.2	83	78	3.72
	25-Jan-10	16.32	85	5.2	84	1.7	84	80	3.70
0260	25-Jan-94	0.32	57	0.3	69	1.8	63	50	3.89
	5-Mar-95	1.42	62	0.5	75	2.8	68	54	3.75
	27-Jan-97	3.32	64	0.9	70	2.6	67	51	3.84
	4-Dec-97	4.18	62	1.5	70	1.3	66	52	3.73
	8-Dec-98	5.19	61	1.8	69	1.6	65	50	3.77
	15-Nov-99	6.12	63	1.4	68	1.4	66	51	3.84
	30-Nov-00	7.16	62	0.8	68	0.8	65	51	3.86
	8-Nov-01	8.10	62	0.5	70	1.4	66	51	3.82
	30-Oct-02	9.08	64	1.2	60	0.7	62	48	3.85
	4-Feb-04	10.34	65	1.6	60	2.1	63	49	3.82
	12-Dec-04	11.20	66	1.9	69	0.6	67	52	3.64
	13-Aug-06	12.87	88	2.7	70	2.4	79	61	3.36
	30-Dec-07	14.25	105	6.8	66	2.2	86	69	2.76
	20-Sep-08	14.97	111	3.8	72	2.0	92	74	2.78
	25-Jan-10	16.32	121	3.1	78	1.3	99	78	2.50
0261	25-Jan-94	0.32	40	0.4	53	1.5	47	39	4.05
	5-Mar-95	1.42	38	0.7	60	1.8	49	40	3.99
	27-Jan-97	3.32	40	0.5	60	1.4	50	40	3.85
	4-Dec-97	4.18	41	0.4	58	2.2	50	40	3.89
	8-Dec-98	5.19	39	0.9	60	1.0	50	40	3.84
	15-Nov-99	6.12	39	1.1	59	1.3	49	39	3.87
	30-Nov-00	7.16	38	0.4	59	0.8	48	40	3.82
	8-Nov-01	8.10	40	0.5	60	0.7	50	40	3.80
	30-Oct-02	9.08	38	0.6	55	1.7	46	38	4.02
	4-Feb-04	10.34	39	0.3	55	1.3	47	37	3.92
	12-Dec-04	11.20	42	2.5	62	1.0	52	42	3.86
	13-Aug-06	12.87	44	1.0	66	1.3	55	44	3.76
	30-Dec-07	14.25	44	0.6	72	3.1	58	48	3.51
	20-Sep-08	14.97	47	1.0	82	3.4	65	52	3.32
	25-Jan-10	16.32	57	0.8	111	2.5	84	69	2.83

Table 30. Roughness Values—Continued.

Section	Date	Years	Left IRI (inches/mi)		Right IRI (inches/mi)		MRI (inches/ mi)	HRI (inches/ mi)	RN
			Average	SD	Average	SD			
0262	25-Jan-94	0.32	72	1.0	67	1.3	70	62	3.76
	5-Mar-95	1.42	67	0.6	70	1.3	69	59	3.71
	27-Jan-97	3.32	112	1.0	110	1.3	111	105	3.44
	4-Dec-97	4.18	122	1.3	118	1.4	120	115	3.35
	8-Dec-98	5.19	137	1.3	138	0.4	137	132	3.14
	15-Nov-99	6.12	144	0.6	150	1.1	147	142	3.08
	30-Nov-00	7.16	139	1.4	155	1.1	147	141	3.02
	8-Nov-01	8.10	158	0.3	175	0.5	166	161	2.84
	30-Oct-02	9.08	155	0.8	174	1.4	165	156	2.79
	4-Feb-04	10.34	158	0.8	171	1.5	164	154	2.73
	12-Dec-04	11.20	163	2.3	193	1.8	178	170	2.60
	11-Aug-06	12.86	195	0.8	225	0.8	210	201	2.33
	30-Dec-07	14.25	186	2.1	234	4.5	210	199	1.80
	20-Sep-08	14.97	204	0.6	249	3.9	227	215	1.76
	25-Jan-10	16.32	195	1.0	229	3.8	212	202	2.13
0263	25-Jan-94	0.32	68	0.8	70	1.8	69	61	3.67
	5-Mar-95	1.42	59	1.9	68	1.4	64	53	3.65
	27-Jan-97	3.32	80	0.7	73	0.7	77	69	3.76
	4-Dec-97	4.18	81	1.5	79	2.1	80	72	3.67
	8-Dec-98	5.19	82	1.2	82	2.3	82	74	3.67
	15-Nov-99	6.12	90	0.3	81	1.3	85	77	3.69
	30-Nov-00	7.16	82	1.7	78	1.6	80	72	3.75
	8-Nov-01	8.10	86	2.4	83	0.3	85	77	3.69
	30-Oct-02	9.08	92	2.6	83	1.4	88	78	3.58
	4-Feb-04	10.34	90	1.7	83	1.8	87	75	3.58
	12-Dec-04	11.20	84	3.9	80	1.9	82	73	3.62
	11-Aug-06	12.86	104	1.4	95	2.0	100	92	3.50
	30-Dec-07	14.25	92	2.1	81	1.8	87	78	3.58
	20-Sep-08	14.97	103	2.4	93	1.9	98	89	3.50
	25-Jan-10	16.32	88	1.4	79	1.4	83	75	3.59
0264	25-Jan-94	0.32	105	1.9	113	2.4	109	93	3.37
	5-Mar-95	1.42	93	1.5	117	2.2	105	89	3.41
	27-Jan-97	3.32	113	1.4	122	2.6	118	98	3.34
	4-Dec-97	4.18	115	2.4	126	1.1	120	103	3.32
	8-Dec-98	5.19	114	2.1	133	1.7	123	106	3.30
	15-Nov-99	6.12	121	1.8	130	2.5	126	108	3.27
	30-Nov-00	7.16	119	0.7	129	2.7	124	107	3.28
	8-Nov-01	8.10	119	1.6	140	3.2	129	113	3.26
	30-Oct-02	9.08	122	4.7	125	1.0	123	108	3.26
	4-Feb-04	10.34	121	5.3	123	3.5	122	107	3.26
	12-Dec-04	11.20	123	4.7	135	4.4	129	114	3.19
	13-Aug-06	12.87	140	1.5	141	0.5	141	126	3.10
	30-Dec-07	14.25	135	1.6	132	2.7	134	119	3.12
	20-Sep-08	14.97	150	1.7	148	1.5	149	135	3.04
	25-Jan-10	16.32	128	3.6	144	3.5	136	122	3.13

Table 30. Roughness Values—Continued.

Section	Date	Years	Left IRI (inches/mi)		Right IRI (inches/mi)		MRI (inches/ mi)	HRI (inches/ mi)	RN
			Average	SD	Average	SD			
0265	25-Jan-94	0.32	84	2.1	89	2.3	86	72	3.55
	5-Mar-95	1.42	81	2.0	96	2.1	89	73	3.50
	27-Jan-97	3.32	96	1.9	106	0.7	101	88	3.44
	4-Dec-97	4.18	99	2.6	115	3.2	107	94	3.37
	8-Dec-98	5.19	107	2.0	123	2.1	115	104	3.27
	15-Nov-99	6.12	109	1.4	128	1.0	118	106	3.29
	30-Nov-00	7.16	107	0.7	133	0.7	120	109	3.21
	8-Nov-01	8.10	118	1.6	146	0.5	132	122	3.11
	30-Oct-02	9.08	114	2.3	141	0.8	127	114	3.12
	4-Feb-04	10.34	112	2.1	145	3.5	129	116	3.05
	12-Dec-04	11.20	114	2.0	156	3.8	135	125	2.97
	13-Aug-06	12.87	136	1.4	168	1.4	152	143	2.90
	30-Dec-07	14.25	123	1.0	168	1.4	146	134	2.82
	20-Sep-08	14.97	143	1.6	182	1.5	163	154	2.79
	25-Jan-10	16.32	133	1.1	180	0.6	156	145	2.75
0266	25-Jan-94	0.32	82	1.2	93	1.8	87	78	3.54
	5-Mar-95	1.42	79	1.1	95	2.4	87	78	3.57
	27-Jan-97	3.32	87	1.5	94	0.4	90	79	3.65
	4-Dec-97	4.18	88	1.5	100	3.2	94	86	3.63
	8-Dec-98	5.19	91	1.6	102	0.5	97	89	3.60
	15-Nov-99	6.12	95	3.5	104	0.8	99	89	3.58
	30-Nov-00	7.16	89	0.7	101	0.7	95	87	3.62
	8-Nov-01	8.10	99	1.1	110	1.0	105	97	3.53
	30-Oct-02	9.08	118	5.2	108	0.9	113	104	3.39
	4-Feb-04	10.34	104	1.0	103	0.9	103	93	3.44
	12-Dec-04	11.20	98	1.9	109	2.1	103	96	3.47
	13-Aug-06	12.87	122	3.5	125	1.9	123	116	3.28
	30-Dec-07	14.25	114	1.6	109	1.1	111	102	3.35
	20-Sep-08	14.97	133	0.6	129	0.8	131	123	3.21
	25-Jan-10	16.32	106	1.7	112	1.1	109	102	3.39
0267	25-Jan-94	0.32	80	1.7	106	2.0	93	78	3.39
	5-Mar-95	1.42	79	0.9	112	4.2	95	79	3.38
	27-Jan-97	3.32	75	2.2	106	1.4	90	75	3.61
	4-Dec-97	4.18	83	5.4	113	3.0	98	83	3.52
	8-Dec-98	5.19	82	1.8	115	1.7	99	84	3.49
	15-Nov-99	6.12	78	0.8	114	1.9	96	83	3.57
	30-Nov-00	7.16	76	0.3	111	1.0	94	82	3.56
	8-Nov-01	8.10	86	2.7	120	1.8	103	90	3.44
	30-Oct-02	9.08	92	6.2	110	2.7	101	86	3.44
	4-Feb-04	10.34	86	1.0	104	1.1	95	82	3.45
	12-Dec-04	11.20	88	1.6	114	1.4	101	89	3.40
	13-Aug-06	12.87	98	1.8	110	1.9	104	92	3.29
	30-Dec-07	14.25	81	1.2	84	1.2	82	71	3.53
	20-Sep-08	14.97	92	1.5	101	1.5	97	87	3.42
	25-Jan-10	16.32	77	2.0	91	1.7	84	74	3.45

Table 30. Roughness Values—Continued.

Section	Date	Years	Left IRI (inches/mi)		Right IRI (inches/mi)		MRI (inches/ mi)	HRI (inches/ mi)	RN
			Average	SD	Average	SD			
0268	25-Jan-94	0.32	85	2.0	94	0.5	89	73	3.39
	5-Mar-95	1.42	80	1.5	96	3.7	88	72	3.36
	27-Jan-97	3.32	91	1.2	92	1.2	91	75	3.53
	4-Dec-97	4.18	89	3.9	95	2.5	92	76	3.48
	8-Dec-98	5.19	93	3.2	98	3.0	95	79	3.45
	15-Nov-99	6.12	94	1.6	98	1.6	96	79	3.52
	30-Nov-00	7.16	92	0.5	97	1.9	95	78	3.48
	8-Nov-01	8.10	97	1.1	104	2.1	101	84	3.42
	30-Oct-02	9.08	102	4.7	96	2.8	99	84	3.40
	4-Feb-04	10.34	99	0.6	91	1.9	95	80	3.39
	12-Dec-04	11.20	97	3.5	98	2.1	97	80	3.35
	13-Aug-06	12.87	116	0.6	112	2.1	114	100	3.26
	30-Dec-07	14.25	99	2.2	94	1.3	97	80	3.40
	20-Sep-08	14.97	106	3.2	107	2.4	107	93	3.32
	25-Jan-10	16.32	94	2.1	100	0.8	97	80	3.33

SD = Standard deviation

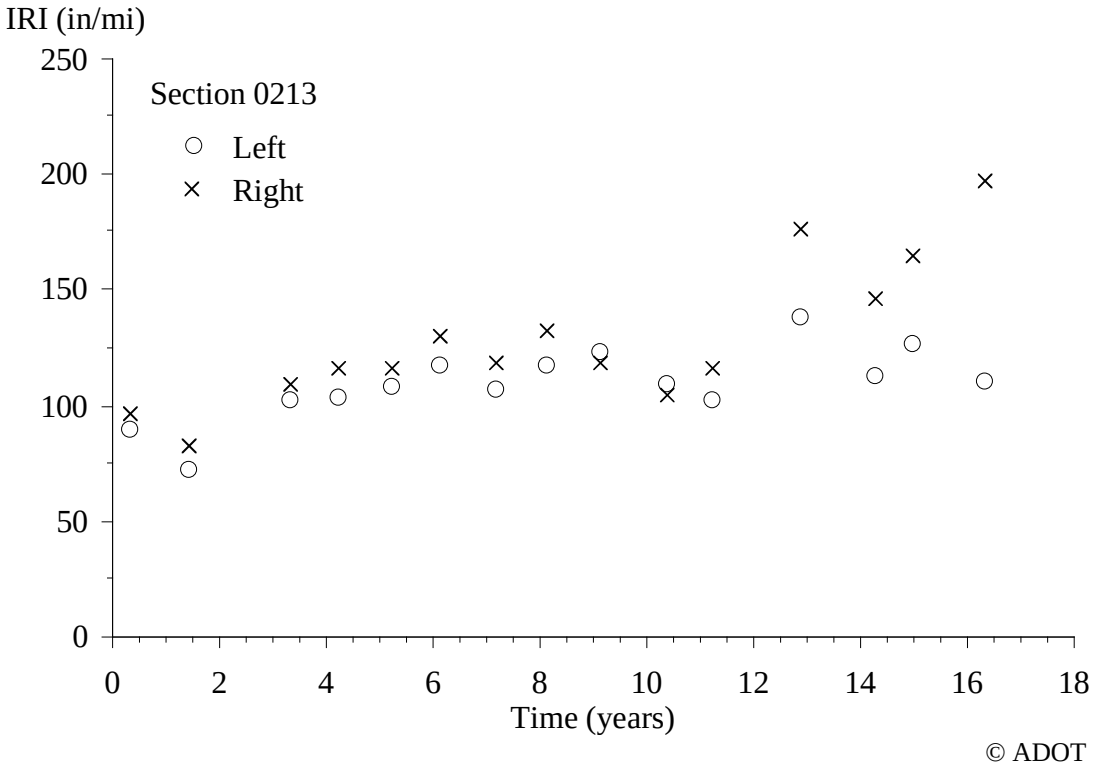

Figure 26. Graph. IRI Progression for Section 0213.

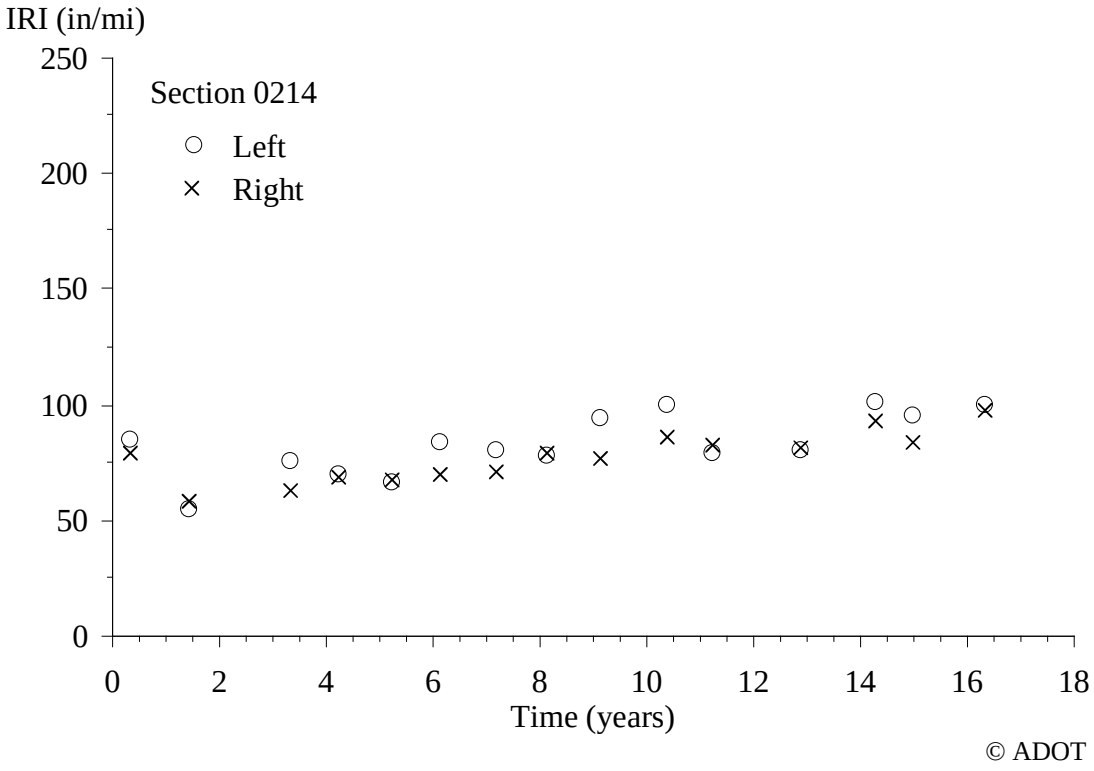

Figure 27. Graph. IRI Progression for Section 0214.

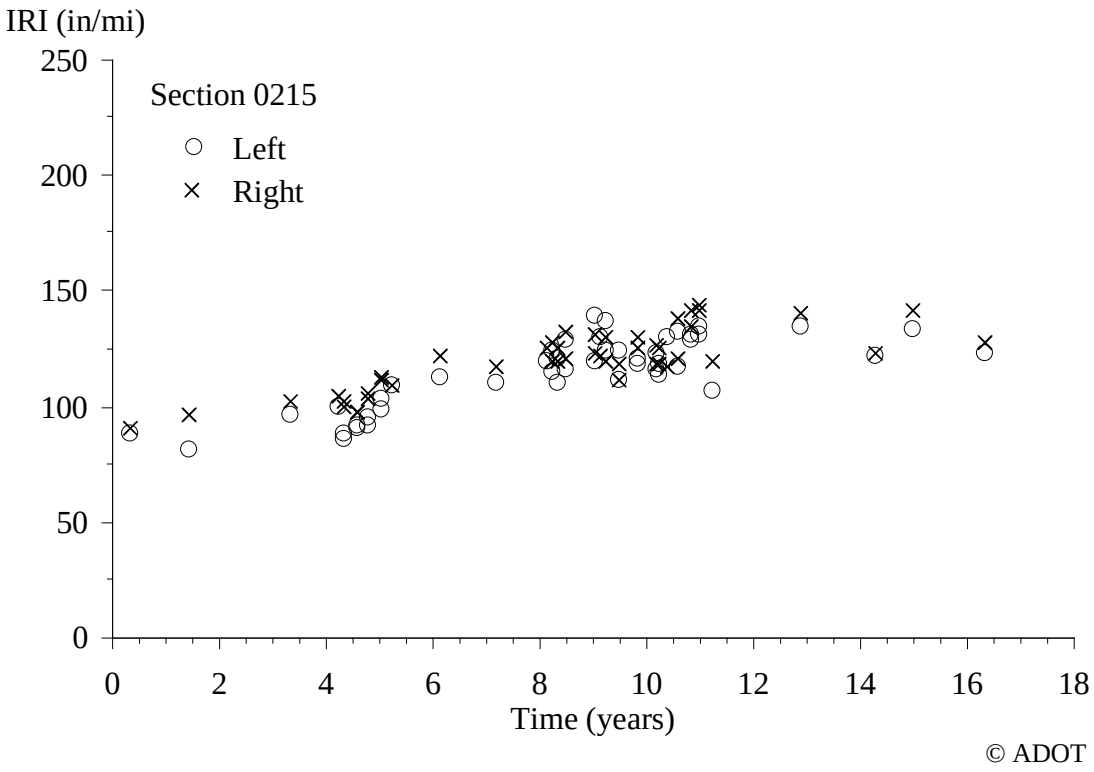

Figure 28. Graph. IRI Progression for Section 0215.

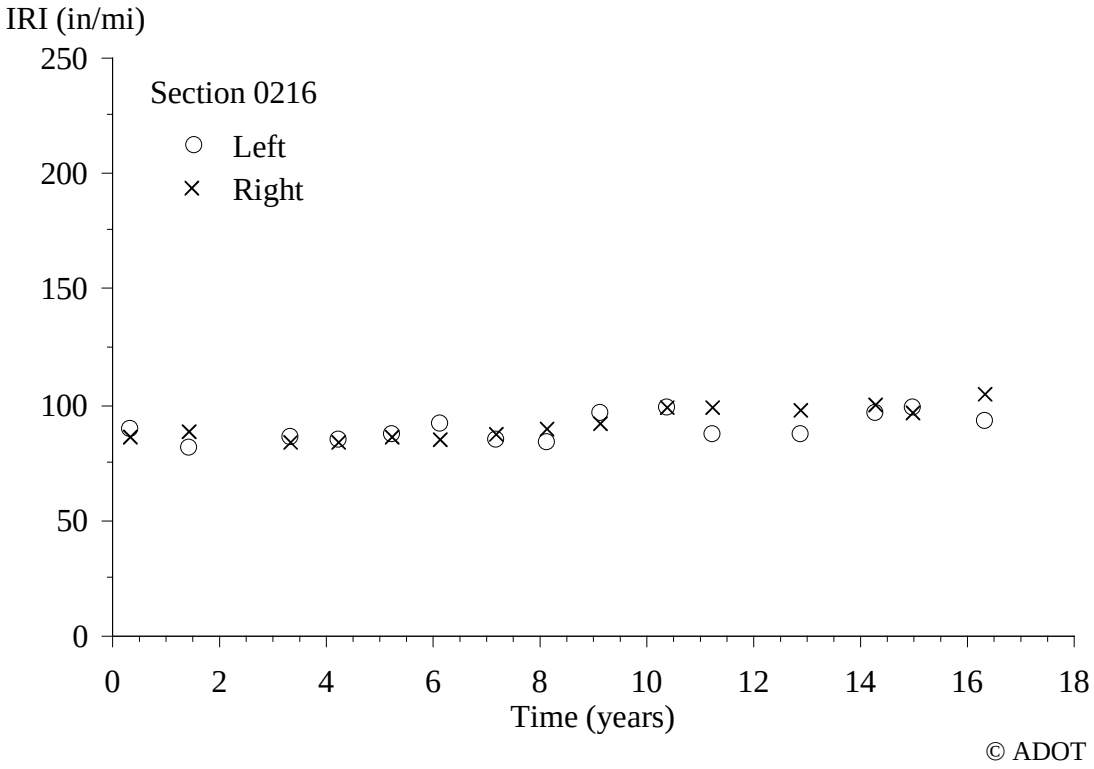

Figure 29. Graph. IRI Progression for Section 0216.

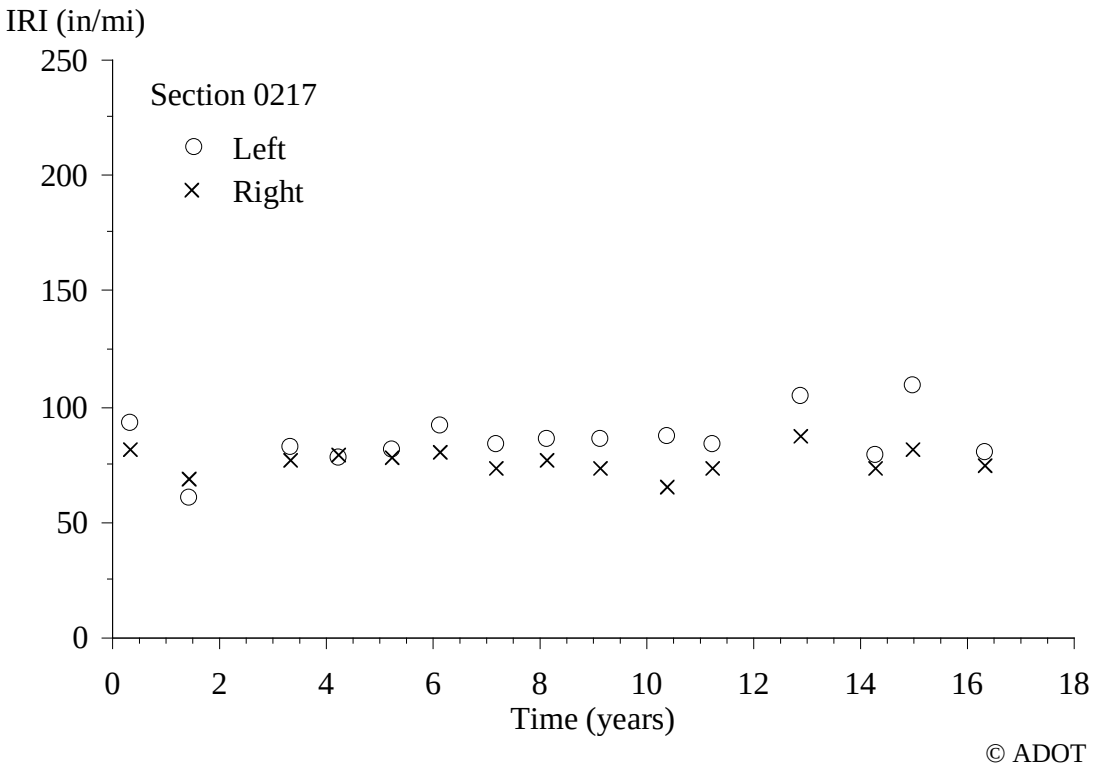

Figure 30. Graph. IRI Progression for Section 0217.

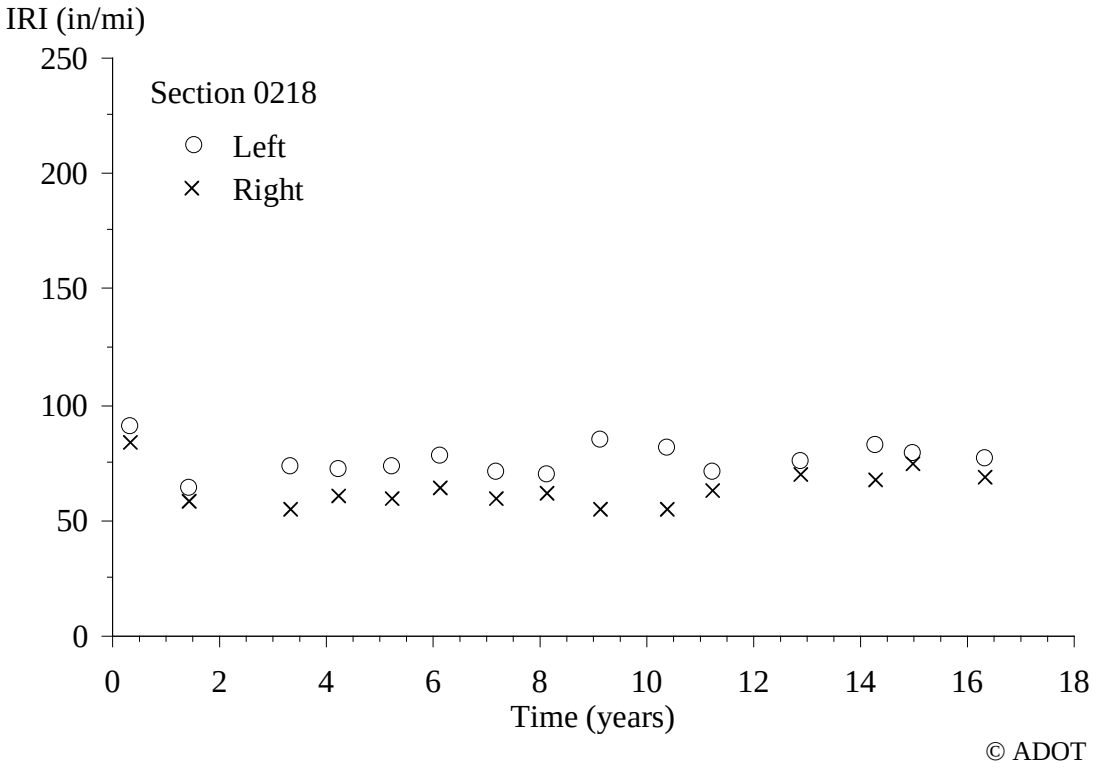

Figure 31. Graph. IRI Progression for Section 0218.

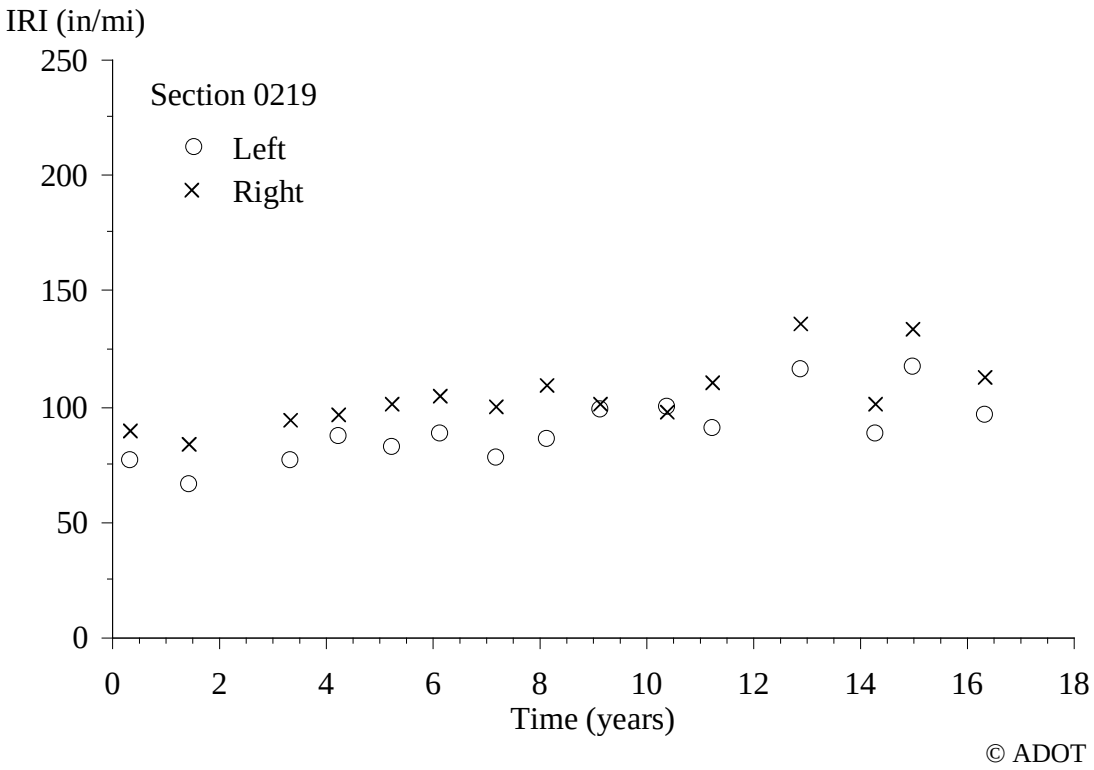

Figure 32. Graph. IRI Progression for Section 0219.

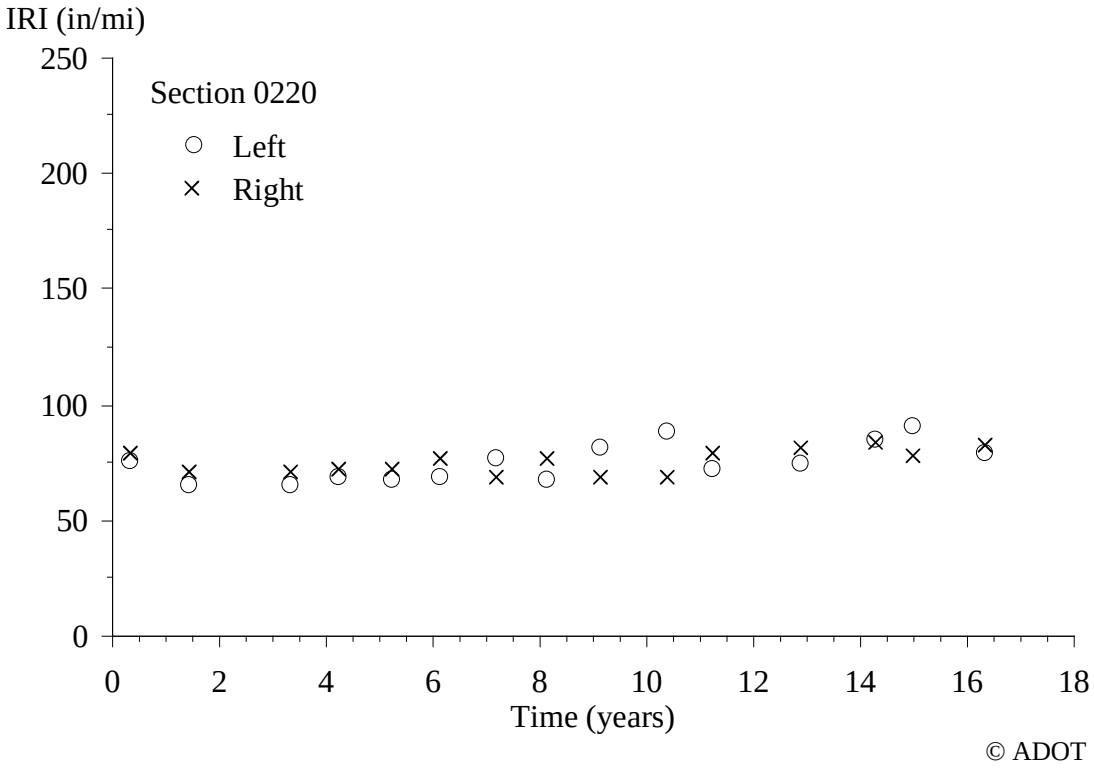

Figure 33. Graph. IRI Progression for Section 0220.

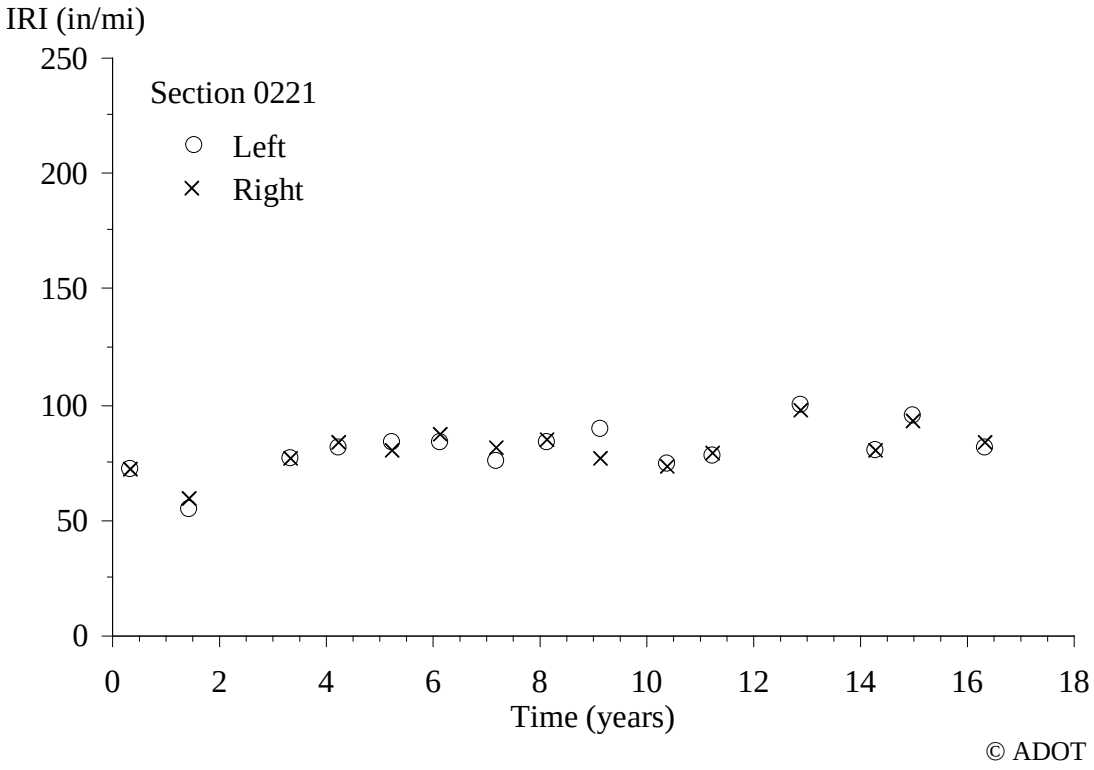

Figure 34. Graph. IRI Progression for Section 0221.

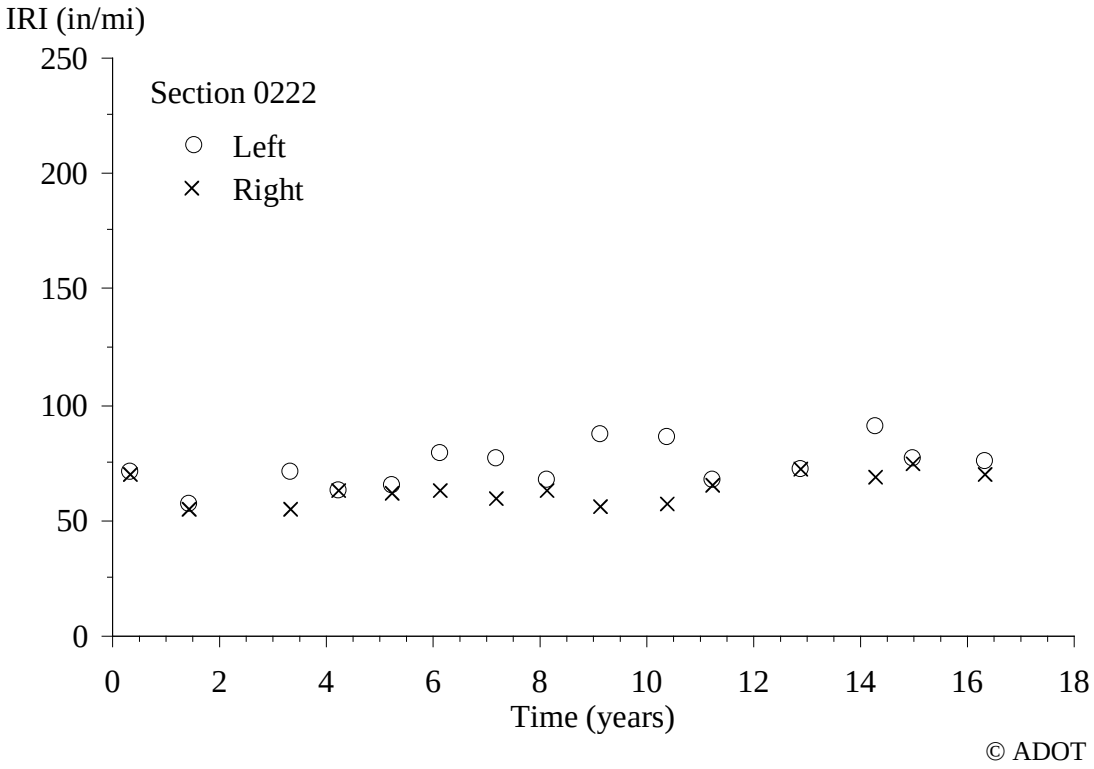

Figure 35. Graph. IRI Progression for Section 0222.

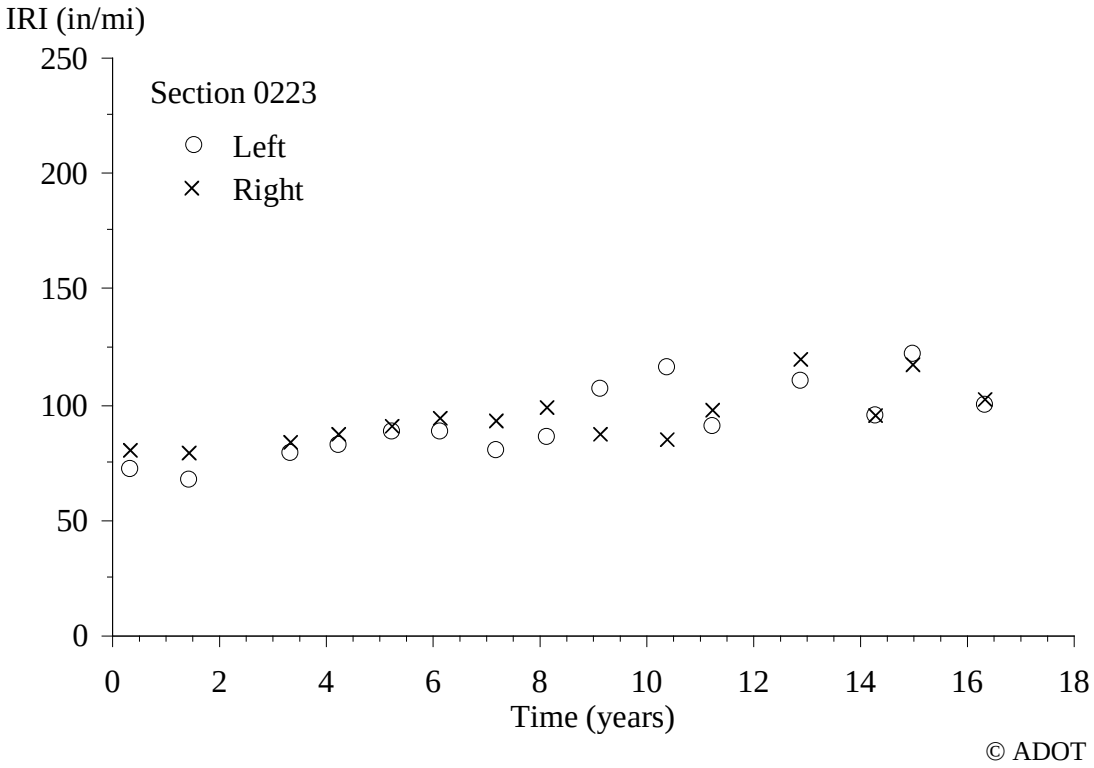

Figure 36. Graph. IRI Progression for Section 0223.

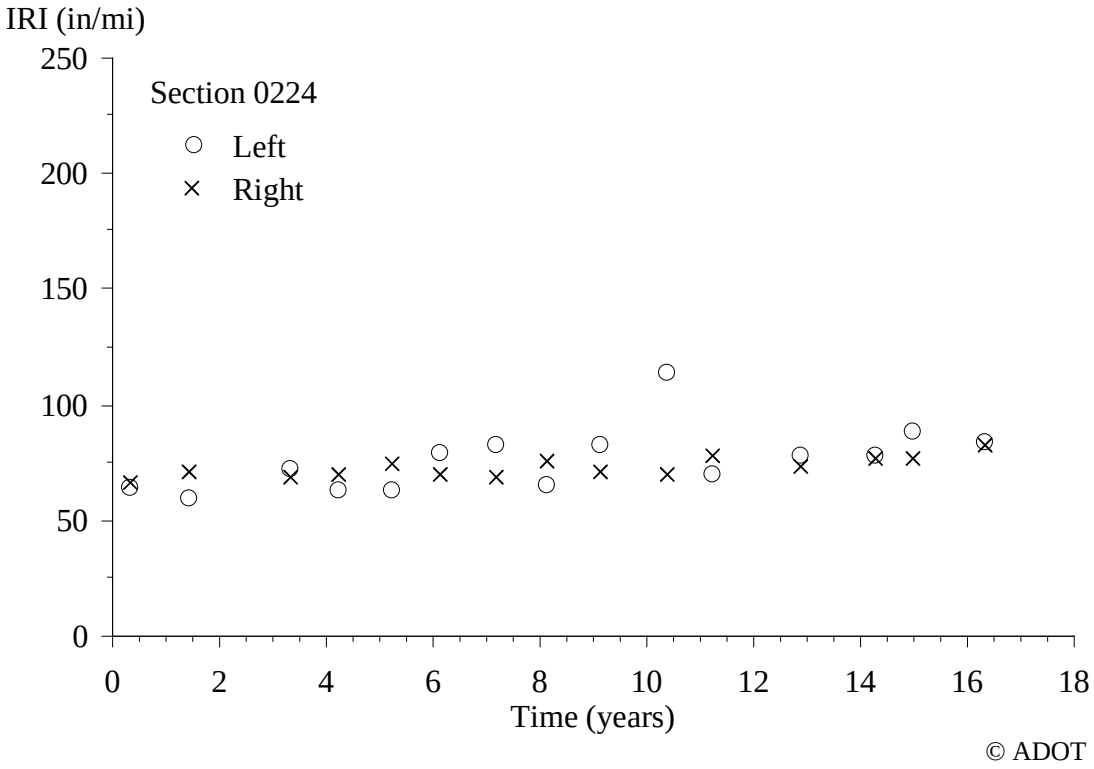

Figure 37. Graph. IRI Progression for Section 0224.

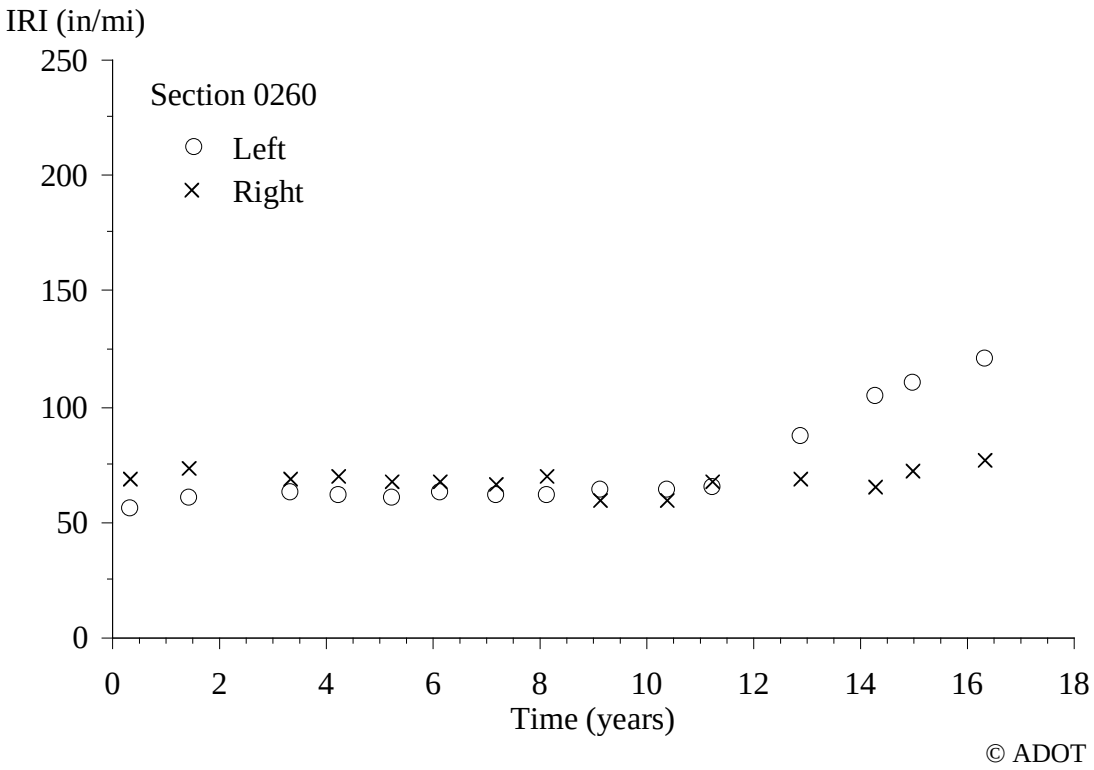

Figure 38. Graph. IRI Progression for Section 0260.

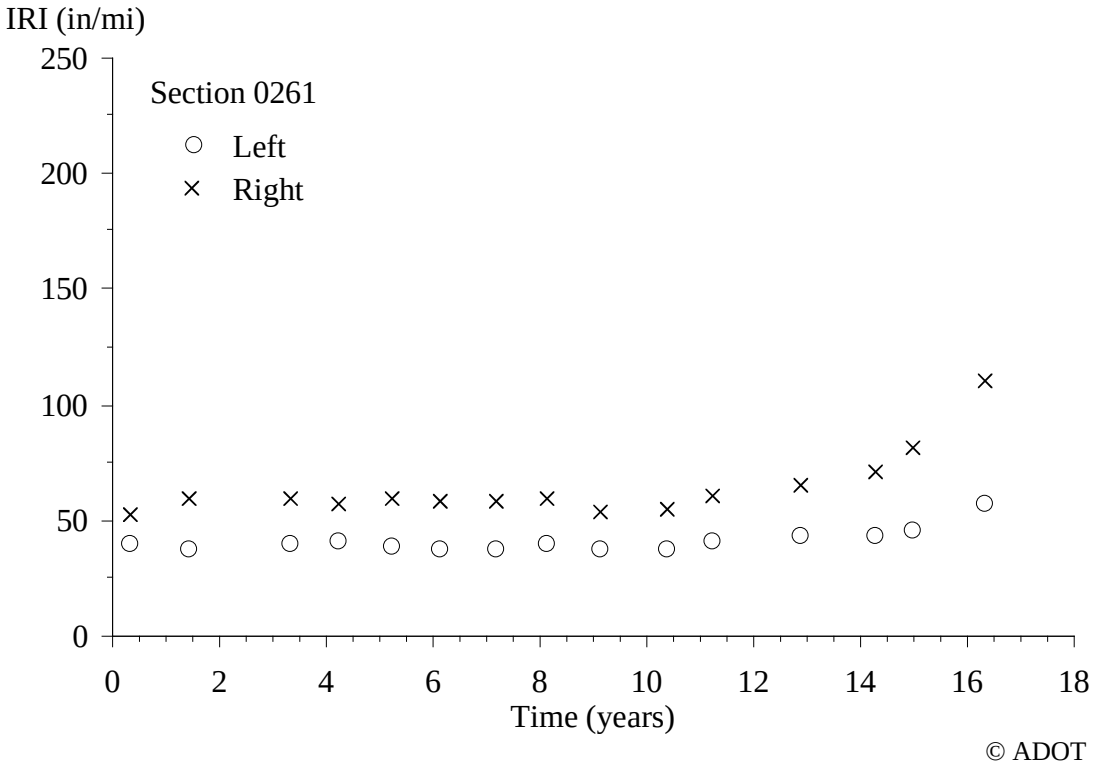

Figure 39. Graph. IRI Progression for Section 0261.

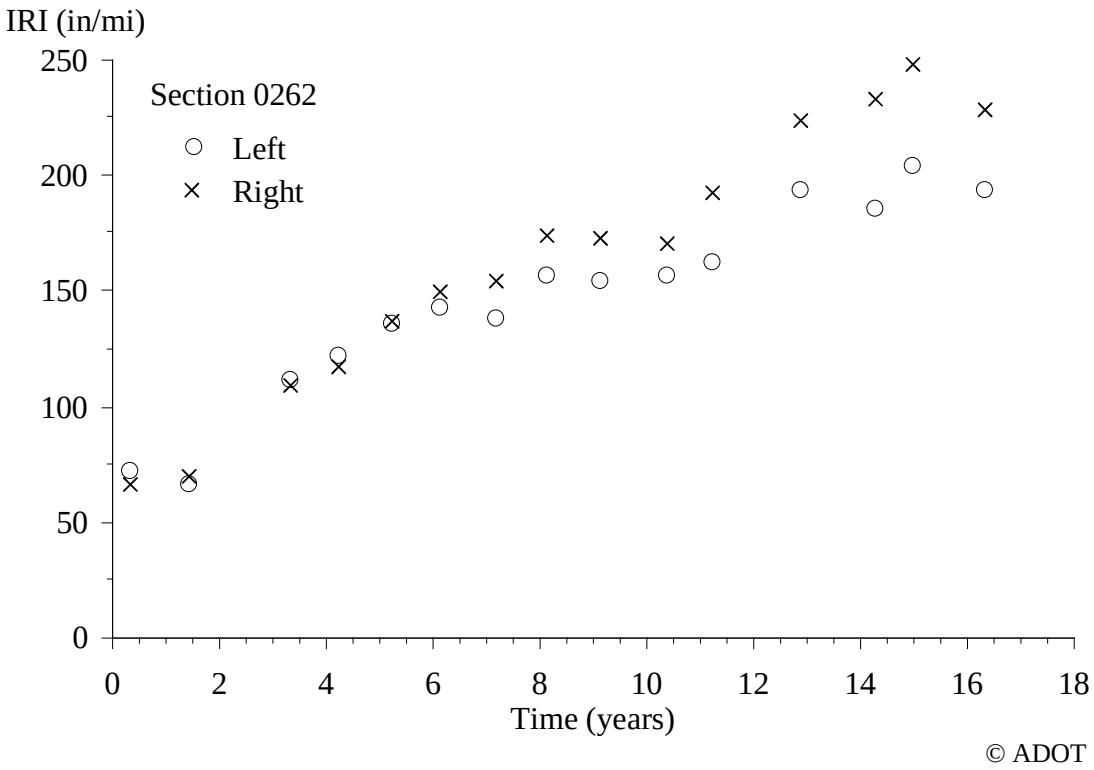

Figure 40. Graph. IRI Progression for Section 0262.

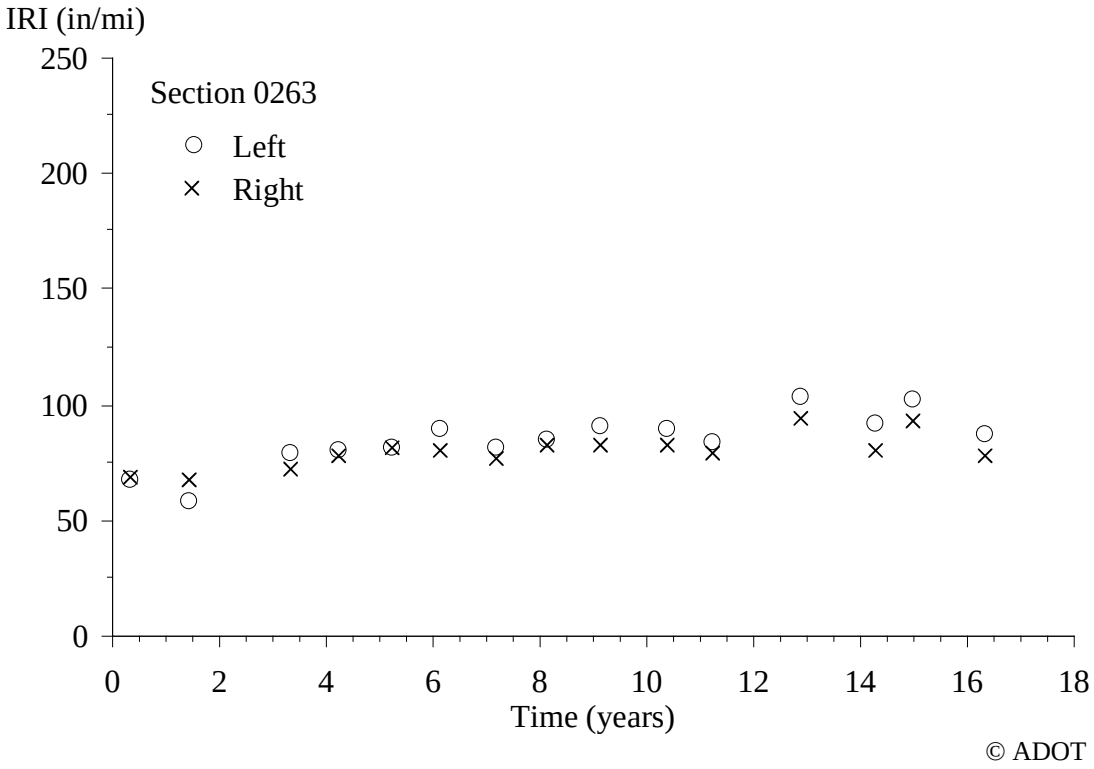

Figure 41. Graph. IRI Progression for Section 0263.

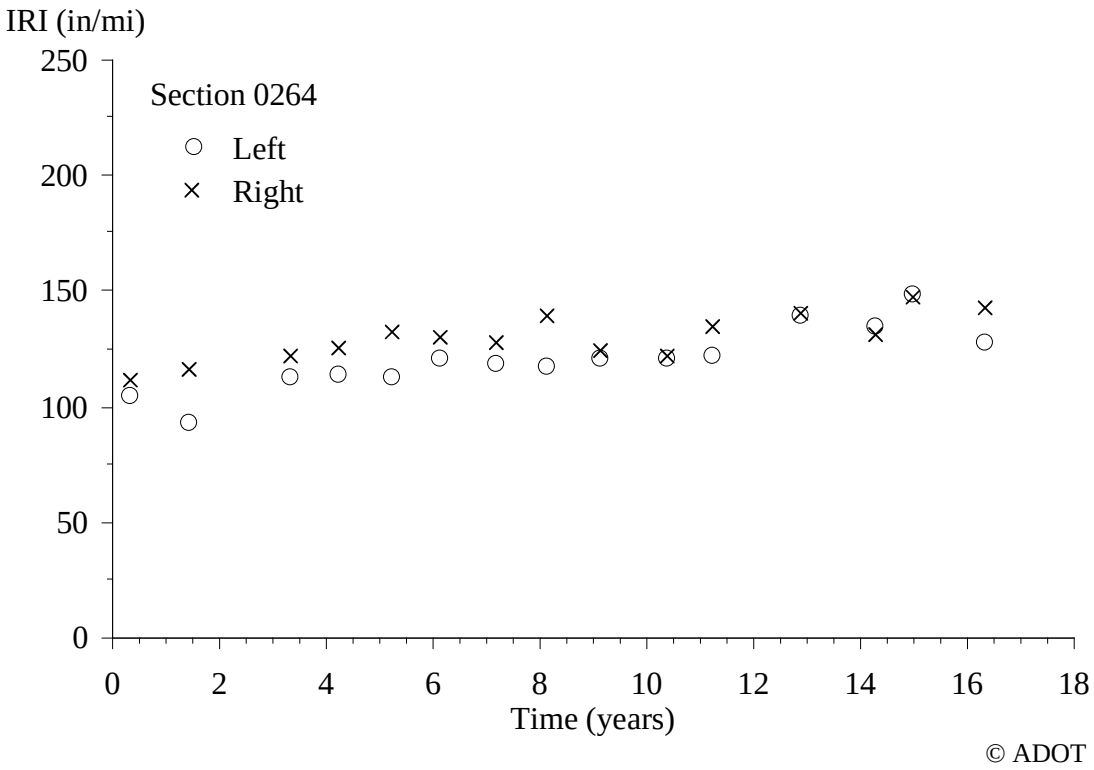

Figure 42. Graph. IRI Progression for Section 0264.

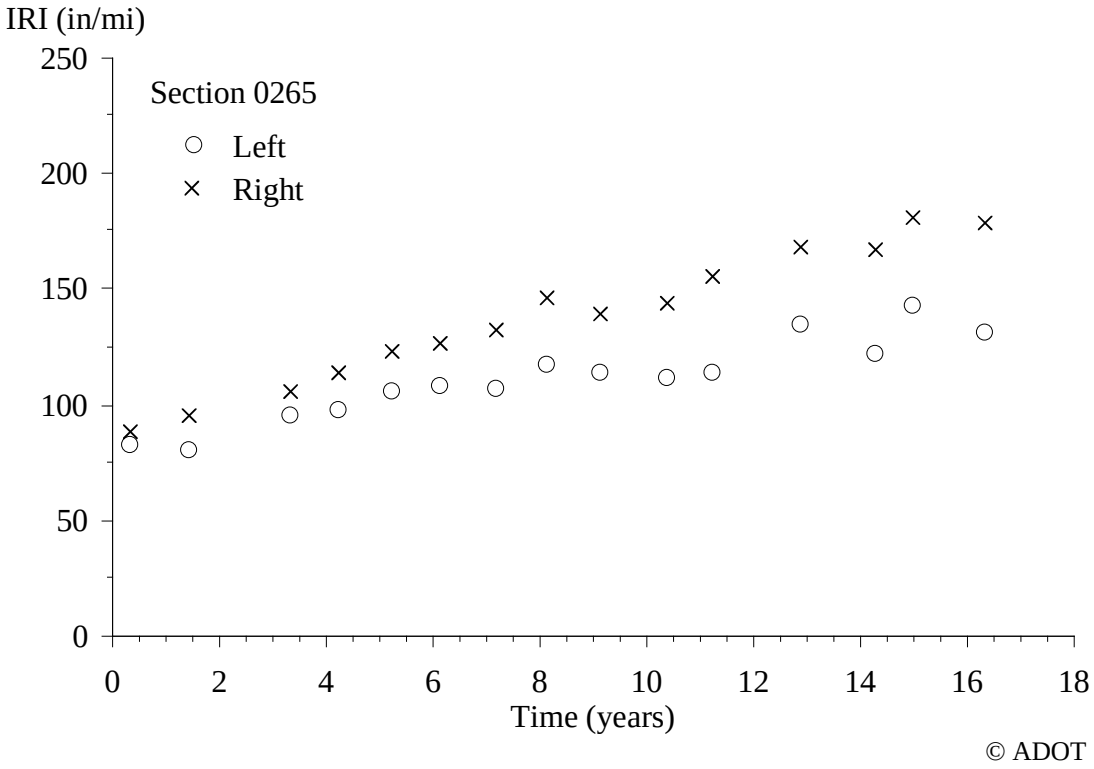

Figure 43. Graph. IRI Progression for Section 0265.

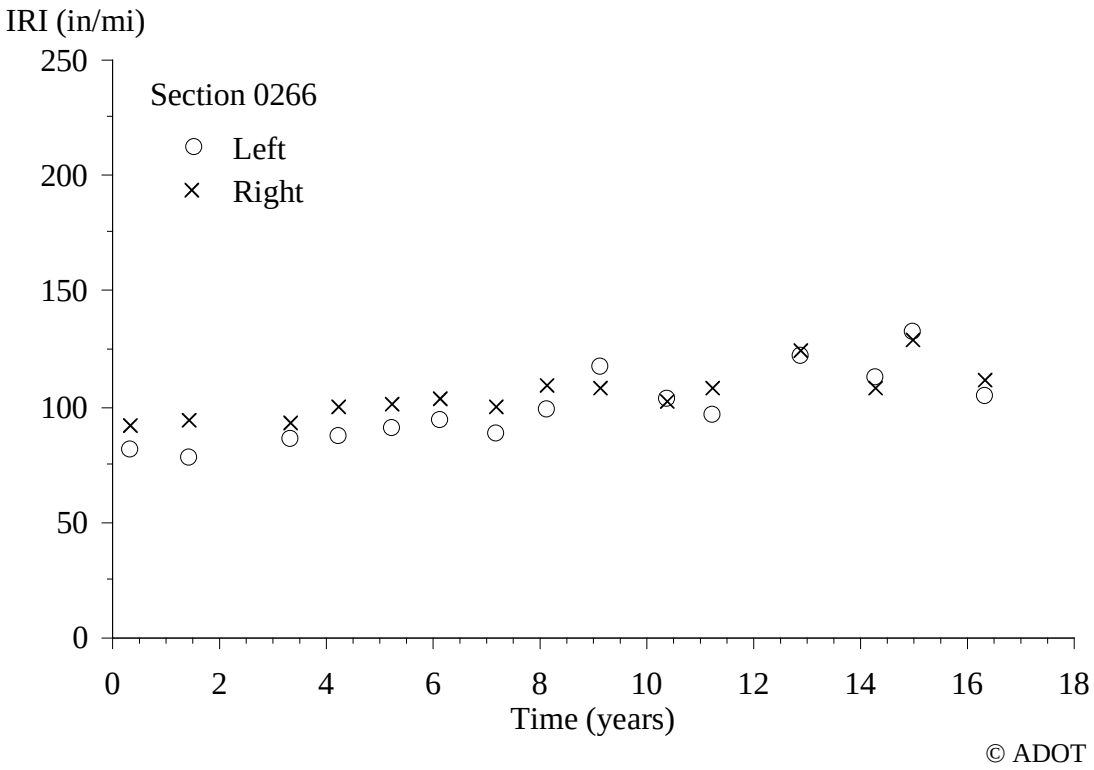

Figure 44. Graph. IRI Progression for Section 0266.

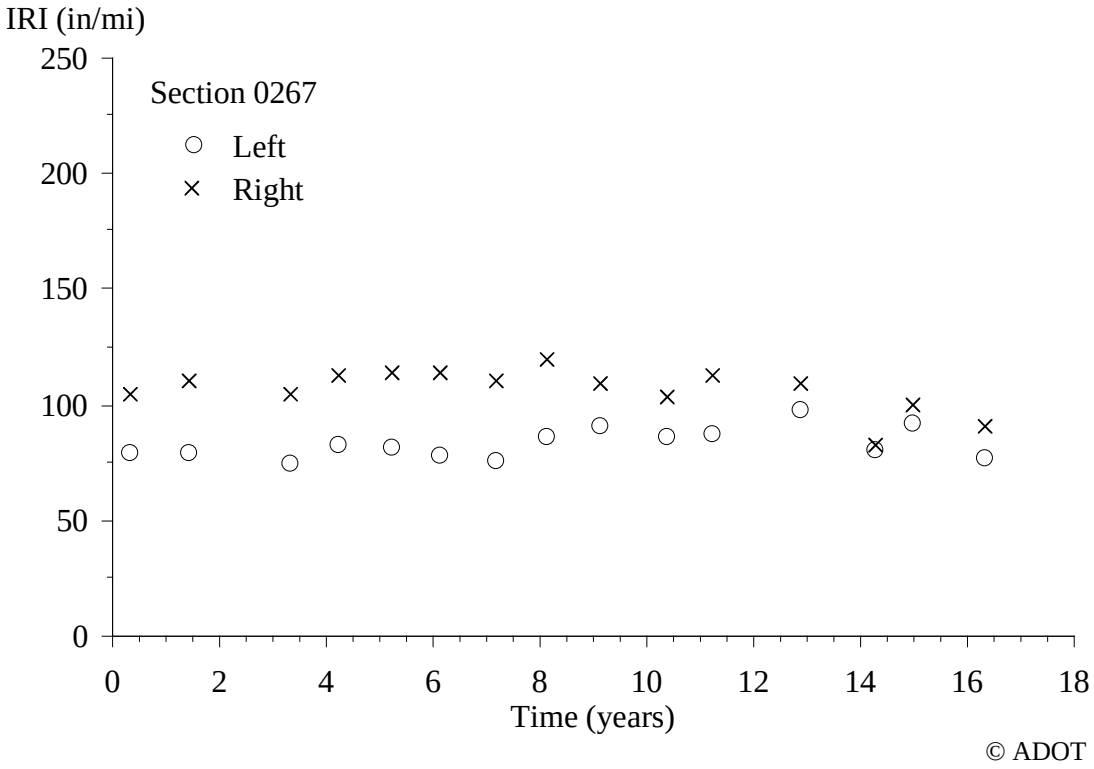

Figure 45. Graph. IRI Progression for Section 0267.

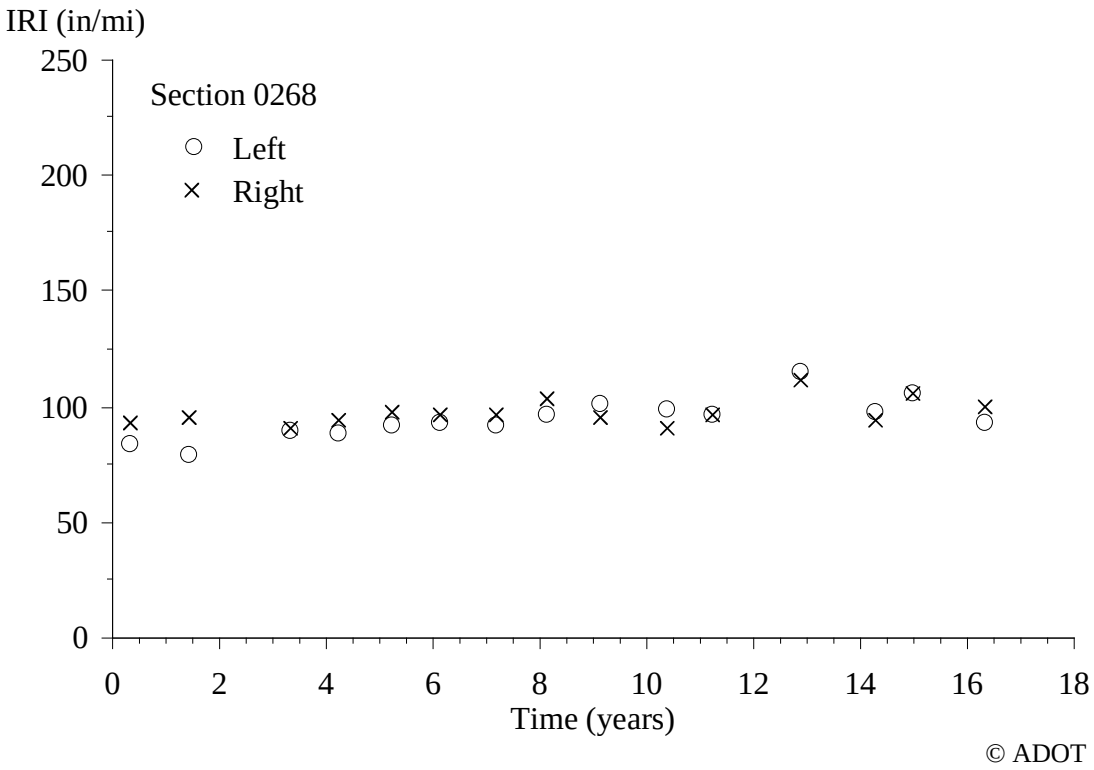

Figure 46. Graph. IRI Progression for Section 0268.

APPENDIX D. TRADITIONAL PROFILE ANALYSES

This appendix provides findings from traditional profile analyses applied to the LTPP SPS-2 site in Arizona. These tools helped study roughness, roughness distribution, and roughness progression of each section, including concentrated roughness-linked pavement distress. The analyses included viewing filtered elevation profile plots, roughness profiles, and power spectral density (PSD) plots. Sayers provides tutorial demonstrations of these methods.[15,16] Karamihas and Senn applied them to other SPS sites in Arizona. (See references 3–7.)

This appendix discusses observations pertinent to IRI but only on those sections where the analyses yielded noteworthy observations. Section 0213 exhibited several features of interest and is used to provide detailed examples of phenomena that appeared on other sections.

SECTION 0213

A simple way to learn about the type of roughness that exists within a profile is to view the trace. However, key details of the profile are often not as obvious in a raw profile trace as they may be after the profile is filtered. Figure 47 shows the right-side profile of section 0213 from visit 03 (27-Jan-1997). Several features are evident from this plot, but they are much more obvious when plotted with filters.

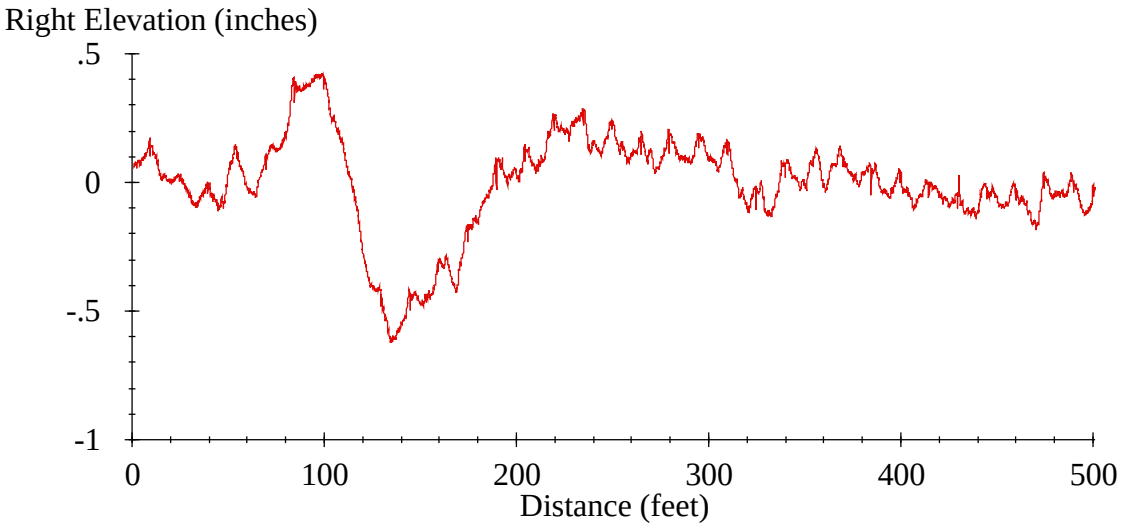

Figure 47. Graph. Raw Profile from Visit 03 of Right Side of Section 0213.

Figure 48 through figure 50 show the profile from figure 47 after application of various moving average filters. Each of the filters helps examine a distinct feature of the roughness on section 0213.

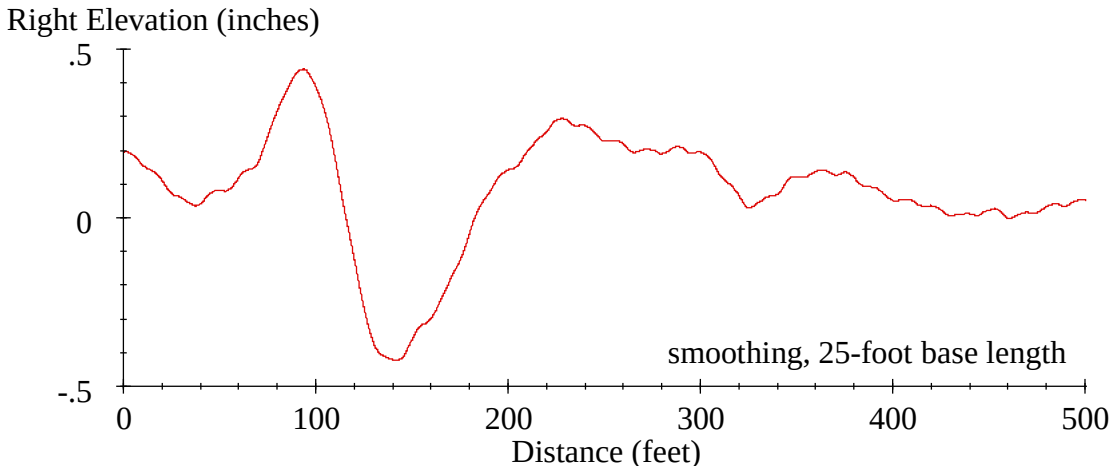

Figure 48. Graph. Profile with Smoothing from Visit 03 of Right Side of Section 0213.

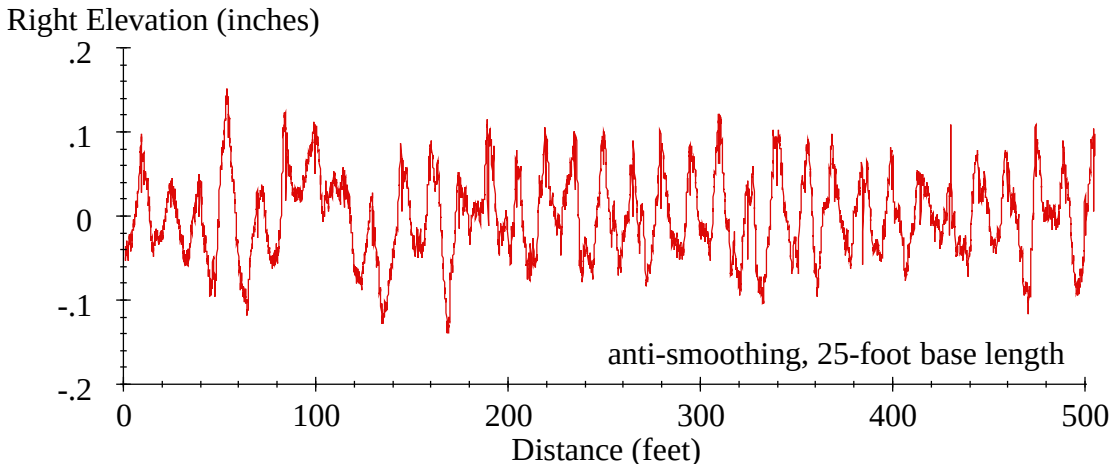

Figure 49. Graph. Profile with Anti-Smoothing from Visit 03 of Right Side of Section 0213.

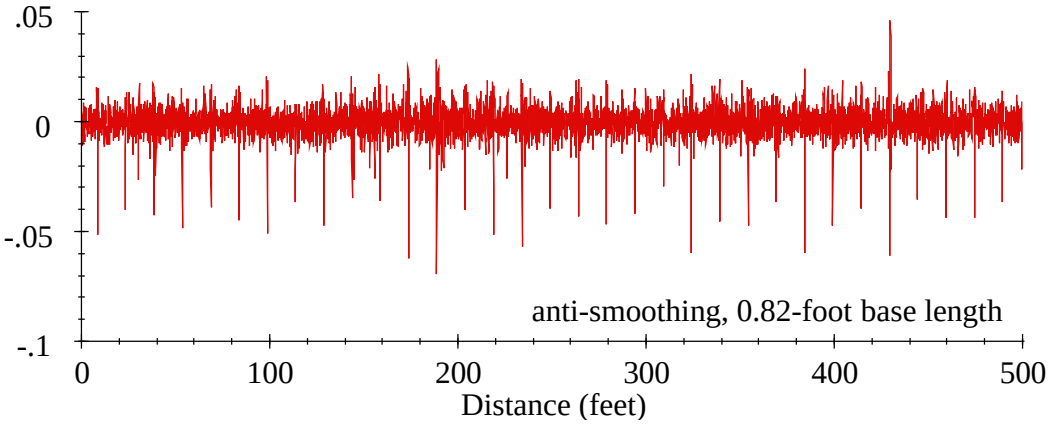

Figure 50. Graph. Profile with Additional Anti-Smoothing from Visit 03 of Right Side of Section 0213.

Figure 48 shows the profile after application of a smoothing filter with a base length of 25 ft. The filter greatly reduces the contribution of deviations that occur over 25 ft and shorter but preserves the trend. This plot shows a long bump followed by a long dip within the profile. This feature appears on both the left and right profiles throughout the monitoring history of section 0213, and it consistently

contributes to the overall IRI of the section. Together, the bump and dip make up a feature so long that the native filters applied to the profile during measurement affect their shape, although the native filters preserve the roughness that most affects IRI. For example, the largest change in this plot occurred between visit 08 (8-Nov-2001) and 09 (30-Oct-2002), when the high-pass filter applied by the profiler had changed.(17)

Figure 49 shows the profile after application of an anti-smoothing filter with a base length of 25 ft. This filter greatly reduces the contribution of deviations that occur over 25 ft and longer, which eliminates the trend and makes the upward curl in the 15-ft-long slabs more obvious.[1] In this plot, local peaks appear 15 ft apart, beginning about 9 ft from the start of the section and ending about 489 ft from the start of the section. These peaks represent the joints that surround the 32 slabs. Even though the vertical scale is much smaller in figure 49 than in figure 48, the contribution to IRI is much larger. For example, IRI of the trace in figure 49 is 104.7 inches/mi, and IRI of the trace in figure 48 is 26.6 inches/mi. Although the trace in figure 48 covers a larger vertical scale, the rapid reversals in the trace in figure 49 create greater roughness.

Figure 50 shows the profile after application of an anti-smoothing filter with a base length of 0.82 ft. Again, eliminating the longer wavelength content reduces the vertical range of the plot. This filter eliminates nearly all the content that affects IRI but retains the narrow dips that appear at the joints.

Inspection of filtered elevation profiles showed that upward slab curl existed throughout the monitoring history of section 0213 and that the level of curl was not consistent. Figure 51 shows part of the left-side profile traces from visits 12 (13-Aug-2006) and 13 (30-Dec-2007). The figure shows a distinct set of upwardly curled slabs. The figure also shows that the extent of curling at each slab is greater in visit 12 than in visit 13. The level of curl that appears on a pavement section is determined by a combination of diurnal, seasonal, and long-term effects. However, a change in temperature gradient may explain the difference in the profiles, since visit 12 took place before sunrise and visit 13 took place after sunrise.

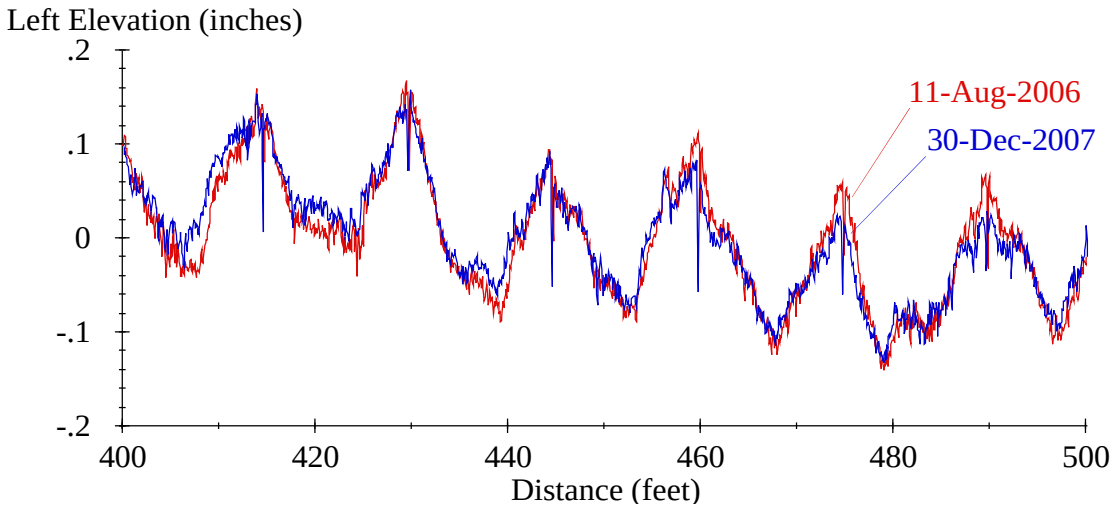

Figure 51. Graph. Changes in Curl on Section 0213.

[1] Distortion of jointed concrete pavement slabs includes curling, which is typically associated with cyclic thermal gradients; warping, which is typically associated with cyclic and long-term changes in moisture gradient; and a small portion of built-in unevenness. In this appendix, the term *curl* is used as shorthand for all three sources of slab distortion.

Over the 100 ft displayed in figure 51, IRI for visit 12 (13-Aug-2006) was 132.0 inches/mi, and IRI for visit 13 (30-Dec-2007) was 106.0 inches/mi. Over the entire section, the difference in IRI was 25.6 inches/mi, which demonstrates the influence a visually modest change in the curling within a profile can have on the roughness of a pavement section (see figure 10 and figure 11).

A PSD plot provides an alternative way of comparing the severity of slab curl within a profile. Figure 52 shows a PSD plot for the two profiles in figure 51. The plot is modified to show PSD of profile slope, rather than elevation, and it uses wavelength as the ordinate axis, instead of wave number (the reciprocal of wavelength). The plot displays spectral density in 24 bands per octave (i.e., 24 values for each increase in wavelength by a factor of 2, with uniform spacing along a logarithmic scale). The PSD plots for both visits include peaks at wavelengths of 15, 7.5, and 5 ft. The peak at 15 ft corresponds to the slab length. Additional peaks appear at 7.5 and 5 ft because the slabs do not curl into a sinusoidal profile. Instead, they curl into a shape that breaks down into an infinite series of sine waves that are as long as the slab, half as long, a third as long, and so on.

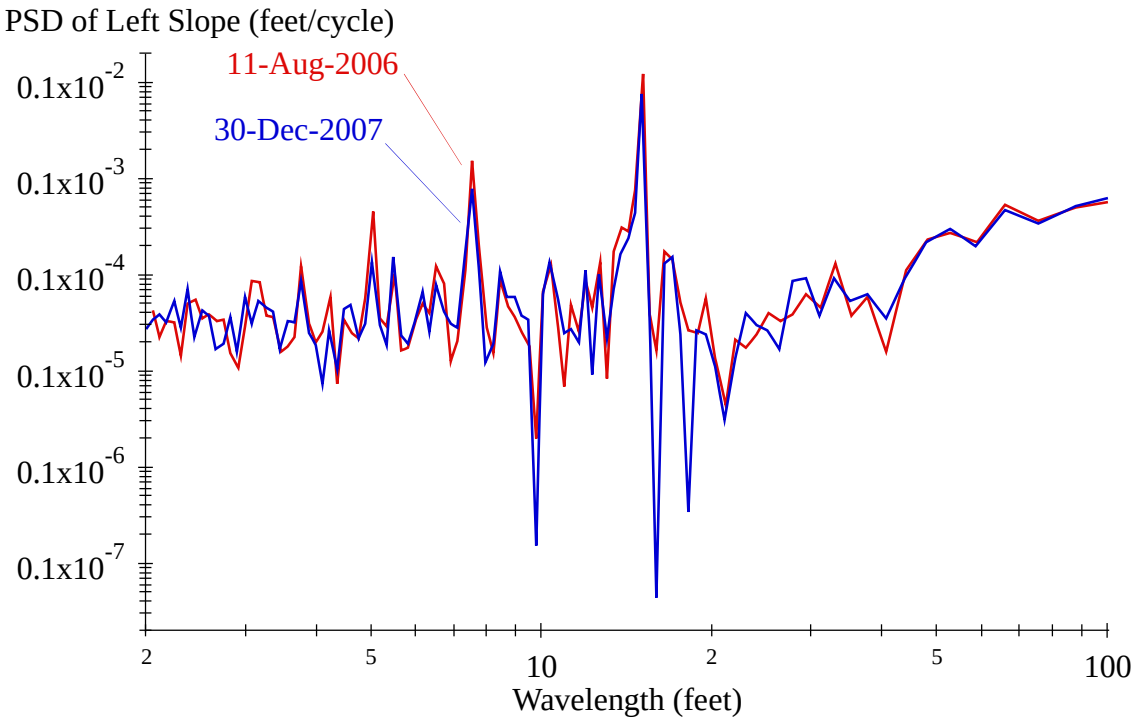

Figure 52. Graph. Slope Spectral Density of Section 0213.

Figure 52 displays the spectral content of the profile in a convenient manner in that values on the ordinate axis map directly to the characteristic length of known pavement features, such as joint spacing. The figure also shows that the influence of curling on variations in profile slope stands out over other profile features. However, the non-standard method of display in figure 52 distorts the relative contribution of each waveband to the overall profile.

Figure 53 provides a more standard display of PSD. The figure displays both axes on a linear scale and provides spectral density versus wave number. When the plots are displayed in this manner, the area under the curve for any range of wave numbers is proportional to the contribution the range makes to the overall mean square. Over the range that affects IRI, shown in figure 53, slab curl dominates the roughness of the section in both visits. Figure 53 also provides a more

representative view of the difference between visit 12 (11-Aug-2006) and visit 13 (30-Dec-2007). At a wave number of 0.066 cycles/ft, which corresponds to a wavelength of 15 ft, the plot for visit 12 has a value of 0.00125 ft/cycle and the plot for visit 13 has a value of 0.00076 ft/cycle. In terms of root mean square, this waveband therefore accounts for 28 percent more roughness in visit 12 than in visit 13.

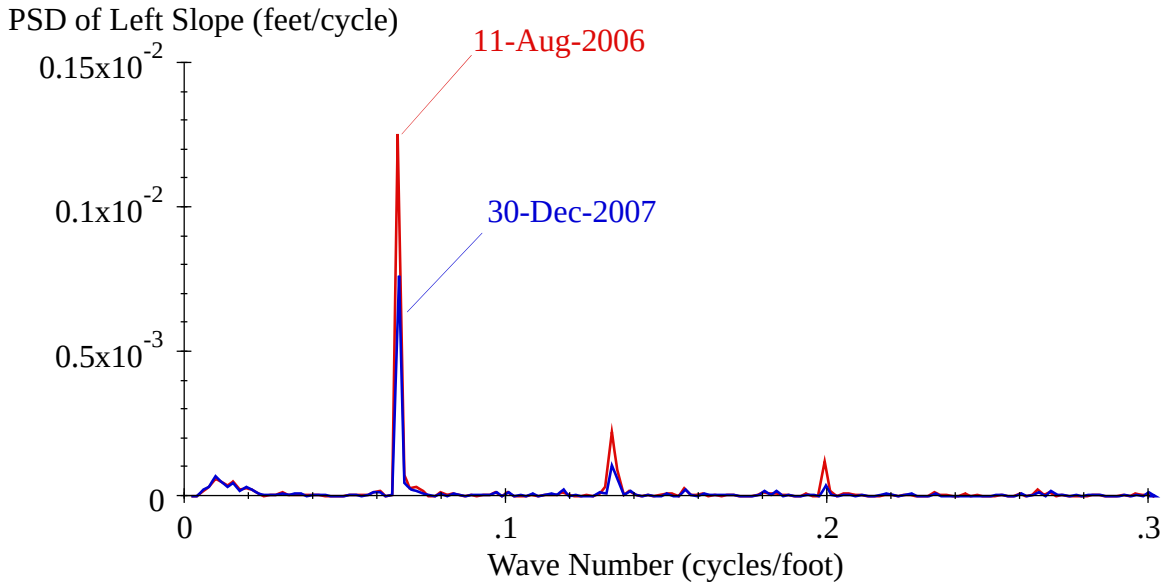

Figure 53. Graph. Slope Spectral Density of Section 0213 with Linear Scaling.

Section 0213 developed distress in the later part of the monitoring history. Starting in visit 12 (11-Aug-2006), narrow dips and groups of densely spaced narrow dips appeared in the right-side profiles. The right-side profiles from visit 12 included narrow dips at 35–47, 143–160, 243–246, 255, and 317–330 ft from the start of the section. These areas correspond to locations where the distress survey showed longitudinal cracking starting in 2004. Starting in 2008, longitudinal cracks appeared either in or near the right wheel path over the first two-thirds of the section. The cracks grew in width from 2008 onward, and some include missing material replaced by asphalt by 2011. Typically, the dips within the profile appear where the cracks wander into the center of the wheel path.

Figure 54 shows three repeat profiles from the right side of section 0213. The area from 143 to 160 ft includes several deep dips. The most severe features in this area appear with the same shape in all three measurements. However, some details of the profiles in this area are not perfectly repeated because they are caused by longitudinal cracks.

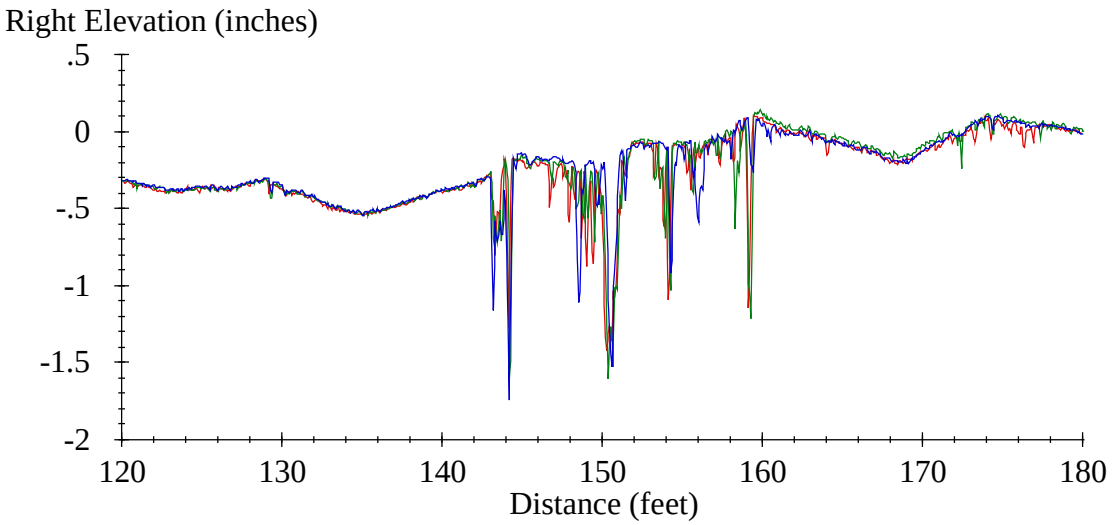

Figure 54. Graph. Right Elevation Profile for Three Repeats from Visit 12 of Section 0213.

A roughness profile provides a way to quantify the severity of isolated disturbances in a profile, such as the dips shown in figure 54. A roughness profile provides a continuous report of road roughness using a given segment length.[(18)] Instead of summarizing the roughness by providing IRI for an entire pavement section, the roughness profile shows the details of how IRI varies with distance along the section. It does this by displaying IRI of every possible segment of a given base length along the pavement, using a sliding window. Figure 55 shows the roughness profile using a 25-ft base length for the profiles shown in figure 54. With a 25-ft base length, isolated roughness is easy to identify and the area with the narrow dips stands out as much rougher than the surrounding area. The peak value in this area was about 600–700 inches/mi. Since this 25-ft-long area accounts for one-twentieth of the section length, this area contributes 30–35 inches/mi to the overall IRI of the section for these repeat measurements.

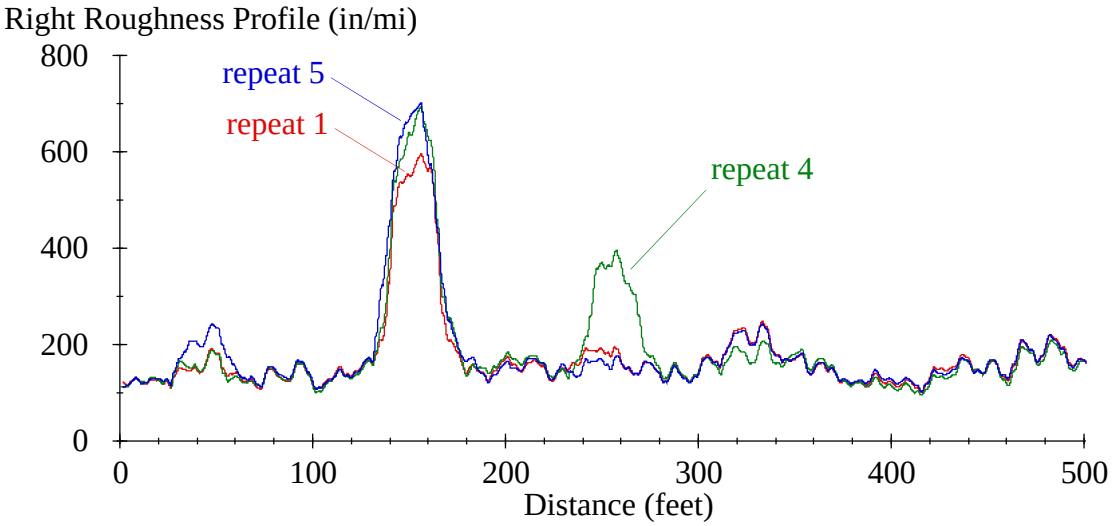

Figure 55. Graph. Right Roughness Profile for Three Repeats from Visit 12 of Section 0213.

One of the repeat measurements shown in figure 55 also includes an area of higher roughness about 250 ft from the start of the section. This is another patch of dips on a longitudinal crack that only one pass detected due to small variations in the tracking position of the profiler.

Inspection of roughness profiles showed that narrow dips at longitudinal cracks account for much of the increase in roughness after visit 11 (12-Dec-2004), although the dips were less severe overall in visit 13 than in visit 12. By visit 15 (25-Jan-2010), two additional areas of isolated roughness appeared along with the area shown in figure 55.

SECTION 0214

Section 0214 profiles included evidence of upward curl in early visits. However, the slabs in the first half of the section gradually changed from upward curl to downward curl, and the upward curl in the second half of the section diminished over time. The slabs changed most aggressively between visit 04 (4-Dec-1997) and visit 10 (4-Feb-2004). Figure 56 shows the right-side profile from visit 01 (25-Jan-1994), and figure 57 shows right-side profiles from visit 10 over part of section 0214. In this part of the section, all of the slabs changed from upward to downward curl.

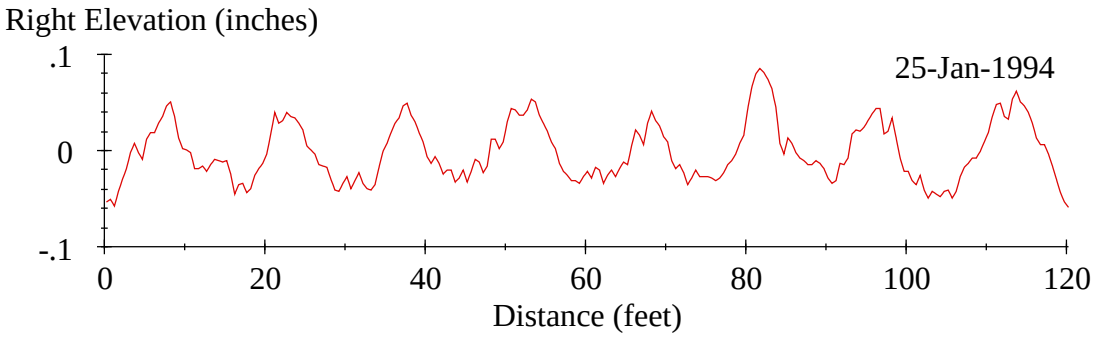

Figure 56. Graph. Right Elevation Profiles from Visit 01 of Section 0214.

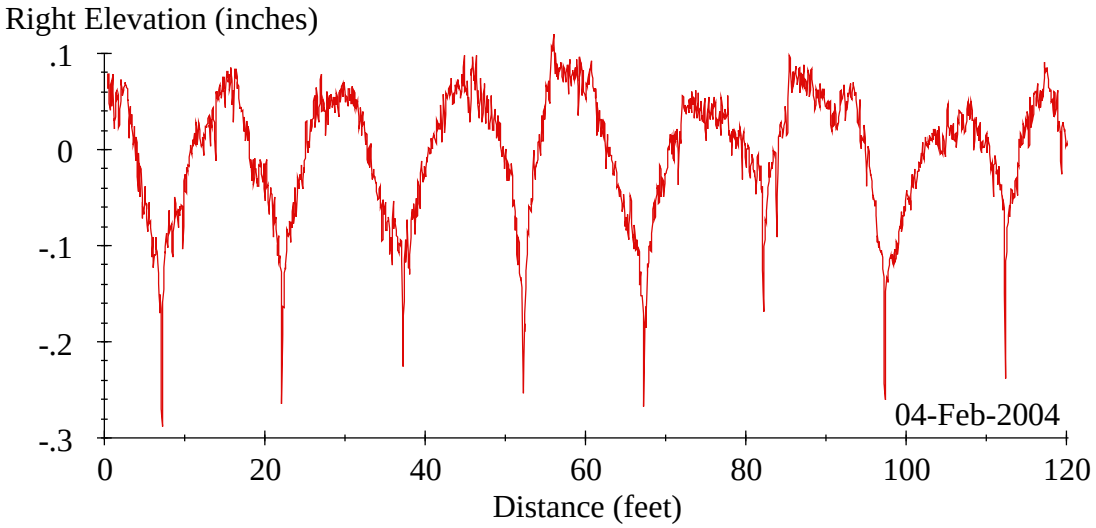

Figure 57. Graph. Right Elevation Profiles from Visit 10 of Section 0214.

Distress surveys noted map cracking on the section starting in 1997. The 1997 survey listed low-severity map cracking throughout the section. By 2008, the distress surveys listed high-severity map cracking in the first part of the section and map cracking in the wheel paths throughout the section. The 2008 distress survey also noted a rough transition from asphalt to concrete pavement upstream of section 0214 and proposed that the resulting dynamic loads imposed on section 0214 may have contributed to the cracking. Figure 58 shows the profile leading to section 0214 in

visit 09 (30-Oct-2002). The figure shows a distance of 0 ft at the section start. The rough features 60–80 ft upstream of the section would exacerbate truck dynamic loading. However, the role of dynamic loading in causing the map cracking is not clear.

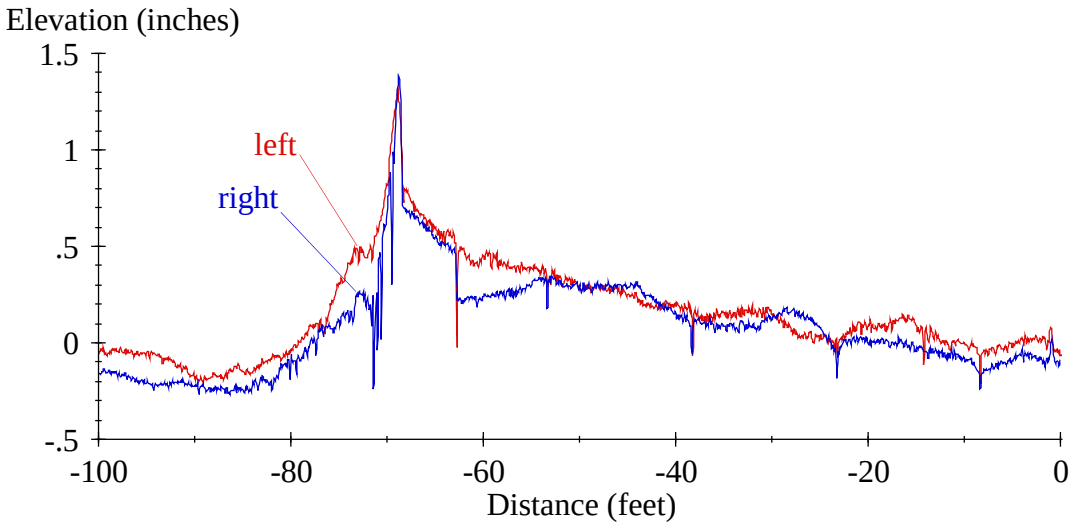

Figure 58. Graph. Profiles Leading to Section 0214.

SECTION 0215

Profile data for section 0215 included measurements on 16 additional SMP dates. On those dates, profiles were collected early (typically in the morning) and late (typically in the afternoon). Together with the 15 routine visits, the data include 47 sets of repeat measurements, with measurements every season in 1998 and from winter 2001 through winter 2004. Plotting of filtered profiles and PSD functions revealed that changes in slab curl caused most of the changes in the roughness of section 0215 over time.

Figure 59 shows the PSD plot for profiles measured in visits S05 (9-Jul-1998, 08:45) and S30 (15-Jul-2004, 09:07). The spectral content for these two profiles is very similar. In addition, the roughness level is about equal over the range shown in the figure, except at wavelengths equal to the slab length (15 ft) and half the slab length (7.5 ft). IRI for the earlier profile was 93.6 inches/mi, and IRI for the later profile was 129.4 inches/mi. Figure 59 shows that changes in slab curl caused most of the difference (see figure 12 and figure 13).

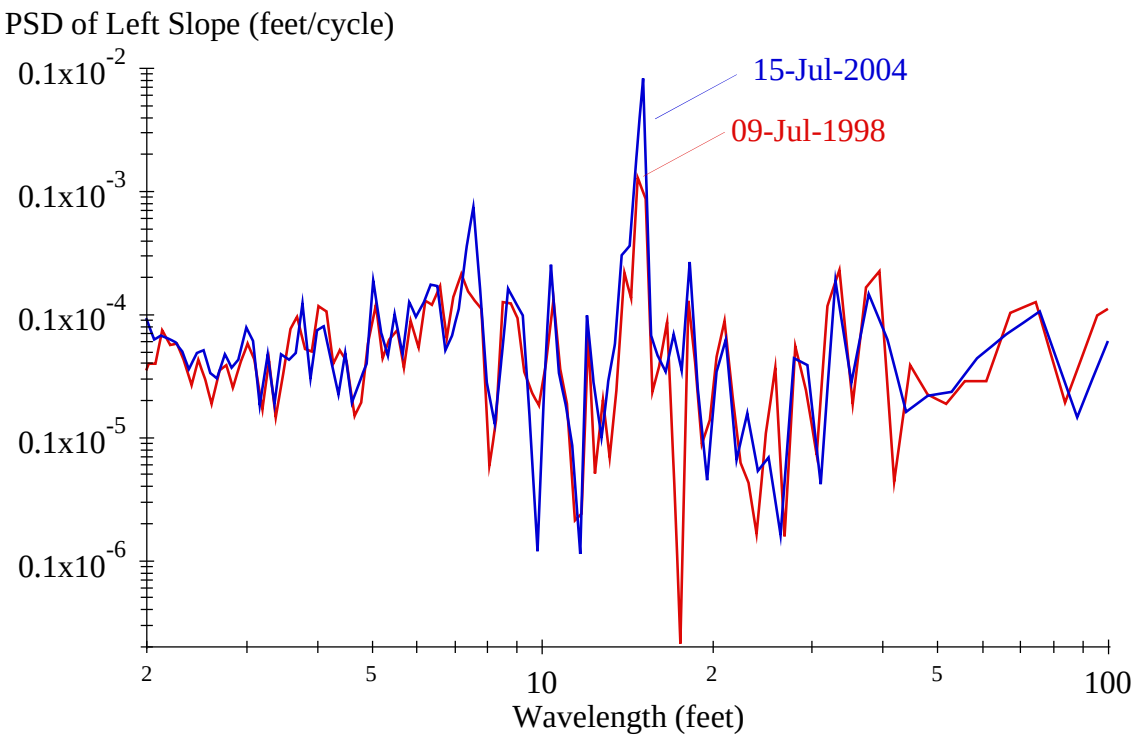

Figure 59. Graph. PSD Plots for Section 0215.

PSD plots of profiles from the 47 visits showed the following:

- The overall level of slab curl exhibited an increasing trend over time, but the trend was not orderly.
- The overall level of curl was higher in visits 12 (13-Aug-2006) and 14 (20-Sep-2008) than in visits 11 (12-Dec-2004), 13 (30-Dec-2007), and 15 (25-Jan-2010). Visits 12 and 14 occurred shortly after midnight, and visits 11, 13, and 15 occurred after sunrise.
- In many of the paired seasonal visits from the same date, the level of curl was higher in the early set of passes than on the following set of passes. This occurred in visits S01–S20, S27, and S28 but not in visits S21–S26, S29, and S30.
- Variations in IRI between visits followed the same trend as the severity of the peak value in the PSD plot at a wavelength of 15 ft.

SECTION 0216

No specific observations are provided for section 0216.

SECTION 0217

The 1997 distress survey recorded longitudinal and transverse cracks, and the level of cracking increased throughout the monitoring period. The 2002 distress survey also listed “map cracking throughout (the) section.”

Narrow dips appeared in both the left and right profiles at positions in the middle third of some slabs starting in visit 09 (30-Oct-2002). The dips appeared in locations where the distress surveys included transverse cracks, although not every transverse crack caused a dip. In visit 15 (25-Jan-2010), the most severe dips appeared 30 ft (0–1.3 inches deep), 407 ft (0–0.9 inches deep), 466.5 ft (0–0.15 inches deep), and 481.5 ft (0–0.6 inches deep) from the start of the section in the left-side profiles and 42–45 ft (0–0.7 inches deep), 238 ft (0–0.4 inches deep), 450 ft (0–1.3 inches deep), and 478 ft (0–1.6 inches deep) from the start of the section in the right-side profiles. The construction report listed transverse cracking in the LCB 480 ft from the start of section 0217 but not at the other locations.[1] Inspection of roughness profiles showed that none of the dips caused the short (25-ft)-interval IRI to exceed 2.5 times the section average.

Throughout the monitoring history, one slab along the right side of section 0217 contributed twice as much to the roughness of the section as the others. Figure 60 shows the right-side profiles from visit 01 (25-Jan-1994) and visit 14 (20-Sep-2008). Joints appear within the plot 444.3, 459.2, 474.2, and 489.3 ft from the start of the section. The slab that extends from 459.2 to 474.2 ft has upward curvature that registers as upward curling to an automated curling analysis based solely on slab profile. However, the upward curvature of this slab may have another cause because (1) no other slab on section 0217 exhibited a similar level of curvature, (2) the overall curvature of this profile along this slab did not change significantly with time, and (3) the left side profiles were relatively flat. The cause of the upward curvature cannot be determined without additional information, and the curling analyses presented in this report depend more heavily on changes in slab shape with time than on the nominal profiles.

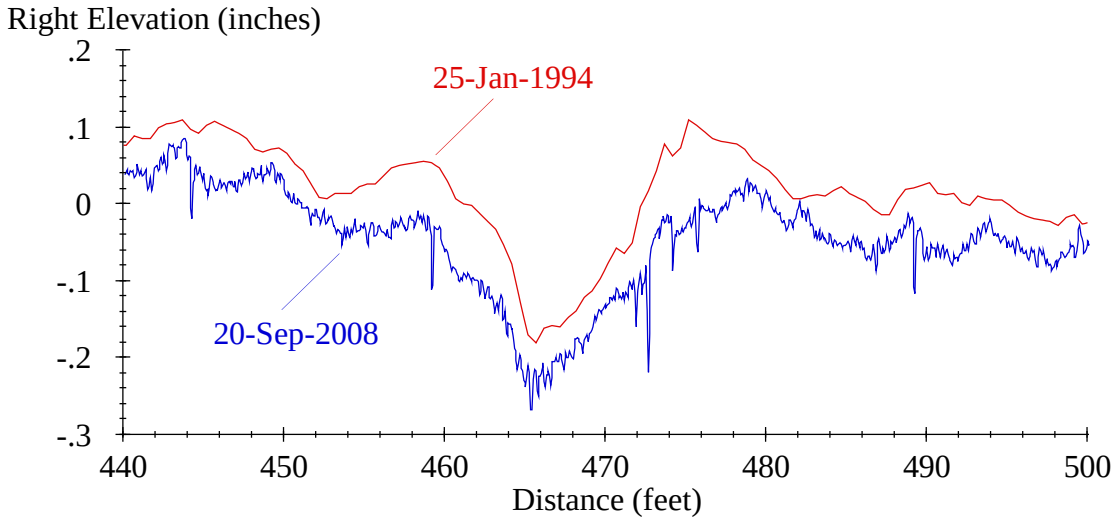

Figure 60. Graph. Right Elevation Profiles for Section 0217.

Profiles from section 0217 included noteworthy spectral content not caused by slab curl. Figure 61 shows the PSD plot for the left profile from visit 08 (8-Nov-2001). Slab curl caused the spikes at 15, 7.5, and 5 ft. Another spike appears at about 33 ft that rivals the others in amplitude. The contractor who built the test pavements confirmed that this was the approximate string line stake spacing. Content at this wavelength was strongest on section 0217, but lesser peaks appear in PSD plots from sections 0214, 0215, 0216, 0218, and 0220.

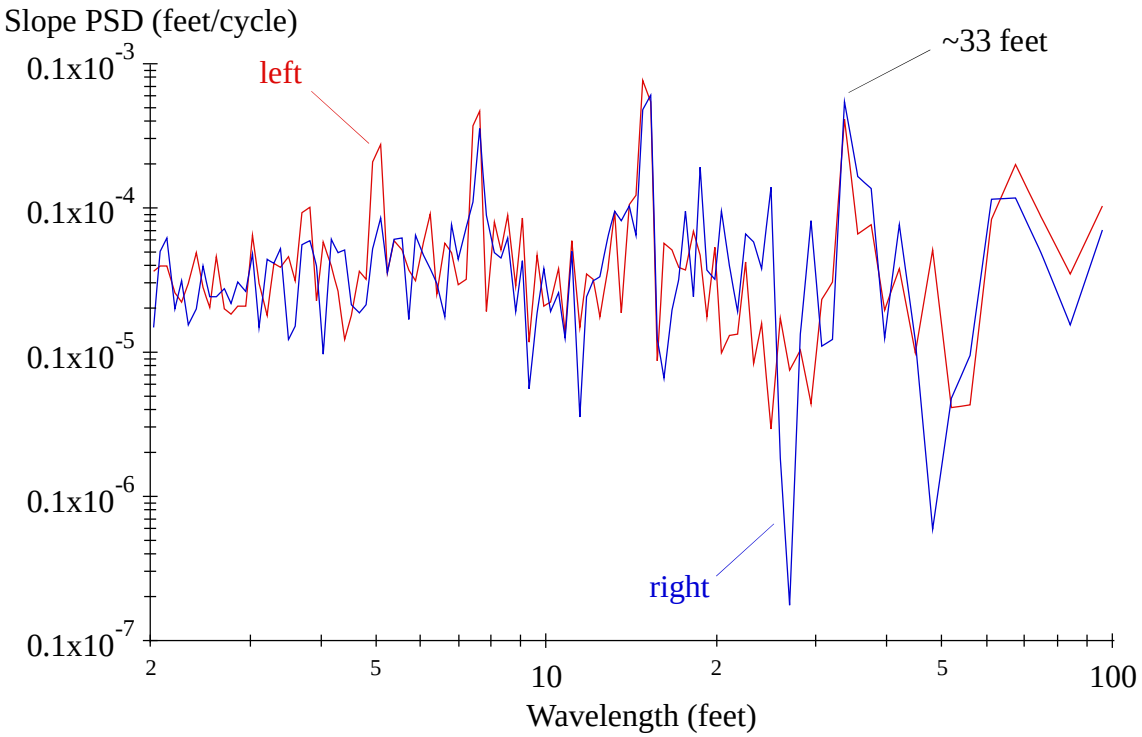

Figure 61. Graph. PSD Plots from Visit 08 of Section 0217.

SECTION 0218

The construction report listed 11 transverse cracks in the LCB within the monitoring range of section 0218.[(1)] Plotting of filtered profiles revealed no localized roughness and no systematic appearance of cracks in the surface layer.

SECTION 0219

Transverse cracks appeared in mid-slab positions on section 0219 beginning in 2002 and on about half of the slabs by the end of the monitoring period. The profiles included narrow dips at some of these locations, particularly on the right side, starting in visit 09 (30-Oct-2002). By visit 15 (25-Jan-2010) narrow dips appeared intermittently in the right-side profiles 195 ft (0–0.15 inches deep), 258 ft (0–0.2 inches deep), 316 ft (0–0.9 inches deep), 384 ft (0–0.3 inches deep), 406 ft (0–0.8 inches deep), and 466 ft (0–0.4 inches deep) from the start of the section. Distress surveys also noted map cracking over most of section 0219 by the end of the monitoring period, but the cracking was less obvious in the photos than on other sections.

SECTION 0220

Profiles from visit 04 (4-Dec-1997) included densely spaced positive and negative spikes at some joint locations on section 0220. Figure 62 shows an example. Similar disturbances appeared in the right-side profiles at the joints about 70, 115, 175, 220, 325, 384, 430, and 474 ft from the start of the section. These disturbances typically appeared in only one or two of the repeat measurements in visit 04 and sparingly in profiles from visit 05 (8-Dec-1998) but not in any of the other visits. They did not correspond to anything noted in the distress survey, although a distress survey in 2003 noted seal damage at joints. The construction report listed 13 transverse cracks in the LCB

within the monitoring range of section 0220.[(1)] Plotting of filtered profiles revealed no localized roughness and no systematic appearance of cracks on the surface.

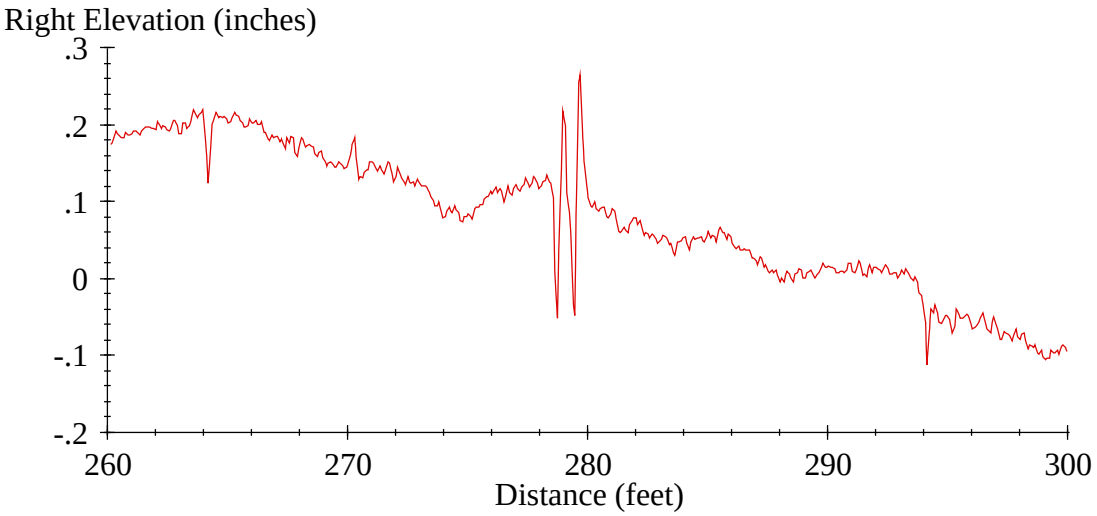

Figure 62. Graph. Profile from Visit 04 of Section 0220.

SECTION 0221

Distress surveys listed distress in the right wheel path of a slab from 410 to 425 ft from the start of section 0221 throughout the monitoring history and distress in neighboring slabs later in the monitoring period. In 1997, the survey noted “severe aggregate loss.” Every survey afterward showed scaling along the right side of that slab, and the survey in 2008 (including the photos) showed fiberglass patching at various locations. Figure 63 shows five repeat measurements of the right-side profile from visit 15 (25-Jan-2010). The dip 421 ft from the start of the section caused localized roughness, and the slab from 410 to 425 ft from the start of the section contributed to IRI 3 times as aggressively as the rest of the section.

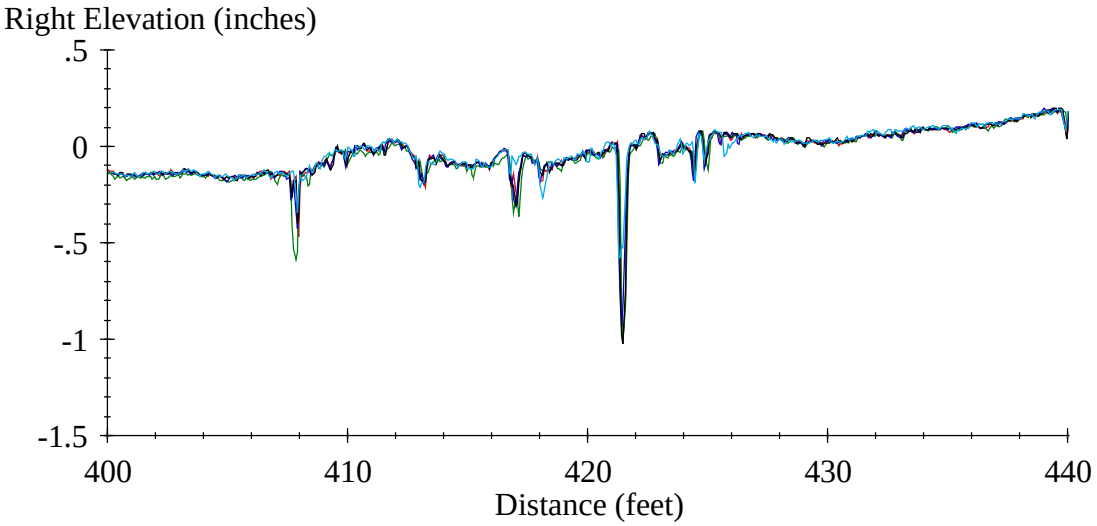

Figure 63. Graph. Right Elevation Profile for Five Repeats from Visit 15 of Section 0221.

SECTION 0222

Some profiles from visit 14 (20-Sep-2008) and visit 15 (25-Jan-2010) included a narrow dip up to 0.7 inches deep at a joint 325 ft from the start of section 0222. Nothing in the distress surveys distinguished this joint from the others, and the dips did not increase the roughness of the section.

SECTION 0223

No specific observations are provided for section 0223.

SECTION 0224

The left IRI value from visit 10 (4-Feb-2004) on section 0224 was 114 inches/mi. This value stood out because the right IRI was 71 inches/mi, the left IRI from visit 09 (30-Oct-2002) was 84 inches/mi, and the left IRI from visit 11 (12-Dec-2004) was 70 inches/mi (see figure 12). As shown in figure 64, a change in spectral content for wavelengths near 8 ft accounts for most of the difference. Although no other obvious explanation could be found, this content is most likely not caused by changes in slab curl, since it only appears on the left side of the lane. The content within the PSD plot at a 15-ft wavelength was not affected strongly, and the high content for wavelengths near 8 ft is not as concentrated as the upper harmonics caused by slab curl in the PSD plots shown for other sections. Furthermore, the peaks and valleys of the approximately 8-ft-long waves do not align with the joint locations in a consistent manner.

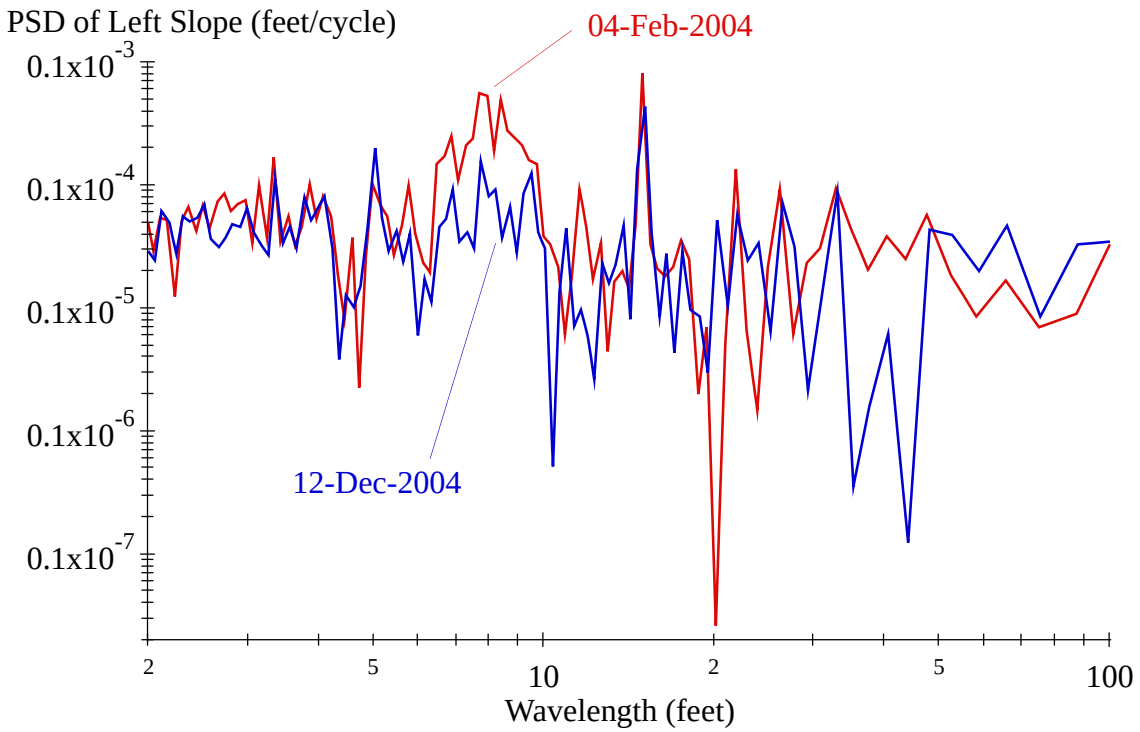

Figure 64. Graph. PSD of Left Slope for Section 0224.

SECTION 0260

The distress surveys reported low-severity raveling on section 0260 starting in 1995 and raveling with no severity qualification in both wheel paths starting in 2004. By 2008, the distress surveys reported significant distress in the left wheel path, and the photos showed fatigue, small potholes, patching, and pools of sealant in the left wheel path. The distress increased in severity by 2010, including more visible cracking along the left wheel path. These observations explain the steady rise in IRI of the left wheel path starting 11 years after the experiment began.

Some areas within the profile showed clear evidence of surface distress. For example, the area from 50 to 70 ft from the start of the section often included patches of narrow dips. The dips appeared starting in visit 06 (15-Nov-1999) on the left side and in visit 11 (12-Dec-2004) on the right side. The dips were not well repeated when they first appeared. However, by the end of the monitoring period, the profile over this segment had a consistent shape, which included a narrow dip 0.7 inches deep and a 3-ft-wide dip that was nearly 0.2 inches deep.

A rough area present since construction exists about 350 ft from the start of the section. Figure 65 shows the roughness profile at various ages, starting with the first profiling visit. The plot uses a 25-ft base length. The rough area progressed from a peak value of 118 inches/mi in visit 01 (25-Jan-1994) to 735 inches/mi by visit 15 (25-Jan-2010). Since the base length is equal to one-twentieth of the section length, this represents a progression in the contribution to overall IRI of the roughest area from 5.9 inches/mi to more than 36 inches/mi.

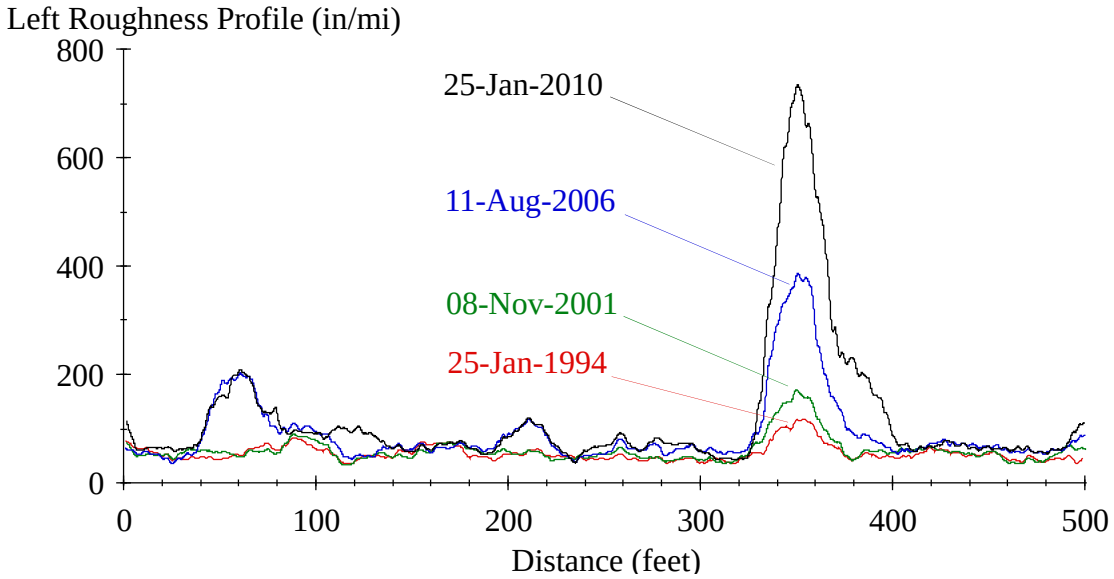

Figure 65. Graph. Left Roughness Profile for Section 0260.

Figure 66 shows profiles from visits 01 (25-Jan-1994) and 15 (25-Jan-2010). The initial disturbance is visible in the plot, although distress was not recorded there until 2000. However, it is not clear if the initial disturbance caused the roughness to progress by increasing the loading experienced at certain locations (i.e., a hot spot), if the disturbance was evidence of structural defects at that location (i.e., a weak spot), or both. In either case, figure 65 shows that the roughest area within section 0260 at the start of its service life progressed to the roughest area much later in its service life. (The peak value would stand out in the plot from visit 01 if not for the large vertical scale needed to accommodate the roughness in later visits.)

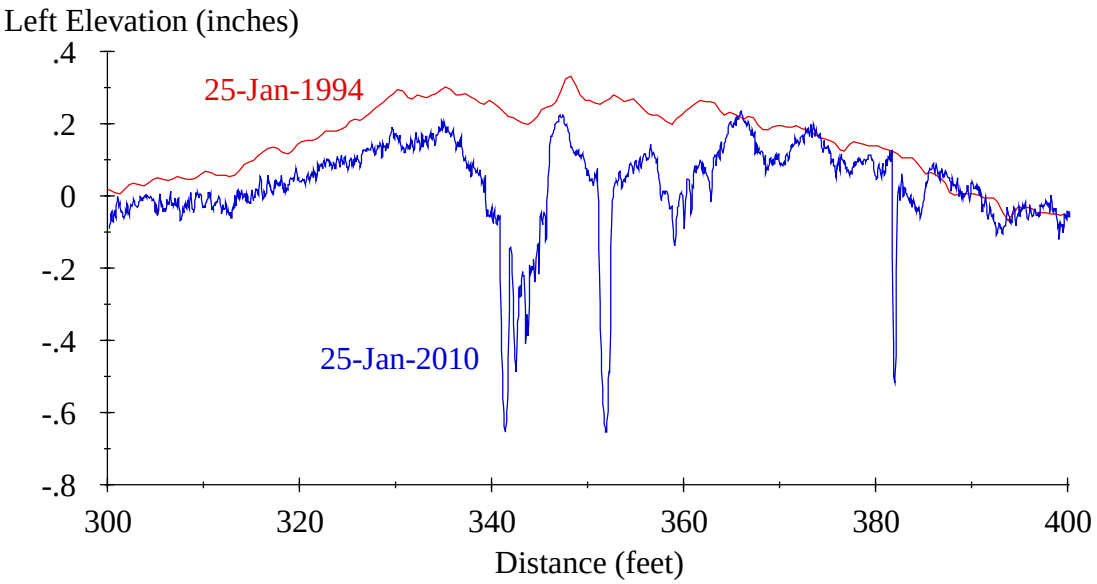

Figure 66. Graph. Left Elevation Profile for a Segment from Section 0260.

SECTION 0261

Distress surveys recorded longitudinal cracking in some areas of section 0261 starting in 1997 and transverse cracking at several locations after 2004. Dips appeared as depressions up to 5 ft wide with a narrow dip up to 1 ft wide in the majority of locations where the 2008 (and later) distress surveys showed transverse cracking. These dips appeared in the profiles starting with visit 11 (12-Dec-2004), and they were prominent late in the experiment. The dips exacerbated the roughness progression. Late in the experiment, localized roughness appeared about 325 ft from the start of the section, where a pothole developed.

The 1997 distress survey recorded the presence of six cores along the right wheel path near the end of the section. A longitudinal crack developed along the line of cores. This area was sealed, but the sealant eventually wore off. A series of bumps and dips appeared in the right-side profiles at that location that grew in roughness throughout the monitoring history.

SECTION 0262

Section 0262 faulted. Filtered profile plots showed that the faulting grew steadily throughout the experiment. Figure 67 shows five repeat profile measurements from a portion of section 0262 in visit 15 (25-Jan-2010). The figure shows a consistent level of faulting along the section and among the repeat measurements. Faulting caused much of the roughness and its progression on section 0262. Figure 68 shows a very short (8-ft)-interval roughness profile for the same set of measurements covered in figure 67. The figure shows the average contribution to IRI of each 8-ft-long segment as a function of the segment midpoint. The figure demonstrates that contributions to overall IRI of the section built up most aggressively at the joints.

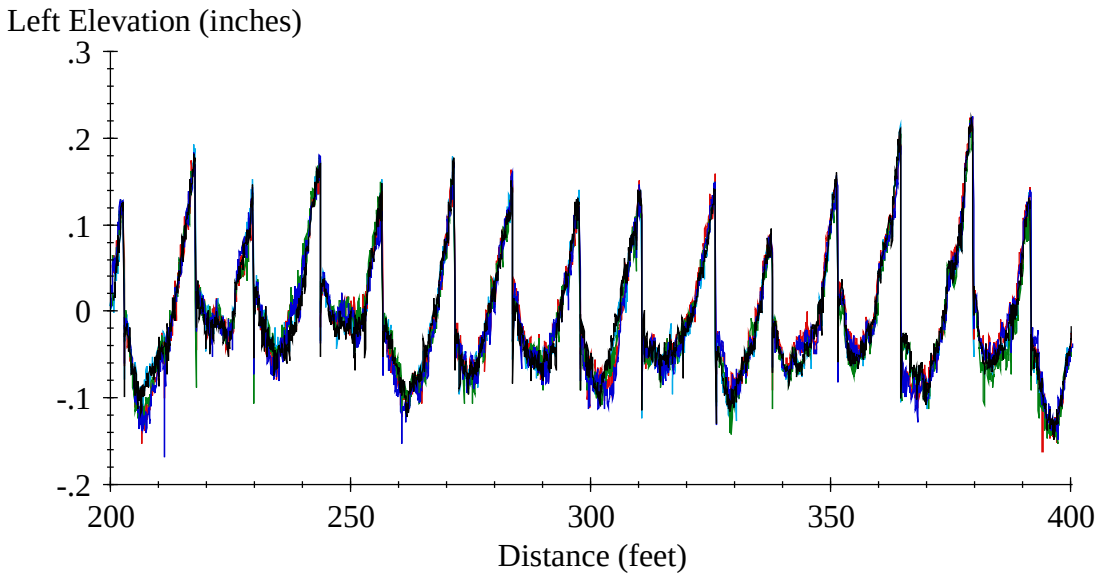

Figure 67. Graph. Left Elevation Profile from Visit 15 of Section 0262.

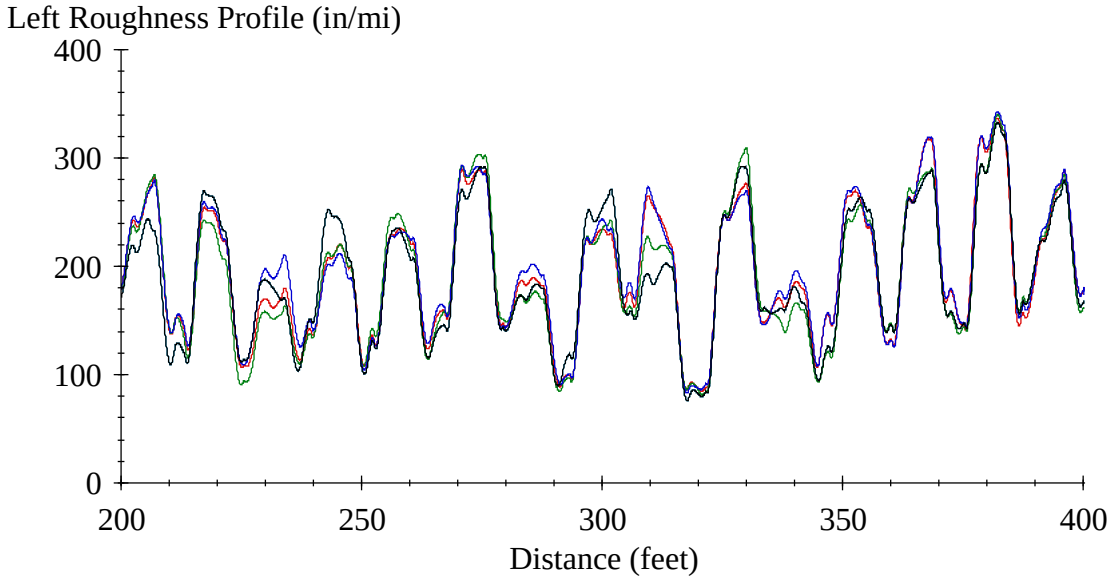

Figure 68. Graph. Left Roughness Profile from Visit 15 of Section 0262.

Starting in visit 12 (11-Aug-2006), the right-side profiles from section 0262 included a narrow dip at the joint 83 ft from the start of the section and a swatch of narrow dips over a half-slab from 129 to 137 ft from the start of the section. Both of these features appeared in areas where distress surveys recorded longitudinal cracking. The roughness at joints caused by the faulting obscured the roughness of these dips.

SECTION 0263

Section 0263 developed very little faulting relative to the other test sections without dowels (0262, 0264, and 0265). In contrast, elevation profile plots showed a high level of slab curl.

SECTION 0264

All profiles from the right side of section 0264 included a rise in elevation of more than 0.5 inches over a 7-ft distance starting 164 ft from the start of the section. The area that included this built-in feature was the roughest of the section throughout the experiment.

SECTION 0265

Section 0265 faulted. Filtered profile plots showed that the faulting grew steadily throughout the experiment. Like section 0262, faulting on section 0265 caused a large portion of the roughness progression. Figure 69 shows the roughness profile for section 0265 at various stages of the experiment. In this case, the roughness profile is plotted using a base length of 100 ft. Thus, every point along the plot represents IRI of a segment of pavement that starts 50 ft upstream and ends 50 ft downstream of that location. The 100-ft base length helps show the distribution of roughness throughout the section, but it is long enough to avoid local peaks caused by a single slab or joint.

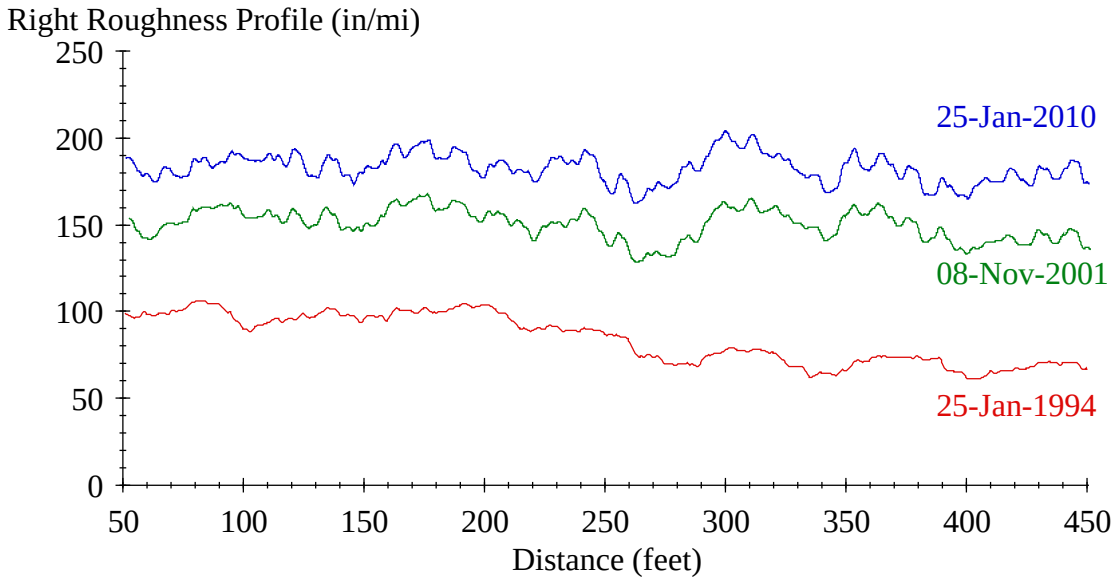

Figure 69. Graph. Right Roughness Profile for Section 0265.

Figure 69 demonstrates that in later visits roughness was distributed evenly along the section. This is because the magnitude of faulting was relatively consistent. The figure also demonstrates that roughness continued to increase throughout the section over the entire experiment.

In later visits, a patch of short-wavelength chatter appeared in the left-side profile within the slab from 314 to 328 ft from the start of the section. Distress surveys recorded scaling over this area and indicated “irregular surface characteristics” on the section. Portions of the section were diamond ground in an effort to alter the surface texture.

SECTION 0266

Section 0266 included a 60-ft-long bump beginning 400 ft from the start of the section. The bump was more than 0.6 inches high throughout the monitoring history. On the left side, a narrow dip appeared 438 ft from the start of the section and grew in severity over time. The dip appeared at

a joint where photos in the 2004 distress survey showed a gap in the sealant and some missing concrete at the aft side of the joint. PSD plots and filtered elevation profile plots showed that the curl on this section was more severe than it was on sections 0267 and 0268.

Distress surveys indicated “irregular surface characteristics” on the section. Diamond grinding was performed on the left wheel path from 405 to 450 ft from the start of the section to adjust the texture. In the photos, it appeared the grinding barely submerged the existing texture. As such, the grinding did not affect IRI.

SECTION 0267

A weigh-in-motion scale was installed in section 0267 between visit 11 (12-Dec-2004) and visit 12 (13-Aug-2006). The scales appeared 206 ft from the start of the section on the left side and 194 ft from the start of the section on the right side. The portion of the section upstream of the scales received diamond grinding as part of the installation procedure. Diamond grinding reduced the IRI of the first 200 ft of the section by about 20 inches/mi on the right side but had very little effect on the left side. Figure 70 shows the profile from visit 12 over a segment that includes the scale. In the figure, the scale is about 0.1 inches above the surrounding pavement and contributes some roughness to the section. The series of closely spaced peaks from 176 to 192 ft along the plot occurs in an area that includes the inductive loop and the approach slab.

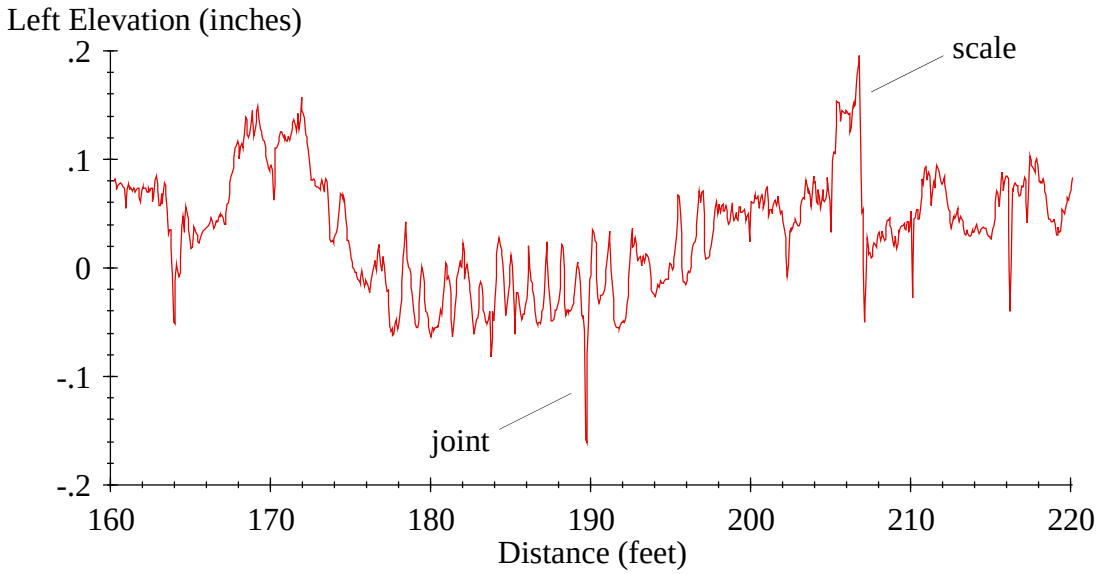

Figure 70. Graph. Weigh-in-Motion Scale on Section 0267.

SECTION 0268

No specific observations are listed for section 0268.

APPENDIX E. JOINT FINDING

The slab-by-slab analysis required careful synchronization of repeat profile measurements and identification of joint locations within a tight tolerance. The joint-finding strategy depended on the following properties of the profile data from each test section:

- Narrow dips appeared in the profiles at many of the joints.
- Repeat measurements on a given section were rigorously synchronized, and the repeated presence of a narrow dip at a given location and in the left- and right-side profiles provided evidence of a potential joint instead of a crack or erroneous sensor reading.
- Narrow dips (i.e., negative spikes) that corresponded to joints appeared in a regular pattern that corresponded to the joint spacing.

The strategy for assembling a list of joint positions exploited the repeated presence of negative spikes at the same location. Each group of five profile measurements from a given visit of a given section formed a set, including both the left- and right-side profiles. For each set of 10 profiles, a list of joint positions for the entire set was found using the steps described in this chapter.

STEP 1: FILTER THE PROFILES

High-pass filter each profile with an anti-smoothing moving average filter using a base length of 0.82 ft.

STEP 2: NORMALIZE

Normalize each filtered profile by its standard deviation. Figure 71 provides an example trace that has been high-pass filtered and normalized. The figure shows the trace produced after application of steps 1 and 2 to a profile from visit 15 of section 0215.

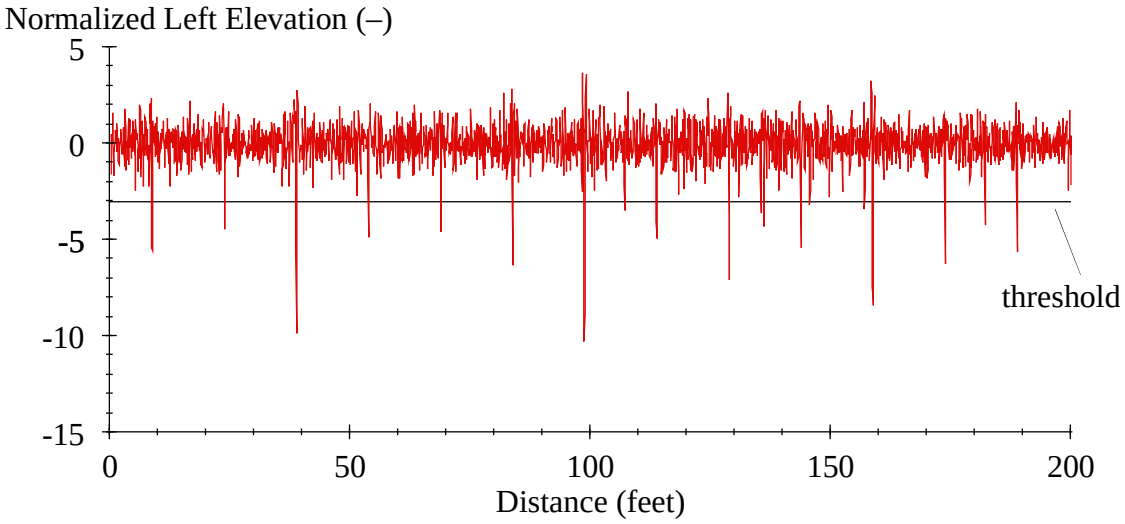

Figure 71. Graph. High-Pass Filtered, Normalized Profile.

STEP 3: SEEK THE NEGATIVE SPIKES

Search the normalized trace. List the longitudinal position of points with a value below -3. This criterion produces a list of longitudinal positions with regular spacing for the trace in figure 71, with some extraneous locations. Extraneous locations often appeared in the list at transverse joints and in multiple locations along distressed slabs.

The threshold value of -3 was used throughout the experiment. The appropriate threshold value for other experiments depends on the length and depth of the gaps at the joints and on the profiler height-sensor footprint, low-pass filtering, and recording interval.

STEP 4: WEED OUT LESSER SPIKES

Eliminate any spike within 0.82 ft of a deeper spike.

STEP 5: AGGREGATE ACROSS THE REPEAT MEASUREMENTS

Assemble the negative spikes for the left and right profiles of all five repeat measurements into a single list. For sections with skewed joints, offset values of longitudinal position for the left side by 0.919 ft. Sections 0262–0265 included skewed joints.

STEP 6: SORT THE LIST

Sort the list of negative spikes in ascending order of longitudinal position.

STEP 7: CONSOLIDATE GROUPS OF NEARBY SPIKES

Consolidate any set of closely spaced spike positions into a group. Merge spike positions for which no gap larger than 1.97 inches exists between consecutive values. For each group, record the range of longitudinal position values and the number of spikes included in the group. To do this, apply the following steps:

- Step 7a: Establish an open group using the first item in the list.
- Step 7b: Promote the next item on the list to the current item. If the list is complete, close the final group.
- Step 7c: If the current item is no more than 1.97 inches downstream of the previous item, add it to the open group and return to step 7b.
- Step 7d: If the current item is more than 1.97 inches downstream, close out the current group. Open a new group with the current item as the first member. Return to step 7b.

This procedure often produces groups that cover a greater longitudinal distance than 1.97 inches but without any gaps within the group greater than that.

Besides the range, record the average value of longitudinal position within each group. These values provide a basis for calculating the actual slab length in subsequent analyses.

On visit 04 of section 0264, the threshold gap value was adjusted to 3.15 inches.

STEP 8: TRIM THE LIST

Eliminate all groups with a count below a given threshold. The threshold value that produced the proper results varied from 2 to 6. Because the joint locations were derived using sets of 10 profiles, this meant retaining groups for which 20–60 percent of the profiles contributed spikes. The most common threshold value was 20 percent. Table 31 provides sample output of step 8 for visit 15 of section 0215.

Table 31. Negative Spike Groups from Visit 15 of Section 0215.

Range (ft)		Average Position (ft)	Number of Spikes	Compatibility Score
Start	End			
-21.04	-20.84	-20.90	10	35
-10.83	*-10.70*	*-10.76*	*2*	*2*
-6.08	-5.82	-5.92	10	35
8.94	9.13	9.07	7	35
24.02	24.22	24.15	10	35
38.98	39.18	39.08	10	35
54.00	54.20	54.11	8	35
69.02	69.22	69.13	10	35
82.16	*82.16*	*82.16*	*2*	*5*
83.98	84.17	84.10	8	35
98.93	99.13	99.05	10	35
104.01	*104.07*	*104.04*	*2*	*0*
113.96	114.15	114.08	9	35
129.04	129.17	129.13	8	35
144.00	144.13	144.08	10	35
158.95	159.15	159.08	8	35
173.98	174.17	174.09	10	35
189.00	189.19	189.10	10	35
204.02	204.08	204.06	5	35
219.04	**219.23**	**219.14**	**9**	**36**
233.86	234.06	233.97	10	36
248.95	249.08	249.01	9	36
263.78	263.97	263.88	9	36
278.80	278.99	278.91	10	36
293.82	294.01	293.93	7	36
308.77	308.97	308.89	10	36
323.80	323.93	323.88	9	36
338.82	339.01	338.93	10	36
353.84	353.97	353.91	7	36
368.79	368.99	368.92	10	36
383.88	383.94	383.91	8	36
398.84	399.03	398.92	9	36
413.79	413.92	413.86	10	36
420.36	*420.42*	*420.38*	*3*	*3*
428.81	428.94	428.88	10	36
436.49	*436.62*	*436.53*	*3*	*5*

Table 31. Negative Spike Groups from Visit 15 of Section 0215—Continued.

Range (ft)		Average Position (ft)	Number of Spikes	Compatibility Score
Start	**End**			
443.77	443.90	443.84	10	35
458.85	458.99	458.91	10	36
473.81	473.94	473.86	10	36
479.79	*479.79*	*479.79*	*2*	*5*
488.77	488.90	488.85	8	36
495.27	*495.33*	*495.29*	*3*	*3*
503.79	503.98	503.88	9	36
505.41	*505.41*	*505.41*	*2*	*2*
510.42	*510.55*	*510.49*	*4*	*3*
512.05	*512.24*	*512.10*	*5*	*3*
515.17	*515.43*	*515.28*	*5*	*2*
518.55	518.87	518.74	9	19

Note: Bold row indicates the group designated as joint location. Italic rows indicate the groups left out by steps 11 and 12.

STEP 9: EVALUATE EACH GROUP ON THE LIST

Calculate a compatibility score for each surviving group. To do this, seek other groups that appear at the expected distances from the group under evaluation within an acceptable tolerance, given the expected saw cut spacing. The tolerance for compatibility was set at 2 percent of the average expected saw cut spacing. (This was 0.27 or 0.30 ft, depending on the section.)

The compatibility score is the number of compatible groups found within the rest of the list. For example, the expected saw cut spacing on section 0215 was 15 ft. The first group in table 31 produced a compatibility score of 35, because 35 other groups appeared within the list that were an integer multiple of 15 ft away, to within 0.3 ft.

Sections 0213–0224 included slabs that were all about 15 ft long. However, the saw cuts in sections 0262–0265 appeared in intervals of about 12, 14, 13, and 15 ft, and the saw cuts in sections 0266–0268 appeared in intervals of 15, 13, 15, and 17 ft. Each group was evaluated four times on sections with irregular joint spacing, once for each of the possible starting points within the pattern. The algorithm retained the highest of the four scores.

STEP 10: DESIGNATE ONE OF THE GROUPS AS A JOINT LOCATION

Designate the group with the highest compatibility score as a joint. If multiple groups share the highest compatibility rating, select the joint that is farthest upstream. For visit 15 of section 0215, a joint was selected that produced negative spikes from 219.04 to 219.23 ft from the start of the profile.

STEP 11: SEEK OTHER JOINTS DOWNSTREAM

Seek the adjacent joint in the forward direction. Designate the adjacent joint as the group with the highest compatibility score that appears between the shortest expected joint spacing for the section (minus 6 percent of its length) and the longest expected joint spacing for the section (plus 6 percent

of its length). Each time a joint is found, seek the next joint using the same criteria until the end of the section is reached.

The search for the next joint location covered a range of 14.1–15.9 ft from the current joint location on sections 0213–0224; the range was 12.72–15.90 ft on sections 0262–0265; and the range was 13.79–18.02 ft on sections 0266–0268.

STEP 12: SEEK OTHER JOINTS UPSTREAM

Repeat step 11 in the reverse direction.

DISCUSSION

This procedure produced a list of joints for each set of five repeat measurements. However, the locations were expressed as a range rather than a precise value. For example, the joint locations listed in table 31 include spike groups that cover a range of 0.130–0.325 ft (2 to 5 times the profile recording interval). The range for spike groups in this experiment typically covered a distance of less than 0.33 ft.[2]

The range at each joint proved to be important in the subsequent slab-by-slab curve fitting analysis, where the profile at each end of the slab was masked over the range where the spikes were detected plus a 0.082-ft-long margin of safety. The average position within a group of spikes was used at each joint to provide slab end locations for calculating overall slab length.

The strategy of searching for narrow dips was successful in all of the profiles after visit 02 because profile data were recorded at a short interval (0.77 or 0.98 inches) and measured using a height sensor with a footprint with a longitudinal dimension equal to or less than the gap at the joint.(17) The joint-finding strategy described here is not suited for profiles measured with the K.J. Law Engineers DNC 690. As a result, the joint locations found for visit 03 of each section were also used in the analysis of visit 01 and visit 02. This practice was successful because the synchronization was very consistent between visits and because the longer recording interval (6 inches) in visits 01 and 02 reduced the requirement on precision of the joint locations.

[2] Of the 10,539 joints, 10,200 covered a range of 0.33 ft or less.

APPENDIX F. PSG ESTIMATION

Analyses were performed to segregate and quantify the portion of roughness caused by slab curl and warp within a profile and the portion associated with other sources of roughness such as built-in defects and surface distress.

The level of curl and warp present within each profile was estimated using slab-by-slab analysis of local profile segments. The automated procedure described in appendix D isolated the profile of each slab by seeking the locations where negative spikes appeared repeatedly in the same locations. The procedure described in this chapter quantifies the level of curl and warp on each slab using PSG, which is the gross strain gradient required to deform a slab into the shape that appears within its measured profile from a flat baseline.

Using PSG to quantify curl and warp represents an approach similar to the calculation of equivalent temperature gradient from measured slab profiles.[19,20] PSG is used rather than equivalent temperature gradient because this study sought to relate curl and warp to IRI rather than relate content within the profile to the environment in which the pavement functions.

Other examples of this analytical strategy for processing slab profiles have been documented by Sixbey and Vandenbossche.[21,22] Those studies applied curve fitting to profiles of individual slabs using appropriately selected polynomials to represent idealized slabs with a strain gradient. The specific approach applied in this study uses an idealized profile for a slab with curling and warping proposed by Westergaard in the classical literature.[23] With only minor exceptions, the step-by-step procedure used in this study follows the analysis methods proposed by Rasmussen and applied by Chang.[2,24] Portions of this appendix duplicate the descriptions by Chang, with additional specific information pertinent to this study.[2,24]

WESTERGAARD

The curve fitting procedure for measured slab profiles used an idealized shape proposed by Westergaard.[23] The idealized profile is based on the assumption of a linear temperature and moisture gradient through the depth of the slab, unrestrained slab ends, and an infinite slab along the undeformed axis. Westergaard provided the solution for an infinitely long pavement of finite width. This study applies the solution to an infinitely wide slab of finite length.

The idealized profile relates the slab elevation (z) to position along the slab as shown in figure 72.

$$z = -z_0 \frac{2\cos\lambda\cosh\lambda}{\sin 2\lambda - \sinh 2\lambda}\left[(-\tan\lambda + \tanh\lambda)\cos\frac{x}{l\sqrt{2}}\cosh\frac{x}{l\sqrt{2}} + (\tan\lambda + \tanh\lambda)\sin\frac{x}{l\sqrt{2}}\sinh\frac{x}{l\sqrt{2}}\right]$$

$$z_0 = \frac{-(1+\mu)(\alpha\Delta T + \Delta\varepsilon_{sh})}{h}l^2 \qquad \lambda = \frac{b}{l\sqrt{8}} \qquad l = \sqrt[4]{\frac{Eh^3}{12(1-\mu^2)k}}$$

Figure 72. Equation. Relationship of Slab Elevation to Position.

Where:

x is the horizontal coordinate along the slab profile, referenced to the slab center (L).

z_0 is the uplift at the slab ends (L).

l is the radius of relative stiffness (L).

b is the slab width (used as slab length here) (L).

E is slab elastic modulus (F/L^2).

μ is Poisson's ratio (–).

k is the modulus of subgrade support ($F/L^2/L$).

Figure 72 is a specialized version of the Westergaard solution that includes both moisture gradient ($\Delta\varepsilon_{sh}/h$) and temperature gradient ($\alpha\Delta T/h$).

The four independent pavement properties *b*, *E*, μ, and *k* are parametric inputs needed to estimate *l*. The curve fitting procedure applied in this study assumes a fixed value for the five aforementioned parameters along a pavement section and seeks the optimal value for total strain gradient on each slab segment as shown in figure 73.

$$PSG = \frac{(\alpha\Delta T + \Delta\varepsilon_{sh})}{h}$$

Figure 73. Equation. PSG.

PSG is given the prefix "pseudo" because it is estimated empirically.

SLAB-BY-SLAB ANALYSIS

The PSG associated with each slab profile was estimated using the following procedure.

Step 1: Crop

Crop the profile of the slab to exclude the negative spikes at the joints. Appendix E describes the procedure for determining the location of the joints. Set the profile starting point to the end of the spike group found at the leading joint plus a small offset. Set the profile ending point to the start of the spike group found at the trailing joint minus a small offset. This study applied an offset of 1 inch.

Step 2: Shift

Shift the longitudinal scale to place the slab center at a value of 0. Assume that the center of the slab is at the midpoint between the two average spike position values, derived as described in appendix E. Figure 74 shows an isolated slab profile after offset of the longitudinal scale.

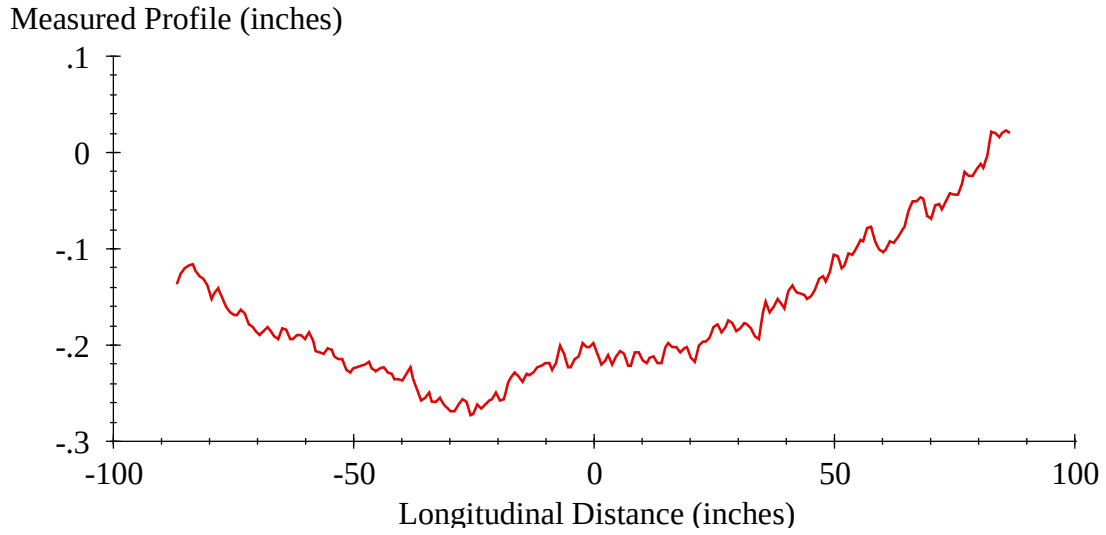

Figure 74. Graph. Measured Slab Profile for Section 0215.

Step 3: Detrend

Detrend the isolated profile. Apply a least-squares linear fit to the profile segment and subtract the best-fit line point by point. The resulting signal will have a zero mean. Figure 75 shows the detrended profile.

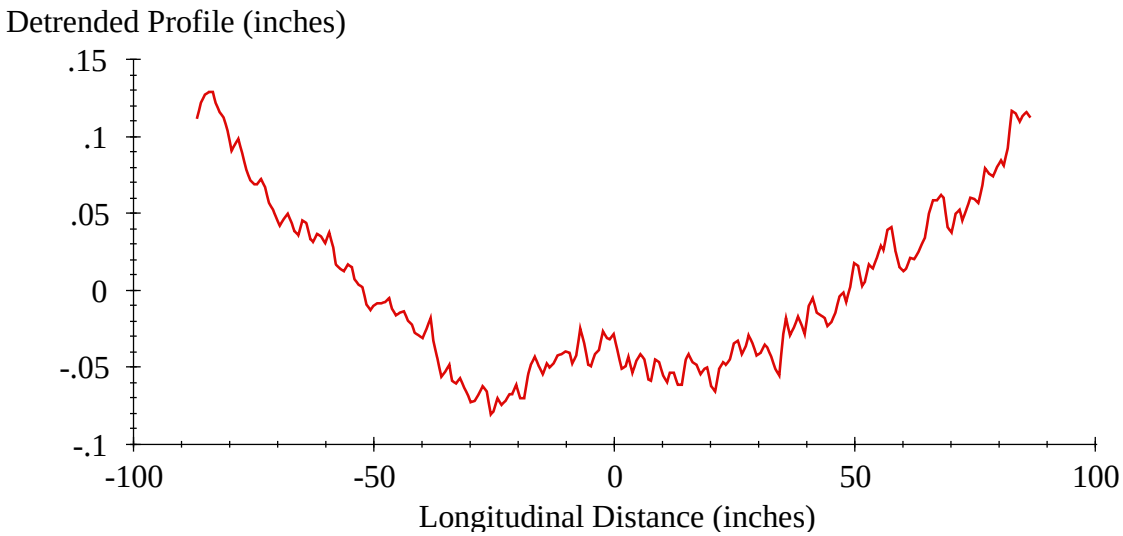

Figure 75. Graph. Detrended Slab Profile for Section 0215.

Step 4: Estimate Pavement Properties

Estimate the pavement properties needed to apply the Westergaard equation for the slab under examination. The LTPP database includes measurements of elastic modulus (E), Poisson's ratio (μ), and slab thickness (h) for each section. For this study, these values were held constant for all slabs within a given section. Values for modulus of subgrade support (k) were not available, and a value of 200 psi/inch was used for the entire experiment. Table 32 lists the values of E, μ, and h for each section, as well as the radius of relative stiffness (l).

Table 32. Pavement Properties.

Section	Elastic Modulus (ksi)	Poisson's Ratio (–)	Slab Thickness (inches)	Radius of Relative Stiffness (inches)
0213	5,100	0.15	7.9	32.2
0214	4,100	0.13	8.3	31.6
0215	4,850	0.15	11.0	40.7
0216	4,300	0.19	11.2	40.2
0217	5,050	0.16	8.1	32.7
0218	4,050	0.14	8.3	31.5
0219	4,900	0.14	10.8	40.2
0220	4,150	0.15	11.2	39.7
0221	4,750	0.15	8.1	32.2
0222	4,075	0.135	8.6	32.4
0223	5,000	0.14	11.1	41.3
0224	5,150	0.15	10.6	40.2
0262	5,150	0.09	8.1	32.7
0263	5,300	0.12	8.2	33.3
0264	5,250	0.13	11.5	42.9
0265	4,300	0.16	10.8	39.0
0266	4,900	0.15	12.3	44.4
0267	5,350	0.13	11.3	42.5
0268	4,850	0.13	8.5	33.5

The joint-finding procedure provided the length of each slab (b). To obtain slab length, calculate the longitudinal distance between the average spike positions at the leading and trailing joint. Each slab requires a distinct estimate.

Step 5: Curve Fit

Perform a non-linear curve fit of the Westergaard model to the measured slab profile. This provides an estimate of the PSG required to optimize the linear fit. In this study, curve fitting was performed using functions MRQMIN and MRQCOF provided in *Numerical Recipes*.[25]

Figure 76 shows a sample curve fit for a slab on section 0215. For this slab, the routine used a slab length of 15.1 ft and radius of relative stiffness of 40.7 inches. For this slab, the routine returned a PSG value of 70.57×10^{-6} in units of strain per inch or 70.57 με/inch.

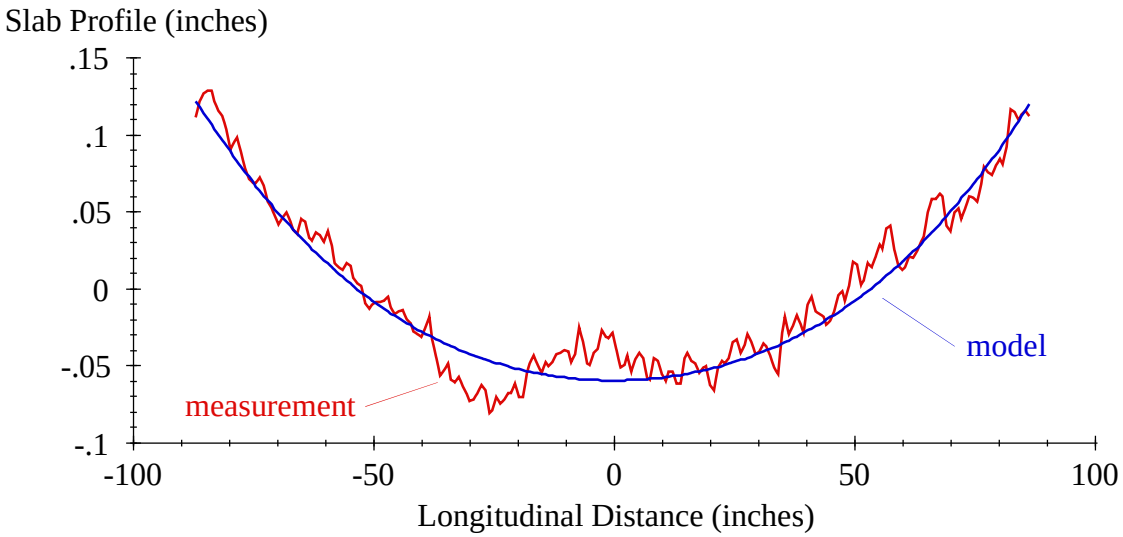

Figure 76. Graph. Curve Fit for Section 0215.

SUMMARY INDEX

Summary PSG values for a section were compiled using a weighted average of the absolute slab-by-slab PSG values. A weighting factor was applied to the PSG values in proportion to their length, relative to the overall section length. For slabs that appeared at the ends of a section, a weighting factor was applied to the PSG values in proportion to the length that appeared within the section, relative to the overall section length.

ACKNOWLEDGEMENTS

The authors of this report would like to thank ADOT and FHWA for their support of this work. This research was originally instigated by ADOT, who supported the work needed to organize the data set, study trends in roughness values, and apply traditional analysis methods to the profile data. Subsequently, the FHWA supported a continuation of the work, including detailed analysis of the influence of curling, warping, and faulting on the development of roughness.

REFERENCES

1. Szrot, R.B. (1994). *Construction Report for Experiment SPS-2,* Nichols Consulting Engineers, Reno, NV.

2. Chang, G., Rasmussen, R., Merritt, D., Garber, S., and Karamihas, S. (2010). *Impact of Temperature Curling and Moisture Warping on Jointed Concrete Pavement Performance*, TechBrief, Publication No. FHWA-HIF-10-010, Federal Highway Administration, Washington, DC.

3. Karamihas, S.M. and Senn, K. (2009). "Profile Analysis of Arizona Specific Pavement Studies 5 Project." *Transportation Research Record 2095*, pp. 144–152, Transportation Research Board, Washington, DC.

4. Karamihas, S.M. (2007). *Profile Analysis of the LTPP SPS-1 Site in Arizona*, Report No. UMTRI-2007-16, University of Michigan Transportation Research Institute, Ann Arbor, MI.

5. Karamihas, S.M. (2007). *Profile Analysis of the LTPP SPS-9A Site in Arizona*, Report No. UMTRI-2007-17, University of Michigan Transportation Research Institute, Ann Arbor, MI.

6. Karamihas, S.M. (2007). *Profile Analysis of the LTPP SPS-9P Site in Arizona*, Report No. UMTRI-2007-18, University of Michigan Transportation Research Institute, Ann Arbor, MI.

7. Karamihas, S.M. and Senn, K. (2010). *Profile Analysis of the LTPP SPS-6 Site in Arizona*, Report No. UMTRI-2010-17, University of Michigan Transportation Research Institute, Ann Arbor, MI.

8. Evans, L.D. and Eltahan, A. (2000). *LTPP Profile Variability*, Report No. FHWA-RD-00-113, Federal Highway Administration, McLean, VA.

9. Sayers, M.W., Gillespie, T.D., and Queiroz, C.A.V. (1986). *The International Road Roughness Experiment*, World Bank Technical Paper Number 45, The World Bank, Washington, DC.

10. Karamihas, S.M. (2004). "Development of Cross Correlation for Objective Comparison of Profiles." *International Journal of Vehicle Design*, Vol. 36, Nos. 2/3, pp. 173–193.

11. Karamihas, S.M., Gillespie, T.D., Kohn, S.D., and Perera, R.W. (1999). *Guidelines for Longitudinal Pavement Profile Measurement*, NCHRP Report 434, Transportation Research Board, Washington, DC.

12. Sayers, M.W. (1989). "Two Quarter-Car Models for Defining Road Roughness: IRI and HRI." *Transportation Research Record 1215*, pp. 165–172, Transportation Research Board, Washington, DC.

13. Karamihas, S.M., Gillespie, T.D., and Riley, S.M. (1995). "Axle Tramp Contribution to the Dynamic Wheel Loads of a Heavy Truck." *Proceedings of the 4th International Symposium on Heavy Vehicle Weights and Dimensions*, Ed. C.B. Winkler, Ann Arbor, MI.

14. Sayers, M.W. and Karamihas, S.M. (1996). “Estimation of Rideability by Analyzing Road Profile.” *Transportation Research Record 1536*, pp 110–116, Transportation Research Board, Washington, DC.

15. Sayers, M.W. and Karamihas, S.M. (1996). *Interpretation of Road Roughness Profile Data*, Report No. FHWA-RD-96-101, Federal Highway Administration, McLean, VA.

16. Sayers, M.W. and Karamihas, S.M. (1998). *The Little Book of Profiling*. University of Michigan, Ann Arbor, MI.

17. Perera, R.W. and Kohn, S.D. (2005). *Quantification of Smoothness Index Differences Related to Long-Term Pavement Performance Equipment Type*, Report No. FHWA-HRT-05-054, Federal Highway Administration, McLean, VA.

18. Sayers, M.W. (1990). “Profiles of Roughness.” *Transportation Research Record 1260*, pp. 106–111, Transportation Research Board, Washington, DC.

19. Mohamed, A.R. and Hansen, W. (1997). “Effect of Nonlinear Temperature Gradient on Curling Stress in Concrete Pavements.” *Transportation Research Record 1568*, pp. 65–71, Transportation Research Board, Washington, DC.

20. Asbahan, R. and Vandenbossche, J. (2011). “Effects of Temperature and Moisture Gradients on Slab Deformation for Jointed Plain Concrete Pavements.” *Journal of Transportation Engineering*, Vol. 137, No. 8, pp. 563–570, American Society of Civil Engineers, Reston, VA.

21. Sixbey, D., et al. (2001). “Measurement and Analysis of Slab Curvature in JCP Pavements Using Profiling Technology.” Proceedings, 7th International Conference on Concrete Pavements, pp. 81–95, International Society for Concrete Pavements, Lake Buena Vista, FL.

22. Vandenbossche, J.M., et al. (2002). *Early and Long-Term Effects of Curling and Warping on Jointed Concrete Pavement*, Draft Report, Contract No. DTFH61-95-C-00021, Federal Highway Administration, Washington, DC.

23. Westergaard, H.M. (1927). “Analysis of Stresses in Concrete Roads Caused by Variations of Temperature.” *Public Roads, Journal of Highway Research*, Vol. 8, No. 3, pp. 54–60.

24. Chang, G., Karamihas, S.M., Rasmussen, R.O., Merritt, D., and Swanlund, M. (2008). “Quantifying the Impact of Jointed Concrete Curling and Warping on Pavement Uneveness.” Presented at the 6th Symposium on Pavement Surface Characteristics, World Road Association, Portorož, Slovenia.

25. Press, W.H., Flannery, B.P., Teukolsky, S.A., and Vetterling, W.T. (1986). *Numerical Recipes: The Art of Scientific Computing*, Cambridge University Press, Cambridge, UK.

HRDI-30/12-12(500)E